CAPITAL UNIVERSITY OF SCIENCE AND TECHNOLOGY, ISLAMABAD

Cattaneo-Christov based Study of a Powell-Eyring Hybrid Nanofluid Flow

by

Muhammad Naveed Sani

A thesis submitted in partial fulfillment for the degree of Master of Philosophy

in the

Faculty of Computing
Department of Mathematics

2022

*I dedicate my dissertation work to my **family** and dignified **teachers**. A special feeling of gratitude to my loving parents who have supported me in my studies.*

CERTIFICATE OF APPROVAL

Cattaneo-Christov based Study of a Powell-Eyring Hybrid Nanofluid Flow

by

Muhammad Naveed Sani

(MMT203028)

THESIS EXAMINING COMMITTEE

(a)	External Examiner	Dr. Amir Ali	COMSATS University Attock
(b)	Internal Examiner	Dr. Rashid Ali	CUST, Islamabad
(c)	Supervisor	Dr. Muhammad Sagheer	CUST, Islamabad

Dr. Muhammad Sagheer
Thesis Supervisor
October, 2022

Dr. Muhammad Sagheer
Head
Dept. of Mathematics
October, 2022

Dr. M. Abdul Qadir
Dean
Faculty of Computing
October, 2022

Author's Declaration

I, **Muhammad Naveed Sani**, hereby state that my MPhil thesis titled "**Cattaneo-Christov based Study of a Powell-Eyring Hybrid Nanofluid Flow**" is my own work and has not been submitted previously by me for taking any degree from Capital University of Science and Technology, Islamabad or anywhere else in the country/abroad.

At any time if my statement is found to be incorrect even after my graduation, the University has the right to withdraw my MPhil Degree.

(Muhammad Naveed Sani)
Registration No: MMT203028

Plagiarism Undertaking

I solemnly declare that research work presented in this thesis titled "**Cattaneo-Christov based Study of a Powell-Eyring Hybrid Nanofluid Flow**" is solely my research work with no significant contribution from any other person. Small contribution/help wherever taken has been dully acknowledged and that complete thesis has been written by me.

I understand the zero tolerance policy of the HEC and Capital University of Science and Technology towards plagiarism. Therefore, I as an author of the above titled thesis declare that no portion of my thesis has been plagiarized and any material used as reference is properly referred/cited.

I undertake that if I am found guilty of any formal plagiarism in the above titled thesis even after award of MPhil Degree, the University reserves the right to withdraw/revoke my MPhil degree and that HEC and the University have the right to publish my name on the HEC/University website on which names of students are placed who submitted plagiarized work.

(Muhammad Naveed Sani)
Registration No: MMT203028

Acknowledgement

I got no words to articulate my cordial sense of gratitude to **Almighty Allah** who is the most merciful and most beneficent to his creation.

I also express my gratitude to the last prophet of **Almighty Allah, Prophet Muhammad (PBUH)** the supreme reformer of the world and knowledge for human being.

I would like to be thankful to all those who provided support and encouraged me during this work.

I would like to be grateful to my thesis supervisor **Dr. Muhammad Sagheer**, the Head of the Department of Mathematics, for guiding and encouraging towards writing this thesis. It would have remained incomplete without his endeavours. Due to his efforts I was able to write and complete this dissertation.

I would like to pay great tribute to my **parents**, for their prayers, moral support, encouragment and appreciation.

Last but not the least, I want to express my gratitude to my **friends** who helped me throughout in my MPhil degree.

(Muhammad Naveed Sani)

Abstract

Hybrid nanofluids are introduced as heat transfer fluids with greater surface stability, diffusion and dispersion capabilities compared to the traditional nanofluids. In this thesis, flow, convective heat transport, mass concentration and volumetric entropy generation in Cattaneo-Christov over Powell-Eyring hybrid nanofluid including magnetic field effects are investigated. Hybrid nanofluid occupies the space over the uniform horizontal porous stretching surface with velocity slip at the interface. Effects of viscous dissipation and linear thermal radiation are also included in the flow model. Mathematical equations for conservation of mass, momentum, energy, mass concentration and entropy are simplified under the assumptions of boundary layer flow of Powell-Eyring hybrid nanofluid. Similarity solutions are obtained by transformation of governing partial differential equations to ordinary differential equations, using similarity variables. Shooting method is then adopted to find the approximate solutions of reduced ordinary differential equations. The influence of various physical parameters on the velocity profile, temperature distribution, concentration profile, skin friction coefficient, Nusselt number, Sherwood number and entropy generation are studied and presented in the graphical and tabular forms. The results obtained reveal that there is an enhancement in the rate of heat transfer with a rise in the nanoparticle volume fraction and permeability parameter. The temperature distribution is also influenced by the presence of the relaxation time parameter, Eckert number, thermal radiation and nanoparticle volume fraction.

Contents

List of Figures

List of Tables

Abbreviations

IVPs	Initial value problems
MHD	Magnetohydrodynamics
ODEs	Ordineary differential equations
PDEs	Partial differential equations
RK	Runge-Kutta

Symbols

μ	Viscosity
ρ	Density
ν	Kinematic viscosity
τ	Stress tensor
k	Thermal conductivity
α	Thermal diffisuitivity
σ	Electrical conductivity
u	x-component of fluid velocity
v	y-component of fluid velocity
B_0	Magnetic field constant
ϖ	Unsteadiness parameter
$\tilde{\beta}$	Material Parameter
ζ^*	Material Parameter
a	Stretching constant
T_w	Temperature of the wall
T_∞	Ambient temperature of the nanofluid
T	Temperature
C_w	Concentration of the wall
C_∞	Ambient concentration of the hybrid nanofluid
C	Concentration
ρ_f	Density of the fluid
μ_f	Viscosity of the fluid
ν_f	Kinematic viscosity of the base fluid

ρ_{nf}	Density of the nanofluid
μ_{nf}	Viscosity of the nanofluid
q_r	Radiative heat flux
q	Heat generation constant
q_w	Heat flux
q_m	Mass flux
σ^*	Stefan Boltzmann constant
k^*	Absorption coefficient
	Stream function
θ	Stream function
ϕ	Stream function
η	Similarity variable
ξ	Similarity variable
C_f	Skin friction coefficient
Nu	Nusselt number
Nu_x	Local Nusselt number
Sh	Sherwood number
Sh_x	Local Sherwood number
Re	Reynolds number
Re_x	Local Reynolds number
ϕ	Nanoparticle volume fraction
Nr	Thermal radiation parameter
m	Shape factor
M	Magnetic parameter
α_f	Thermal diffusivity
Δ	Material Parameter
ω	Material Parameter
Ec	Eckert number
Pr	Prandtl number
S	Suction/injection parameter
Λ	Velocity slip parameter

Bi	Biot number
Sc	Schmidt number
K_1	Chemical reaction number
Br	Brinkmann number
Ω	Dimensionless temperature gradient
ρ_{hnf}	Density of the hybrid nanofluid
ρ_f	Density of the pure fluid
ρ_{p_1}	Density of Cu
ρ_{p_2}	Density of Al_2O_3
μ_{hnf}	Viscosity of the hybrid nanofluid
μ_f	Viscosity of the base fluid
$(\rho C_p)_{hnf}$	Heat capacitance of hybrid nanofluid
$(\rho C_p)_f$	Heat capacitance of base fluid
$(\rho C_p)_{p_1}$	Heat capacitance of Cu
$(\rho C_p)_{p_2}$	Heat capacitance of Al_2O_3
σ_{hnf}	Electrical conductivity of the hybrid nanofluid
σ_f	Electrical conductivity of the base fluid
σ_{p_1}	Electrical conductivity of the Cu
σ_{p_2}	Electrical conductivity of the Al_2O_3
κ_{hnf}	Thermal conductivity of the hybrid nanofluid
κ_{nf}	Thermal conductivity of the nanofluid
κ_f	Thermal conductivity of the base fluid
κ_{p_1}	Thermal conductivity of the Cu
κ_{p_2}	Thermal conductivity of the Al_2O_3
D_{hnf}	Mass diffusion of the hybrid nanofluid
D_f	Diffusivity of the base fluid
f	Dimensionless velocity
θ	Dimensionless temperature
ϕ	Dimensionless concentration
λ	Thermal relaxation time period

Chapter 1

Introduction

Hybrid nanofluids are a mixture of metal, polymeric or non-metallic nano-sized strengths with base fluid (water, ethylene, glycol, oil and many others) used to enhance the rate of heat transfer in a variety of applications. Hybrid nanofluid has a higher heat transfer rate than pure fluid. Entropy generation is the quantity of entropy that is usually produced during the irreversible process by the flow of heat across thermal resistance and some other irreversible pocesses like diffusion, chemical reaction, joule heating etc.

Some of the most important industrial applications of heat transfer by fluid flow are solar thermal systems, food processing techniques, fabrication of composite materials, thermal insulation, oil recovery, and subterranean water transportation. On a horizontal stretching sheet, the momentum and heat transfer in a laminar liquid layer are analysed by Andersson et al.[1]. Under the effects of suction/injection, viscous dissipation, and thermal radiation, an analysis of the steady non-linear viscous flow of an incompressible viscous fluid across a horizontal surface of changing temperature with a power-law velocity is provided by Cortell [2]. By utilizing porous materials, Ali et al. [3] examined enhanced thermal characteristics and heat transfer of phase change material. Extended surfaces, heat pipes, and the inclusion of highly conductive nanoparticles can improve the heat transmission of PCMs. Ghadikolaei et al. [4] examine the flow and heat transfer of a homogenous, incompressible fluid over a strecthing sheet. To understand thermal as well as fluid

flow analysis, readers are recommended to study [5–11]. These uses were expected while manufacturing nanofluids by Choi [12] to improve the heat transmission capabilities of conventional fluids. Thermodynamics analysis, Newtonian and non-Newtonian fluid models, different flow geometries, bounding surface conditions, shape and type of nanoparticles, nanoparticle concentration and the effect of external forces etc. were all taken into consideration by researchers shortly after the introduction of nanofluids. Qing et al. [13, 14] examine entropy generation on porous medium across stretching/shrinking sheet using the MHD Casson nanofluid model. Tausif et al. [15] calculated the melting heat transfer (MHT) boundary layer emission of a Casson fluid containing suspended ZrO_2 nanoparticles of four distinct shapes across a flat surface. Two distinct scenarios of controlling nanoparticles (i.e active and passive control) have been taken into consideration.

Relevant research on nanofluid flow and heat transfer processes, particularly over large moving surfaces can be found in [16–23]. Although it is important to consider the concentration of nanoparticles, their form, size, and interactions with one another, adding nanoparticles to a Newtonian fluid often results in a non-Newtonian behaviour. Additionally, abrupt motion and temperature changes can affect viscosity and thermal conductivity.

Suresh et al. [24] expanded the concept of nanofluids and introduced hybrid nanofluids by incorporating two different types of nanoparticles into a base fluid. Devi and Devi [25, 26] numerically examine the mathematical model of 3D MHD flow of Cu-Al_2O_3/H_2O Hybrid and conventional nanofluids over the surface that is linearly extending in one direction. Comparison of the heat transfer rates between hybrid and traditional nanofluids revealed that the rate of heat transfer of hybrid nanofluid Cu-Al_3/H_2O is more as compare to nano-fluid Cu-H_2O.

Afrand et al. [27] keeping up the same diretion and concentrating on the impact of nanoparticle concentration on magnetite Fe_3O_4-$Ag/Engine\ Oil$ hybrid nanofluid. They came to the conclusion that shear rates cause the viscosities of non-Newtonian samples to drop, indicating that the nanofluid samples exhibit shear thinning behaviour. Hussain et al. [28] describe results for Cu-Al_2O_3/H_2O

hybrid nanofluid is flowing inside the blocked cavity. They acquire FEM for numerical solutions and concentrated on physical factors and how they affected hybrid nanofluids heat transfer properties.

Acharya et al. [29] examined the impact of Hall current on the radiative transport of the hybrid nanofluid over the rotating disc. For this numerical study they considered Cu-TiO_2/H_2O hybrid nanofluid and utilizing the shooting method similarity solutions are obtained. Temperature profiles are found to be higher when compared to traditional nanofluid, hybrid nanofluid's. Additionally, the Hall parameter reduces nanofluid temperature and increases radial skin friction at the border. Maskeen et al. [30] discuss numerical soltions for the effects of heat transfer and flow characteristics of Cu-Al_2O_3/H_2O hybrid nanofluid flowing across an expanding cylinder. They incorporated linear thermal radiation and Lorentz magnetic forces into their model. They demonstrated that the hybrid nanofluid is more efficient than traditional nanofluids in heat transfer procedures.

Aziz et al. [31] numerical calculations are made for the hybrid Powell-Eyring nanofluid flow, heat transfer, and total volumetric entropy analysis. Hybrid nanofluids are made by adding copper and alumina nanoparticles to water. The water-based hybrid nanofuid covers an infinitely porous flat surface, and the flow is produced as a result of the surface being stretched. Velocity slip is also expected to occur at the interface. Analysis of the combined effects of thermal radiation and viscous dissipation on the system's total entropy, flow and temperature profiles, and rate of heat transfer is the main objective.

Ghadikolaei et al. [32] examin the thermophysical characteristics of TiO_2-Cu/H_2O hybrid nanofliud with shape factor when Lorentz forces are present. Jamshed et al. [33] the Cattaneo-Cahristov heat flux theory to study the flow, heat transfer, and entropy formation of an electrically conducting non-Newtonian hybrid nanofluid across a stretched surface. For the hybrid nanofluid, the Casson fluid model is used combined with slip and convective boundary conditions at the surface. The flow is created by nonlinearly stretching a porous horizontal surface, and the flow is then subjected to a uniform magnetic field in the transverse direction. The mathematical formulation also incorporates the Cattaneo-Christov heat

flux model and thermal radiation and the numerical results for the Copper Oxide with base fluid Ethylene glycol *CuO-EG* and TiO_2-*CuO/EG* hybrid nanofluid. The influence of various shape factors parameters increases the temperature fluctuation, and entropy of Casson hybrid nanofluid inside boundary layer.
Nazir et al. [34] numerical analysis is used to examine how hybrid nanostructures might improve two-dimensional heat transport. Comparisons are made between the results of pure Carreau-Yasuda fluid and fluid incorporating nanostructures.

1.1 Thesis Contributions

In this thesis, we provide a review study of Aziz et al. [31]. The present survey is focused on the numerical analysis of Cattaneo-Christov bases study of Powell-Eyring hybrid nanofluid flow with magnetic field effect and chemical reaction. Through the use of similarity transformations, the presented nonlinear PDEs are transformed into a system of ODEs. Furthermore, the shooting approach is used to determine the numerical solutions of nonlinear ODEs.Utilizing MATLAB, the numerically acquired findings are computed. The impact of significant parameters on velocity distribution $f'(\eta)$, temperature distribution $\theta(\eta)$, concentration distribution $\phi(\eta)$ and entropy generation NG ,skin friction coefficient Cf, local Nusselt number Nu_x and local Sherwood number Sh_x have been discussed in graphs and tables.

1.2 Layout of Thesis

The following is a quick summary of the thesis's contents.

Chapter 2 covers some fundamental terminologies and definitions that are essential to understanding the concepts discussed later.

Chapter 3 provides the proposed analytical evaluation ofentropy anaysis of Powell-Eyring hybrid nanofluid with thermal radiation effect and shooting methodology

is used to generate the numerical solutions of the governing flow model.

Chapter 4 extends the proposed model flow mentioned in Chapter 3 by including the Cattaneo-Christov heat flux, Powell-Eyring hybrid nanofluid and magnetic field effects.The shooting methodology is used to generate the numerical solutions of the governing flow model.

Chapter 5 provides the thesis's final remarks.

References used in the thesis are mentioned in **Biblography**.

Chapter 2

Preliminaries

This chapter mentions some basic definitions and governing laws which will be helpful in later chapters.

2.1 Some Fundamental Terminologies

Definition 2.1.1 (Fluid)

"A fluid is a substance that deforms continuously under the application of a shear (tangential) stress no matter how small the shear stress may be." [35]

Definition 2.1.2 (Fluid Mechanics)

"Fluid mechanics is that branch of science which deals with the behavior of the fluid (liquids or gases) at rest as well as in motion." [36]

Definition 2.1.3 (Fluid Dynamics)

"The study of fluid if the pressure forces are also considered for the fluids in motion, that branch of science is called fluid dynamics." [36]

Definition 2.1.4 (Fluid Statics)

"The study of fluid at rest is called fluid statics." [36]

Definition 2.1.5 (Viscosity)

"Viscosity is defined as the property of a fluid which offers resistance to the movement of one layer of fluid over another adjacent layer of the fluid. Mathematically,

$$\mu = \frac{\tau}{\frac{\partial u}{\partial y}},$$

where μ is viscosity coefficient, τ is shear stress and $\frac{\partial u}{\partial y}$ represents the velocity gradient." [36]

Definition 2.1.6 (Kinematic Viscosity)

"It is defined as the ratio between the dynamic viscosity and density of fluid. It is denoted by symbol ν called **nu**. Mathematically,

$$\nu = \frac{\mu}{\rho}." \text{ [36]}$$

Definition 2.1.7 (Thermal Conductivity)

"The Fourier heat conduction law states that the heat flow is proportional to the temperature gradient. The coefficient of proportionality is a material parameter known as the thermal conductivity which may be a function of a number of variables." [37]

Definition 2.1.8 (Thermal Diffusivity)

"The rate at which heat diffuses by conducting through a material depends on the thermal diffusivity. It can be defined as,

$$\alpha = \frac{k}{\rho C_p},$$

where α is the thermal diffusivity, k is the thermal conductivity, ρ is the density and C_p is the specifc heat at constant pressure." [37]

2.2 Types of Fluid

There are following types of fluid:

Definition 2.2.1 (Ideal Fluid)

"A fluid, which is incompressible and has no viscosity, is known as an ideal fluid. Ideal fluid is only an imaginary fluid as all the fluids, which exist, have some viscosity." [36]

Definition 2.2.2 (Real Fluid)

"A fluid, which possesses viscosity, is known as a real fluid. In actual practice, all the fluids are real fluids." [36]

Definition 2.2.3 (Newtonian Fluid)

"A real fluid, in which the shear stress is directly proportional to the rate of shear strain (or velocity gradient), is known as a Newtonian fluid." [36]

Definition 2.2.4 (Non-Newtonian Fluid)

"A real fluid in which the shear stress is not directly proportional to the rate of shear strain (or velocity gradient), is known as a non-Newtonian fluid.

$$\tau_{xy} \propto \left(\frac{du}{dy}\right)^m, \qquad m \neq 1$$
$$\tau_{xy} = \mu\left(\frac{du}{dy}\right)^m ." \text{ [36]}$$

Definition 2.2.5 (Magnetohydrodynamics)

"Magnetohydrodynamics(MHD) is concerned with the mutual interaction of fluid flow and magnetic fields. The fluids in question must be electrically conducting and non-magnetic, which limits us to liquid metals, hot ionised gases (plasmas) and strong electrolytes." [38]

2.3 Types of Flow

The following types of flow are:

Definition 2.3.1 (Rotational Flow)

"Rotational flow is that type of flow in which the fluid particles while flowing along stream-lines, also rotate about their own axis." [36]

Definition 2.3.2 (Irrotational Flow)

"Irrotational flow is that type of flow in which the fluid particles while flowing along stream-lines, do not rotate about their own axis then this type of flow is called irrotational flow." [36]

Definition 2.3.3 (Compressible Flow)

"Compressible flow is that type of flow in which the density of the fluid changes from point to point or in other words the density (ρ) is not constant for the fluid, Mathematically,

$$\rho \neq k,$$

where k is constant." [36]

Definition 2.3.4 (Incompressible Flow)

"Incompressible flow is that type of flow in which the density is constant for the fluid. Liquids are generally incompressible while gases are compressible, Mathematically,

$$\rho = k,$$

where k is constant." [36]

Definition 2.3.5 (Steady Flow)

"If the flow characteristics such as depth of flow, velocity of flow, rate of flow at any point in open channel flow do not change with respect to time, the flow is said to be steady flow. Mathematically,

$$\frac{\partial Q}{\partial t} = 0,$$

where Q is any fluid property." [36]

Definition 2.3.6 (Unsteady Flow)

"If at any point in open channel flow, the velocity of flow, depth of flow or rate of flow changes with respect to time, the flow is said to be unsteady. Mathematically,

$$\frac{\partial Q}{\partial t} \neq 0,$$

where Q is any fluid property." [36]

Definition 2.3.7 (Internal Flow)

"Flows completely bounded by a solid surfaces are called internal or duct flows." [35]

Definition 2.3.8 (External Flow)

"Flows over bodies immersed in an unbounded fluid are said to be an external flow." [35]

2.4 Kinds of Heat Transfer

There are following kinds of heat transfer:

Definition 2.4.1 (Heat Transfer)

"Heat transfer is a branch of engineering that deals with the transfer of thermal energy from one point to another within a medium or from one medium to another due to the occurrence of a temperature difference. For example, heat is transferred from stove to the cooking pan." [37]

Definition 2.4.2 (Conduction)

"The transfer of heat within a medium due to a diffusion process is called conduction. For example, a radiator is a good of example of conduction." [37]

Definition 2.4.3 (Convection)

"Convection heat transfer is usually defined as energy transport effected by the motion of a fluid. The convection heat transfer between two dissimilar media is governed by Newtons law of cooling." [37]

Definition 2.4.4 (Thermal Radiation)

"Thermal radiation is defined as radiant (electromagnetic) energy emitted by a medium and is solely to the temperature of the medium. Sometimes radiant energy is taken to be transported by electromagnetic wave while at other times it is supposed to be transported by particle like photons. " [37]

2.5 Dimensionless Numbers

There are different types of dimensionless numbers:

Definition 2.5.1 (Eckert Number)

"It is the dimensionless number used in continuum mechanics. It describes the relation between flows and the boundary layer enthalpy difference and it is used for characterized heat dissipation. Mathematically,

$$Ec = \frac{u^2}{C_p \nabla T}$$

where C_p denotes the specific heat." [35]

Definition 2.5.2 (Prandtl Number)

"It is the ratio between the momentum diffusivity ν and thermal diffusivity α. Mathematically, it can be defined as

$$Pr = \frac{\nu}{\alpha} = \frac{\frac{\mu}{\rho}}{\frac{k}{C_p \rho}} = \frac{\mu C_p}{k}$$

where μ represents the dynamic viscosity, Cp denotes the specific heat and k stands for thermal conductivity. The relative thickness of thermal and momentum

boundary layer is controlled by Prandtl number. For small Pr, heat distributed rapidly corresponds to the momentum." [35]

Definition 2.5.3 (Skin Friction Coefficient)

"The steady flow of an incompressible gas or liquid in a long pipe of internal D. The mean velocity is denoted by u_w. The skin friction coefficient can be defined as

$$C_f = \frac{2\tau_0}{\rho u_w^2}$$

where τ_0 denotes the wall shear stress and ρ is the density." [39]

Definition 2.5.4 (Nusselt Number)

"The hot surface is cooled by a cold fluid stream. The heat from the hot surface, which is maintained at a constant temperature, is diffused through a boundary layer and convected away by the cold stream. Mathematically,

$$Nu = \frac{qL}{k}$$

where q stands for the convection heat transfer, L for the characteristic length and k stands for thermal conductivity." [40]

Definition 2.5.5 (Sherwood Number)

"It is the nondimensional quantity which show the ratio of the mass transport by convection to the transfer of mass by diffusion. Mathematically:

$$Sh = \frac{kL}{D}$$

here L is characteristics length, D is the mass diffusivity and k is the mass transfer" coeffcient." [41]

Definition 2.5.6 (Reynolds Number)

"It is defined as the ratio of inertia force of a flowing fluid and the viscous force

of the fluid. Mathematically,

$$Re = \frac{VL}{\nu},$$

where V denotes the free stream velocity, L is the characteristic length and ν stands for kinematic viscosity." [36]

Definition 2.5.7 (Schmidt Number)

"It is the ratio between kinematic viscosity and molecular diffusion$D$. It is denoted by Sc and mathematically we can write it as:

$$Sc = \frac{\nu}{D}$$

where ν is the kinematic viscosity and D is the mass diffusivity." [37]

2.6 Governing Laws

Definition 2.6.1 (Continuity Equation)

"The principle of conservation of mass can be stated as the time rate of change of mass is fixed volume is equal to the net rate of flow of mass across the surface. Mathematically, it can be written as

$$\frac{\partial \rho}{\partial t} + \nabla.(\rho \mathbf{u}) = 0." \text{ [37]}$$

Definition 2.6.2 (Momentum Equation)

"The momentum equation states that the time rate of change of linear momentum of a given set of particles is equal to the vector sum of all the external forces acting on the particles of the set, provided Newtons Third Law of action and reaction governs the internal forces. Mathematically, it can be written as:

$$\frac{\partial}{\partial t}(\rho \mathbf{u}) + \nabla.[(\rho \mathbf{u})\mathbf{u}] = \nabla.\mathbf{T} + \rho g." \text{ [37]}$$

Definition 2.6.3 (Energy Equation)

"The law of conservation of energy states that the time rate of change of the total energy is equal to the sum of the rate of work done by the applied forces and change of heat content per unit time.

$$\frac{\partial \rho}{\partial t} + \nabla.\rho\mathbf{u} = -\nabla.\mathbf{q} + Q + \phi,$$

where ϕ is the dissipation function." [37]

Definition 2.6.4 (Conservation Equation)

"The principle of conservation of mass can be stated as the time rate of change of mass is fixed volume is equal to the net rate of flow of mass across the surface. Mathematically, it can be written as:

$$\frac{\partial \rho}{\partial t} + \nabla.\rho\mathbf{u} = 0,$$

where t is time, the fluid density is , and the fluid velocity is u." [37]

2.7 Shooting Method

To estimate the solution of following boundary value problem by Shooting method.

$$\left.\begin{aligned} &g'''(x) = g''(x) + g(x)g'(x) \\ &g(0) = 0, \qquad g'(0) = 1, \qquad g(h) = R. \end{aligned}\right\} \tag{2.1}$$

Introduce the following notations to reduce the order of the above boundary value problem.

$$\left.\begin{aligned} &g = z_1 \\ &g' = z_1' = z_2, \\ &g'' = z_2' = z_3. \end{aligned}\right\} \tag{2.2}$$

As a result, (2.1) is transformed into the following system of first order ODEs.

$$z_1' = z_2, \qquad z_1(0) = 0 \tag{2.3}$$

$$z_2' = z_3, \qquad z_2(0) = 1 \tag{2.4}$$

$$z_3' = z_3 + z_1 z_2, \qquad z_3(0) = t \tag{2.5}$$

where t is the missing initial condition which will be guessed.
The above IVP will be numerically solved by the RK-4 method. The missing condition t is to be chosen such that.

$$z_1(h, t) = R. \tag{2.6}$$

For convenience, now onward $z_1(h, t)$ will be denoted by $z_1(t)$.
Let us further denote $z_1(t) - R$ by $\phi(t)$, so that

$$\phi(t) = 0. \tag{2.7}$$

The above equation can be solved by using Newton's method with the following iterative formula.

$$t_{n+1} = t_n - \frac{\phi(t_n)}{\left(\frac{\partial \phi(t)}{\partial t}\right)_{t=t_n}},$$

or

$$t_{n+1} = t_n - \frac{z_1(t_n) - R}{\left(\frac{\partial z_1(t)}{\partial t}\right)_{t=t_n}}. \tag{2.8}$$

For $\frac{\partial z_1(t)}{\partial t}$, we introduce the following notations.

$$\frac{\partial z_1}{\partial t} = z_4, \quad \frac{\partial z_2}{\partial t} = z_5, \quad \frac{\partial z_3}{\partial t} = z_6. \tag{2.9}$$

By using these notations Newton's iterative scheme, will then get the following form

$$t_{n+1} = t_n - \frac{z_1(t_n) - R}{z_4(t_n)}. \tag{2.10}$$

Now differentiate the system of first order ODEs (2.3)-(2.4) with respect to t, we get another system of ODEs, as follows.

$$z_4' = z_5, \qquad z_4(0) = 0. \tag{2.11}$$

$$z_5' = z_6, \qquad z_5(0) = 0. \tag{2.12}$$

$$z_6' = z_6 + z_1 z_5 + z_4 z_2, \qquad z_6(0) = 1. \tag{2.13}$$

Writing all the four ODEs (2.3), (2.4), (2.10) and (2.11) together, we have the following IVP.

$$\begin{aligned}
z_1' &= z_2, & z_1(0) &= 0.\\
z_2' &= z_3, & z_2(0) &= 1.\\
z_3' &= z_3 + z_1 z_2, & z_3(0) &= t.\\
z_4' &= z_5, & z_4(0) &= 0.\\
z_5' &= z_6, & z_5(0) &= 0.\\
z_6' &= z_6 + z_1 z_5 + z_4 z_2, & z_6(0) &= 1.
\end{aligned}$$

The above IVP will be solved numerically by using Runge-Kutta method of order four.

The stopping criteria for the Shooting method is set as,

$$\mid z_1(t) - R \mid < \epsilon,$$

where $\epsilon > 0$ is an sufficiently small positive number.

Chapter 3

Entropy Analysis of Powell-Eyring Hybrid Nanofluid Including Effect of Linear Thermal Radiation and Viscous Dissipation

3.1 Introduction

In this chapter, we will perform numerical analysis of flow, heat transfer and total volumetric entropy of hybrid Powell-Eyring nanofluids. The numerical solution for this model was computed by Aziz et al. [31] by the Keller-Box method. In the present chapter a review of this work is included by using the shooting method. In this study, hybrid nanofluids are made by adding copper and alumina nanoparticles to water. Water-based hybrid nanofluid occupies more space on an infinite porous flat surface, and its flow is caused by the interface in surface tension and speed. The main purpose is to analyze the effect of viscous dissipation

and thermal radiation on flow, temperature profile, heat transfer rate and the general entropy of the framework set by Tiwari and Das [42].

3.2 Mathematical Modeling

Consider an unstable, laminar, stable, boundary layer flow of inviscid optically thick hybrid nanofluid above infinite penetrable plate. The non-Newtonian Powell-Eyring mathematical model is assumed for Hybrid nanofluids. Cartesian dimensional coordinates are assumed with x-axis to have porous surface along it and the y-axis normal to this. In current study, nanofluids are prepared by adding copper *(Cu)* nanoparticles in pure water with the volume fraction ϕ also alumina (Al_2O_3) and copper *(Cu)* nanoparticles with volume fractions ϕ_1 and ϕ_2 are dispersed in the pure water to manufacture hybrid nanofuid. The nanoparticle volume concentration of hybrid nanofluid is defined as $\phi_{hnf} = \phi_1 + \phi_2$. The constitutive equations of Powell-Eyring fluid model are derived from the theory of liquids and not from the empirical relationship as in the power-law model. The Powell-Eyring fluid model reduces Newtonian flux at low and high shear rates. The Cauchy stress tensor for Powell-Eyring fluid is given as [43]:

$$\tau_{ij} = \mu_{hnf}\Big(\frac{\partial u_i}{\partial x_j}\Big) + \frac{1}{\tilde{\beta}} Sinh^{-1}\Big(\frac{1}{\zeta^*}\frac{\partial u_i}{\partial x_j}\Big), \tag{3.1}$$

where μ_{hnf} is the hybrid dynamic viscosity and β, ζ^* are material constants of Powell-Eyring hybrid nanofluid. The stretching speed and porous surface temperature are

$$U_w(x,t) = \frac{cx}{1-\varpi t}, \qquad T_w(x,t) = T_\infty + \frac{cx}{1-\varpi t}. \tag{3.2}$$

Here t is the time, c is a +ve constant and T_∞ the ambient temperature.

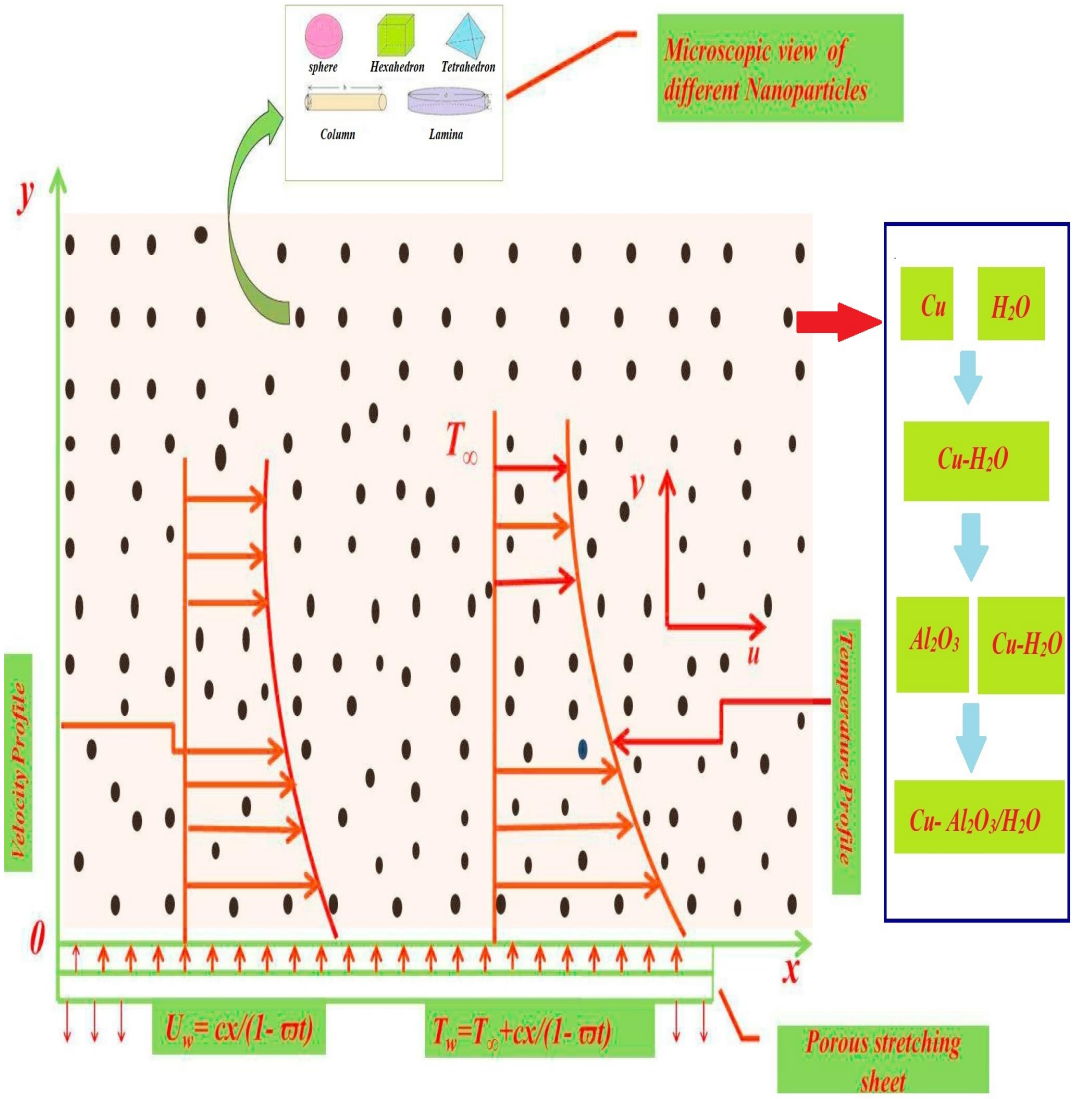

FIGURE 3.1: systematic representation of physical model.

The governing equations of the mathematical model for hybrid Powell-Eyring nanofluid can be expressed as Aziz et al. [31]:

$$\frac{\partial u}{\partial x}+\frac{\partial v}{\partial y}=0, \tag{3.3}$$

$$\frac{\partial u}{\partial t}+u\frac{\partial u}{\partial x}+v\frac{\partial u}{\partial y}=\left(\nu_{hnf}+\frac{1}{\rho_{hnf}\tilde{\beta}\zeta^{*}}\right)\frac{\partial^{2}u}{\partial y^{2}}-\frac{1}{2\tilde{\beta}\zeta^{*3}\rho_{hnf}}\left(\frac{\partial u}{\partial y}\right)^{2}\frac{\partial^{2}u}{\partial y^{2}}, \tag{3.4}$$

$$\frac{\partial T}{\partial t}+u\frac{\partial T}{\partial x}+v\frac{\partial T}{\partial y}=\frac{\kappa_{hnf}}{(\rho C_{p})_{hnf}}\left(\frac{\partial^{2}T}{\partial y^{2}}\right)-\frac{1}{(\rho C_{p})_{hnf}}\left(\frac{\partial q_{r}}{\partial y}\right)+\frac{\nu_{hnf}}{(\rho C_{p})_{hnf}}\left(\frac{\partial u}{\partial y}\right)^{2}. \tag{3.5}$$

The associated BCs have been taken as:

$$\left.\begin{aligned} &u(x,0) = U_w + \nu_{hnf}\Big(\frac{\partial u}{\partial y}\Big), \quad v(x,0) = V_w, \\ &-\kappa_f\Big(\frac{\partial T}{\partial y}\Big) = h_f(T_w - T), \quad at \quad y = 0, \\ &u \to 0, \quad T \to T_\infty, \quad as \quad y \to \infty. \end{aligned}\right\} \tag{3.6}$$

The radiative heat flux is given by

$$q_r = -\frac{4\sigma^*}{3k^*}\frac{\partial T^4}{\partial y}, \tag{3.7}$$

where σ^* is the Stefan-Boltzman constant and k^* is the absorption coefficient. If the temperature difference is very small, then the temperature T^4 can be expanded about T_∞ using Taylor series, as follows.

$$T^4 = T_\infty^4 + 4T_\infty^3(T - T_\infty) + 6T_\infty^2(T - T_\infty)^2 + ...$$

Ignoring the higher order terms, we have

$$\begin{aligned} T^4 &= T_\infty^4 + 4T_\infty^3(T - T_\infty) \\ &= T_\infty^4 + 4T_\infty^3 T - 4T_\infty^4 \\ &= -3T_\infty^4 + 4T_\infty^3 T \\ &= 4T_\infty^3 T - 3T_\infty^4. \end{aligned}$$

TABLE 3.1: Thermo-physical properties of Hybrid naonofluid

Feature	Hybrid nanofluid Al_2O_3-Cu/H_2O
Viscosity (ν)	$\mu_{hnf} = \mu_f(1-\phi_1)^{-2.5}(1-\phi_2)^{-2.5}$
Density (ρ)	$\rho_{hnf} = (1-\phi_2)\big((1-\phi_1)\rho_f + \phi_1\rho_{p_1}\big) + \phi_2\rho_{p_2}$
Heat Capacity (ρC_p)	$(\rho C_p)_{hnf} = (1-\phi_2)[(1-\phi_1)(\rho C_p)_f + \phi_1(\rho C_p)_{p_1}] + \phi_2(\rho C_p)_{p_2}$
Thermal conductivity (κ)	$\frac{\kappa_{hnf}}{\kappa_{nf}} = \left[\frac{\kappa_{p_2}+(m-1)\kappa_{nf}-(m-1)\phi_2(\kappa_{nf}-\kappa_{p_2})}{\kappa_{p_2}+(m-1)\kappa_{nf}+\phi_2(\kappa_{nf}-\kappa_{p_2})}\right]$, $\frac{\kappa_{nf}}{\kappa_f} = \left[\frac{\kappa_{p_1}+(m-1)\kappa_f-(m-1)\phi_1(\kappa_{1f}-\kappa_{p_1})}{\kappa_{p_1}+(m-1)\kappa_f+\phi_1(\kappa_f-\kappa_{p_1})}\right]$
Electrical conductivity (σ)	$\frac{\sigma_{hnf}}{\sigma_f} = \left[1 + \frac{3(\frac{\phi_1\sigma_{p_1}+\phi_2\sigma_{p_2}}{\sigma_f}-(\phi_1+\phi_2))}{(\frac{\phi_1\sigma_{p_1}+\phi_2\sigma_{p_2}}{(\phi_1+\phi_2)\sigma_f}+2)-(\frac{\phi_1\sigma_{p_1}+\phi_2\sigma_{p_2}}{\sigma_f}-(\phi_1+\phi_2))}\right]$

For convenience, the following notations have been introduced:

$$P_a = (1-\phi_1)^{2.5}(1-\phi_2)^{2.5}, \tag{3.8}$$

$$P_b = (1-\phi_2)\left((1-\phi_1)+\phi_1\frac{\rho_{p_1}}{\rho_f}\right)\frac{\rho_{p_2}}{\rho_f}, \tag{3.9}$$

$$P_c = (1-\phi_2)\left((1-\phi_1)+\phi_1\frac{(\rho C_p)_{p_1}}{(\rho C_p)_f}\right)+\phi_2\frac{(\rho C_p)_{p_2}}{(\rho C_p)_f}, \tag{3.10}$$

$$P_d = \left[\frac{\kappa_{p_2}+2\kappa_{nf}-2\phi_2(\kappa_{nf}-\kappa_{p_2})}{\kappa_{p_2}+2\kappa_{nf}+\phi_2(\kappa_{nf}-\kappa_{p_2})}\right]\times\left[\frac{\kappa_{p_1}+2\kappa_f-2\phi_1(\kappa_{1f}-\kappa_{p_1})}{\kappa_{p_1}+2\kappa_{1f}+\phi_1(\kappa_f-\kappa_{p_1})}\right]. \tag{3.11}$$

For the conversion of the mathematical model in the form of partial differential equations (3.3)-(3.5) into the ODEs, the following similarity transformation was used by Hayat et al. [44].

$$\left.\begin{aligned}\eta(t,y) &= \sqrt{\frac{c}{\nu_f(1-\varpi t)}}y,\\ \psi(x,y) &= \sqrt{\frac{\nu_f c}{(1-\varpi t)}}xf(\eta), \qquad \theta(\eta) = \frac{T-T_\infty}{T_w-T_\infty},\end{aligned}\right\} \tag{3.12}$$

where ψ denotes the stream function.

The step-by-step process for transforming (3.3)-(3.5) into the dimensionless form has been described below.

$$\begin{aligned} u &= \frac{\partial\psi}{\partial y}\\ &= \frac{\partial}{\partial y}\left(\sqrt{\frac{\nu_f c}{1-\varpi t}}xf(\eta)\right)\\ &= \sqrt{\frac{\nu_f c}{1-\varpi t}}xf'\frac{\partial\eta}{\partial y}\\ &= \left(\frac{c}{1-\varpi t}\right)xf'. \end{aligned} \tag{3.13}$$

$$\begin{aligned} v &= -\frac{\partial\psi}{\partial x}\\ &= -\frac{\partial}{\partial x}\left(\sqrt{\frac{\nu_f c}{1-\varpi t}}xf(\eta)\right)\\ &= -\sqrt{\frac{\nu_f c}{1-\varpi t}}.1.f(\eta)-\sqrt{\frac{\nu_f c}{1-\varpi t}}x.f'.(0)\\ &= -\sqrt{\frac{\nu_f c}{1-\varpi t}}f(\eta). \end{aligned} \tag{3.14}$$

$$\begin{aligned}\frac{\partial u}{\partial x} &= \frac{\partial}{\partial x}\left(\frac{c}{1-\varpi t}xf'\right)\\ &= \frac{c}{1-\varpi t}.1.f'(\eta)+\frac{c}{1-\varpi t}xf''\frac{\partial \eta}{\partial x}\\ &= \frac{c}{1-\varpi t}f'(\eta). \qquad (3.15)\\ \frac{\partial u}{\partial y} &= \frac{\partial}{\partial y}\left[\frac{c}{1-\varpi t}xf'(\eta)\right]\\ &= \frac{c}{1-\varpi t}\sqrt{\frac{c}{\nu_f(1-\varpi t)}}xf''. \qquad (3.16)\\ \frac{\partial^2 u}{\partial y^2} &= \frac{c^2}{\nu_f(1-\varpi t)}xf'''. \qquad (3.17)\\ \frac{\partial v}{\partial y} &= \frac{\partial}{\partial y}\left(-\sqrt{\frac{\nu_f c}{1-\varpi t}}f(\eta)\right)\\ &= -\sqrt{\frac{\nu_f c}{1-\varpi t}}f'(\eta)\frac{\partial \eta}{\partial y}\\ &= -\sqrt{\frac{\nu_f c}{1-\varpi t}}f'(\eta)\sqrt{\frac{c}{\nu_f(1-\varpi t)}}\\ \frac{\partial v}{\partial y} &= -\frac{c}{1-\varpi t}f'(\eta). \qquad (3.18)\\ \frac{\partial u}{\partial t} &= \frac{\partial}{\partial t}\left(\frac{c}{1-\varpi t}xf'(\eta)\right)\\ &= -1.\frac{c}{(1-\varpi t)^2}xf'+\frac{c}{1-\varpi t}x.f''.\frac{1}{2}\frac{1}{\sqrt{\frac{c}{\nu_f(1-\varpi t)}}}(-1)\frac{c}{\nu_f(1-\varpi t)^2}(-\tilde{\omega})y\\ &= \frac{cx}{(1-\varpi t)^2}f'+\frac{1}{2}\frac{c\varpi}{(1-\varpi t)^2}\sqrt{\frac{c}{\nu_f(1-\varpi t)}}xyf''. \qquad (3.19)\end{aligned}$$

Equation (3.3) is easily satisfied by using (3.15) and (3.18), as follows

$$\frac{\partial u}{\partial x}+\frac{\partial v}{\partial y}=\frac{c}{1-\varpi t}f'(\eta)-\frac{c}{1-\varpi t}f'(\eta)=0. \qquad (3.20)$$

Now, the dimensionless form of the momentum equation (3.4) can be obtained by using equations (3.13) - (3.19) as follows,

$$\frac{\partial u}{\partial t}+u\frac{\partial u}{\partial x}+v\frac{\partial u}{\partial y}=\left[\nu_{hnf}+\frac{1}{\rho_{hnf}\tilde{\beta}\zeta^*}\right]\frac{\partial^2 u}{\partial y^2}-\frac{1}{2\tilde{\beta}\zeta^{*3}\rho_{hnf}}\left[\frac{\partial u}{\partial y}\right]^2\frac{\partial^2 u}{\partial y^2}.$$

$$\Rightarrow \frac{cx}{(1-\varpi t)^2}f' + \frac{1}{2}\frac{c\varpi}{(1-\varpi t)^2}\sqrt{\frac{c}{\nu_f(1-\varpi t)}}xyf'' + (\frac{c}{1-\varpi t})xf'.\frac{c}{1-\varpi t}f'(\eta)$$
$$- \sqrt{\frac{\nu_f c}{1-\varpi t}}f(\eta).\frac{c}{1-\varpi t}\sqrt{\frac{c}{\nu_f(1-\varpi t)}}xf'' = \Big[\nu_{hnf} + \frac{1}{\rho_{hnf}\tilde{\beta}\zeta^*}\Big].\frac{c^2}{\nu_f(1-\varpi t)}xf'''$$
$$- \frac{1}{2\tilde{\beta}\zeta^{*3}\rho_{hnf}}\Big[\frac{c}{1-\varpi t}\sqrt{\frac{c}{\nu_f(1-\varpi t)}}xf''\Big]^2.\frac{c^2}{\nu_f(1-\varpi t)}xf'''.$$

$$\Rightarrow \frac{cx}{(1-\varpi t)^2}f' + \frac{1}{2}\frac{c\varpi}{(1-\varpi t)^2}\sqrt{\frac{c}{\nu_f(1-\varpi t)}}xyf'' + \frac{c^2}{(1-\varpi t)^2}xf'^2 - \frac{c^2}{(1-\varpi t)^2}xff''$$
$$= \Big[\nu_{hnf} + \frac{1}{\rho_{hnf}\tilde{\beta}\zeta^*}\Big]\frac{c^2}{\nu_f(1-\varpi t)}xf''' - \frac{1}{2\tilde{\beta}\zeta^{*3}\rho_{hnf}}\frac{c^5}{\nu_f^2(1-\varpi t)^5}x^3f''^2f'''$$

$$\Rightarrow \frac{\varpi}{c}f' + \frac{1}{2}.\frac{\varpi}{c}.\sqrt{\frac{c}{\nu_f(1-\varpi t)}}yf'' + f'^2 - ff'' = \Big[\nu_{hnf} + \frac{1}{\rho_{hnf}\tilde{\beta}\zeta^*}\Big]\frac{1}{\nu_f}f'''$$
$$- \frac{1}{2}\frac{c^3x^2}{(1-\varpi t)^3\rho_{hnf}\nu_f^2\tilde{\beta}\zeta^{*3}}f''^2f'''.$$

$$\Rightarrow \Big[\frac{\nu_{hnf}}{\nu_f} + \frac{1}{\nu_f\rho_{hnf}\tilde{\beta}\zeta^*}\Big]f''' - \frac{1}{2}\Big[\frac{c^3x^3}{(1-\varpi t)^3\rho_{hnf}\nu_f^2\tilde{\beta}\zeta^{*3}x}\Big]f''^2f''' - f'^2 + ff''$$
$$- \frac{\varpi}{c}\Big[f' + \frac{1}{2}\sqrt{\frac{c}{\nu_f(1-\varpi t)}}yf''\Big] = 0.$$

$$\Rightarrow \Big[\frac{\nu_{hnf}}{\nu_f} + \frac{1}{\nu_f\rho_{hnf}\tilde{\beta}\zeta^*}\Big]f''' - \Big[\frac{\frac{c^3x^3}{(1-\varpi t)^3}}{2\nu_f^2\rho_{hnf}\tilde{\beta}\zeta^{*3}x}\Big]f''^2f''' - f'^2 + ff''$$
$$- \frac{\varpi}{c}\Big[f' + \frac{1}{2}\sqrt{\frac{c}{\nu_f(1-\varpi t)}}yf''\Big] = 0.$$

Since, $\nu = \frac{\mu}{\rho}$, so

$$\left(\frac{\frac{\mu_{hnf}}{\rho_{hnf}}}{\frac{\mu_f}{\rho_f}} + \frac{1}{\frac{\mu_f}{\rho_f}\rho_{hnf}\tilde{\beta}\zeta^*}\right)f''' - \left(\frac{U_w^3}{(2\zeta^{*2}\nu_f x)(\rho_{hnf}\frac{\mu_f}{\rho_f}\tilde{\beta}\zeta^* x)}\right)f''^2f''' - f'^2 + ff''$$
$$- \frac{\varpi}{c}\left(f' + \frac{1}{2}\sqrt{\frac{c}{\nu_f(1-\varpi t)}}yf''\right) = 0.$$
$$\because \frac{\frac{\mu_{hnf}}{\rho_{hnf}}}{\frac{\mu_f}{\rho_f}} = \frac{\mu_f(1-\phi_1)^{-2.5}(1-\phi_2)^{-2.5}\rho_f}{\mu_f[(1-\phi_2)(1-\phi_1)\rho_f + \phi_1\rho_{p_1}] + \phi_2\rho_{p_2}} = \frac{1}{P_1P_2},$$
$$\rho_{hnf}\frac{\mu_f}{\rho_f} = \left(\big((1-\phi_2)(1-\phi_1)\rho_f + \phi_1\rho_{p_1}\big) + \phi_2\rho_{p_2}\right) \times \frac{\mu_f}{\rho_f},$$

therefore, the dimensionless form of the momentum equation gets the form:

$$\Big(\frac{1}{P_aP_b} + \frac{\omega}{P_b}\Big)f''' + ff'' - f'^2 - A\Big(f' + \frac{\eta}{2}f''\Big) - \frac{\omega\Delta}{P_b}f''^2f''' = 0. \tag{3.21}$$

The following dimensionless parameters are used in equation (3.21),

$$A = \frac{\varpi}{c}, \qquad \omega = \frac{1}{\mu_f \tilde{\beta} \zeta^*}, \qquad \Delta = \frac{U_w^3}{2\zeta^{*2}\nu_f x}.$$

Now, for the conversion of energy equation (3.5), the following derivatives are required.

$$\begin{aligned}
\theta(\eta) &= \frac{T - T_\infty}{T_w - T_\infty}. \\
\Rightarrow \qquad T &= \theta(\eta)(T_w - T_\infty) + T_\infty \\
&= \theta(\eta)\Big(T_\infty + \frac{cx}{1-\varpi t} - T_\infty\Big) + T_\infty \\
&= \theta(\eta)\Big(\frac{cx}{1-\varpi t}\Big) + T_\infty. \\
\frac{\partial T}{\partial x} &= \frac{\partial}{\partial x}\Big(\frac{cx}{1-\varpi t}\Big)\theta^(\eta) \\
&= \Big(\frac{c}{1-\varpi t}\Big)\theta(\eta). \qquad (3.22) \\
\frac{\partial T}{\partial y} &= \frac{\partial}{\partial y}\Big[\theta(\eta)\Big(\frac{cx}{1-\varpi t}\Big) + T_\infty\Big] \\
&= \Big(\frac{cx}{1-\varpi t}\Big)\theta' \frac{\partial \eta}{\partial y} \\
&= \Big(\frac{cx}{1-\varpi t}\Big)\theta' \sqrt{\frac{c}{\nu_f(1-\varpi t)}}. \qquad (3.23) \\
\frac{\partial^2 T}{\partial y^2} &= \Big(\frac{c^2 x}{\nu_f(1-\varpi t)^2}\Big)\theta''. \qquad (3.24)
\end{aligned}$$

Now, the time derivative of temperature is,

$$\begin{aligned}
\frac{\partial T}{\partial t} &= \frac{\partial}{\partial t}\left(\theta(\eta)\Big(\frac{cx}{1-\varpi t}\Big) + T_\infty\right) \\
&= (-1)\frac{cx}{(1-\varpi t)^2}(-\varpi)\theta \\
&\quad + \frac{cx}{1-\varpi t}\theta' \frac{1}{2}\sqrt{\frac{\nu_f(1-\varpi t)}{c}}(-1)\frac{c}{\nu_f(1-\varpi t)^2}(-\varpi)y \\
&= \frac{cx\varpi}{(1-\varpi t)^2}\theta + \frac{1}{2}\frac{c^2\varpi}{\nu_f(1-\varpi t)^3}\sqrt{\frac{\nu_f(1-\varpi t)}{c}}xy\theta' \\
&= \frac{cx\varpi}{(1-\varpi t)^2}\theta + \frac{1}{2}\frac{c\,\varpi}{(1-\varpi t)^2}\sqrt{\frac{c}{\nu_f(1-\varpi t)}}xy\theta'. \qquad (3.25)
\end{aligned}$$

$$
\begin{aligned}
\textit{Also} \qquad q_r &= -\frac{4\sigma^*}{3k^*}\frac{\partial T^4}{\partial y} \\
&= -\frac{4\sigma^*}{3k^*}\frac{\partial}{\partial y}(4T_\infty^3 T - 3T_\infty^4) \\
&= -\frac{4\sigma^*}{3k^*}\frac{\partial}{\partial y}(4T_\infty^3 T) \\
&= -\frac{16\sigma^*}{3k^*}T_\infty^3\frac{\partial T}{\partial y}. \\
\Rightarrow \qquad \frac{\partial q_r}{\partial y} &= -\frac{16\sigma^*}{3k^*}T_\infty^3\frac{\partial^2 T}{\partial y^2} \\
&= -\frac{16\sigma^*}{3k^*}T_\infty^3\left(\frac{c^2 x}{\nu_f(1-\varpi t)^2}\right)\theta''. \qquad (3.26)
\end{aligned}
$$

The governing equation for the conservation of energy is

$$
\begin{aligned}
&\frac{\partial T}{\partial t} + u\frac{\partial T}{\partial x} + v\frac{\partial T}{\partial y} = \frac{\kappa_{hnf}}{(\rho C_p)_{hnf}}\left(\frac{\partial^2 T}{\partial y^2}\right) - \frac{1}{(\rho C_p)_{hnf}}\left(\frac{\partial q_r}{\partial y}\right) + \frac{\nu_{hnf}}{(\rho C_p)_{hnf}}\left(\frac{\partial u}{\partial y}\right)^2. \\
\Rightarrow\ &\frac{cx\varpi}{(1-\varpi t)^2}\theta + \frac{1}{2}\frac{c\,\varpi}{(1-\varpi t)^2}\sqrt{\frac{c}{\nu_f(1-\varpi t)}}xy\theta' + \left(\frac{cx}{1-\varpi t}f'\right)\left(\frac{c}{1-\varpi t}\right)\theta(\eta) \\
&+ \left(-\sqrt{\frac{\nu_f c}{1-\varpi t}}f\right)\frac{cx}{1-\varpi t}\theta'\sqrt{\frac{c}{\nu_f(1-\varpi t)}} = \frac{\kappa_{hnf}}{(\rho C_p)_{hnf}}\left(\frac{c^2 x}{\nu_f(1-\varpi t)^2}\right)\theta'' \\
&- \frac{1}{(\rho C_p)_{hnf}}\left(-\frac{16\sigma^*}{3k^*}T_\infty^3\left(\left(\frac{c^2 x}{\nu_f(1-\varpi t)^2}\right)\theta''\right)\right) \\
&+ \frac{\nu_{hnf}}{(\rho C_p)_{hnf}}\left(\frac{c^2x^2}{(1-\varpi t)^2}\frac{c}{\nu_f(1-\varpi t)}f''^2\right). \\
\Rightarrow\ &\frac{\varpi}{c}\theta + \frac{1}{2}\frac{\varpi}{c}\eta\theta' + f'\theta - f\theta' = \frac{\kappa_{hnf}}{(\rho C_p)_{hnf}}\frac{1}{\nu_f}\theta'' + \frac{16\sigma^*}{3\kappa^*}\frac{1}{(\rho C_p)_{hnf}}\frac{1}{\nu_f}\theta' T_\infty^3 \\
&\qquad + \frac{\nu_{hnf}}{(\rho C_p)_{hnf}}\frac{cx}{\nu_f(1-\varpi t)}f''^2.
\end{aligned}
$$

From Table 3.1,

$$
\begin{aligned}
\kappa_{hnf} &= \left[\frac{\kappa_{p_2} + (m-1)\kappa_{nf} - (m-1)\phi_2(\kappa_{nf} - \kappa_{p_2})}{\kappa_{p_2} + (m-1)\kappa_{nf} + \phi_2(\kappa_{nf} - \kappa_{p_2})}\right] \\
&\quad \times \left[\frac{\kappa_{p_1} + (m-1)\kappa_f - (m-1)\phi_1(\kappa_{1f} - \kappa_{p_1})}{\kappa_{p_1} + (m-1)\kappa_f + \phi_1(\kappa_f - \kappa_{p_1})}\right]\kappa_f \\
\Rightarrow \quad \kappa_{hnf} &= P_d\kappa_f. \\
(\rho C_p)_{hnf} &= \Big[(1-\phi_2)[(1-\phi_1)(\rho C_p)_f + \phi_1(\rho C_p)_{p_1}] + \phi_2(\rho C_p)_{p_2}\Big] \times \frac{(\rho C_p)_{hnf}}{(\rho C_p)_{hnf}} \\
&= P_c(\rho C_p)_f.
\end{aligned}
$$

$$
\begin{aligned}
So, \quad & \frac{\varpi}{c}\theta+\frac{1}{2}\frac{\varpi}{c}\eta\theta'+f'\theta-f\theta'=\frac{P_d\kappa_f}{P_c(\rho C_p)_f}\frac{1}{\nu_f}\theta''+\frac{16\sigma^*}{3\kappa^*}\frac{1}{P_c(\rho C_p)_f}\frac{1}{\nu_f}\theta' T_\infty^3 \\
& \qquad +\frac{\frac{\nu_f}{P_a}}{P_c(\rho C_p)_f}\frac{cx}{\frac{\nu_f}{\rho_f}(1-\varpi t)}f''^2. \\
\Rightarrow \quad & \frac{\varpi}{c}\theta+\frac{1}{2}\frac{\varpi}{c}\eta\theta'+f'\theta-f\theta'=\frac{P_d}{P_c}\frac{\kappa_f}{(\rho C_p)_f}\frac{1}{\nu_f}\theta''+\frac{1}{P_c}\frac{16\sigma^*}{3\kappa^*}\frac{T_\infty^3}{\nu_f(\rho C_p)_f}\theta' \\
& \qquad +\frac{1}{P_aP_c}\frac{c^2x^2}{(1-\varpi t)^2}\frac{1-\varpi t}{cx}\frac{1}{(C_p)_f}f''^2. \\
\Rightarrow \quad & \frac{\varpi}{c}\theta+\frac{1}{2}\frac{\varpi}{c}\eta\theta'+f'\theta-f\theta'=\frac{P_d}{P_c}\frac{\kappa_f}{(\rho C_p)_f}\frac{1}{\nu_f}\theta''+\frac{1}{P_c}\frac{16\sigma^*}{3\kappa^*}\frac{T_\infty^3}{\nu_f(\rho C_p)_f}\theta' \\
& \qquad +\frac{1}{P_aP_c}\frac{U_w^3}{(C_p)_f(T_w-T_\infty)}f''^2. \\
\Rightarrow \quad & A\theta+\frac{1}{2}A\theta'+f'\theta-f\theta'=\frac{P_d}{P_c}\frac{1}{Pr}\theta''+\frac{Nr}{P_c}\theta'+\frac{E^c}{P_aP_c}f''^2. \\
\Rightarrow \quad & \frac{P_d}{P_c}\frac{1}{Pr}\theta''+\frac{Nr}{P_c}\theta'+\frac{E^c}{P_aP_c}f''^2-A\theta-\frac{1}{2}A\theta'-f'\theta+f\theta'=0. \\
& \left(1+\frac{PrNr}{P_d}\right)\theta''+Pr\frac{P_c}{P_d}\times\left(f\theta'-f'\theta-A\left(\theta+\frac{\eta}{2}\theta'\right)+\frac{E^c}{P_aP_c}f''^2\right)=0.
\end{aligned}
\tag{3.27}
$$

The dimensionless parameters used in equation (3.27) are:

$$
\begin{aligned}
A&=\tfrac{\varpi}{c}, \qquad \alpha_f=\tfrac{\kappa_f}{(\rho C_p)_f}, \qquad Pr=\tfrac{\nu_f}{\alpha_f}, \\
E^c&=\tfrac{U_w^3}{(C_p)_f(T_w-T_\infty)}, \qquad Nr=\tfrac{16\sigma^*}{3\kappa^*}\tfrac{T_\infty^3}{\nu_f(\rho C_p)_f}.
\end{aligned}
$$

The final dimensionless form of the governing equations is

$$
\left(\frac{1}{P_aP_b}+\frac{\omega}{P_b}\right)f'''+ff''-f'^2-A\left(f'+\frac{\eta}{2}f''\right)-\frac{\omega\Delta}{P_b}f''^2f'''=0, \tag{3.28}
$$

$$
\left(1+\frac{PrNr}{P_d}\right)\theta''+Pr\frac{P_c}{P_d}\times\left(f\theta'-f'\theta-A\left(\theta+\frac{\eta}{2}\theta'\right)+\frac{E^c}{P_aP_c}f''^2\right)=0. \tag{3.29}
$$

The related BCs are converted into the dimensionless form by the following procedure.

$$
\begin{aligned}
& v(x,0)=V_w, && at \quad y=0. \\
\Rightarrow \quad & V_w=-\sqrt{\frac{\nu_f c}{1-\varpi t}}f(\eta), && at \quad \eta=0.
\end{aligned}
$$

$$
\begin{aligned}
\Rightarrow \quad & f(\eta) = -\sqrt{\frac{1-\varpi t}{\nu_f c}}, && at \quad \eta = 0.\\
\Rightarrow \quad & f(0) = S.\\
& u(x,0) = U_w(x) + \mu_{hnf}\Big(\frac{\partial u}{\partial y}\Big), && at \quad y = 0.\\
\Rightarrow \quad & \frac{cx}{1-\varpi t} f'(\eta) = \frac{cx}{1-\varpi t} + \frac{cx}{1-\varpi t}\sqrt{\frac{c}{\nu_f(1-\varpi t)}}\frac{\mu_f}{P_a} f''(\eta), && at \quad \eta = 0.\\
\Rightarrow \quad & \frac{cx}{1-\varpi t} f'(\eta) = \frac{cx}{1-\varpi t}\Big(1 + \sqrt{\frac{c}{\nu_f(1-\varpi t)}}\mu_f\Big) f'', && at \quad \eta = 0.\\
\Rightarrow \quad & f'(\eta) = 1 + \frac{\Lambda}{P_a} f''(\eta), && at \quad \eta = 0.\\
\Rightarrow \quad & f'(0) = 1 + \frac{\Lambda}{P_a} f''(0).\\
& -\kappa_f\Big[\frac{\partial T}{\partial y}\Big] = h_f(T_w - T), && at \quad y = 0.\\
\Rightarrow \quad & -\kappa_f \frac{cx}{1-\varpi t}\sqrt{\frac{c}{\nu_f(1-\varpi t)}}\theta' = h_f\Big(T_\infty + \frac{cx}{1-\varpi t} - T\Big), && at \quad \eta = 0.\\
\Rightarrow \quad & \frac{cx}{1-\varpi t}\theta'(\eta) = \frac{-h_f}{\kappa_f}\sqrt{\frac{\nu_f(1-\varpi t)}{c}}\Big(\frac{cx}{1-\varpi t} - (T - T_w)\Big), && at \quad \eta = 0.\\
\Rightarrow \quad & \frac{cx}{1-\varpi t}\theta'(\eta) = -\frac{h_f}{\kappa_f}\sqrt{\frac{\nu_f(1-\varpi t)}{c}}\Big(\frac{cx}{1-\varpi t} - \frac{cx}{1-\varpi t}\theta(\eta)\Big), && at \quad \eta = 0.\\
\Rightarrow \quad & \theta'(\eta) = -Bi(1-\theta(\eta)), && at \quad \eta = 0.\\
\Rightarrow \quad & \theta'(0) = -Bi(1-\theta(0)).
\end{aligned}
$$

Similarly,

$$
\begin{aligned}
& u \to 0, && as \quad y \to \infty.\\
\Rightarrow \quad & f'(\eta) \to 0, && as \quad \eta \to \infty.\\
& T \to T_\infty, && as \quad y \to \infty.\\
\Rightarrow \quad & \theta(\eta) \to 0 && as \quad \eta \to \infty.
\end{aligned}
$$

The associated BCs (3.6) in the dimensionless form are:

$$
\left.
\begin{aligned}
& f(0) = S, \quad f'(0) = 1 + \frac{\Lambda}{P_a} f''(0), \quad f'(\eta) \to 0, \quad as \;\; \eta \to \infty,\\
& \theta'(0) = -Bi(1-\theta(0)), \quad \theta(\eta) \to 0, \quad as \;\; \eta \to \infty.
\end{aligned}
\right\} \tag{3.30}
$$

The skin friction coefficient, is given as follows,

$$C_f = \frac{\tau_w}{\rho_f U_w^2}, \tag{3.31}$$

where

$$\tau_w = -\left(\left(\mu_{hnf} + \frac{1}{\tilde{\beta}\zeta^*} \right) \frac{\partial u}{\partial y} - \frac{1}{6\tilde{\beta}\zeta^{*3}} \left(\frac{\partial u}{\partial y} \right)^3 \right)_{y=0}. \tag{3.32}$$

Therefore

$$\begin{aligned}
C_f &= \frac{-\left[\left(\mu_{hnf} + \frac{1}{\tilde{\beta}\zeta^*} \right) \frac{c}{1-\varpi t} \sqrt{\frac{c}{\nu_f(1-\varpi t)}} x f'' - \frac{1}{6\tilde{\beta}\zeta^{*3}} \frac{c^3}{(1-\varpi t)^3} \left(\sqrt{\frac{c}{\nu_f(1-\varpi t)}} x f'' \right)^3 \right]_{y=0}}{\rho_f U_w^2} \\
&= \frac{-\left[\left(\frac{\mu_f}{P_a} + \frac{1}{\tilde{\beta}\zeta^*} \right) U_w \sqrt{\frac{c}{\nu_f(1-\varpi t)}} x f'' - \frac{1}{6\tilde{\beta}\zeta^{*3}} U_w^3 \left(\sqrt{\frac{c}{\nu_f(1-\varpi t)}} x f'' \right)^3 \right]_{y=0}}{\rho_f U_w^2} \\
&= \frac{-\left[\left(\frac{\mu_f}{\mu_f P_a} + \frac{1}{\mu_f \tilde{\beta}\zeta^*} \right) U_w \sqrt{\frac{c}{\nu_f(1-\varpi t)}} x f'' - \frac{1}{6\mu_f \tilde{\beta}\zeta^{*3}} U_w^3 \left(\sqrt{\frac{c}{\nu_f(1-\varpi t)}} x f'' \right)^3 \right]_{y=0}}{\frac{\rho_f}{\mu_f} U_w^2} \\
&= \frac{-\left[\left(\frac{1}{P_a} + \frac{1}{\mu_f \tilde{\beta}\zeta^*} \right) f''(0) - \frac{1}{6\mu_f \tilde{\beta}\zeta^{*3}} U_w^2 \frac{c}{\nu_f(1-\varpi t)} f'''^3(0) \right] \sqrt{\frac{c}{\nu_f(1-\varpi t)}}}{\frac{1}{\nu_f} U_w} \\
&= \frac{-\left[\left(\frac{1}{P_a} + \frac{1}{\mu_f \tilde{\beta}\zeta^*} \right) f''(0) - \frac{1}{6\mu_f \tilde{\beta}\zeta^{*3}} U_w^2 \frac{cx}{\nu_f(1-\varpi t)x} f'''^3(0) \right] \sqrt{\frac{c}{\nu_f(1-\varpi t)}} x}{\frac{U_w x}{\nu_f}} \\
&= \frac{-\left[\left(\frac{1}{P_a} + \frac{1}{\mu_f \tilde{\beta}\zeta^*} \right) f''(0) - \frac{1}{3} \frac{1}{\mu_f \tilde{\beta}\zeta^*} \frac{U_w^3}{2\zeta^* \nu_f x} f'''^3(0) \right] \sqrt{\frac{cx}{\nu_f x(1-\varpi t)}} x}{\frac{U_w x}{\nu_f}} \\
&= \frac{-\left[\left(\frac{1}{P_a} + \frac{1}{\mu_f \tilde{\beta}\zeta^*} \right) f''(0) - \frac{1}{3} \frac{1}{\mu_f \tilde{\beta}\zeta^*} \frac{U_w^3}{2\zeta^* \nu_f x} f'''^3(0) \right] \sqrt{\frac{U_w}{\nu_f x}} x}{\frac{U_w x}{\nu_f}} \\
&= \frac{-\left[\left(\frac{1}{P_a} + \frac{1}{\mu_f \tilde{\beta}\zeta^*} \right) f''(0) - \frac{1}{3} \frac{1}{\mu_f \tilde{\beta}\zeta^*} \frac{U_w^3}{2\zeta^* \nu_f x} f'''^3(0) \right] \sqrt{\frac{U_w x}{\nu_f}}}{\frac{U_w x}{\nu_f}} \\
&= \frac{-\left[\left(\frac{1}{P_a} + \omega \right) f''(0) - \frac{\omega\Delta}{3} f'''^3(0) \right] \sqrt{Re_x}}{Re_x} \\
&= -\frac{\left[\left(\frac{1}{P_a} + \omega \right) f''(0) - \frac{\omega\Delta}{3} f'''^3(0) \right]}{\sqrt{Re_x}}.
\end{aligned}$$

$$\Rightarrow \quad C_f Re_{x^{\frac{1}{2}}} = -\left[\left(\frac{1}{P_a} + \omega \right) f''(0) - \frac{\omega\Delta}{3} f'''^3(0) \right]. \tag{3.33}$$

Here $Re_x = \frac{U_w x}{\nu_f}$ denotes the local Reynolds number.

Local Nusselt number is defined as follows.

$$Nu_x = \frac{xq_w}{\kappa_f(T_w - T_\infty)}. \tag{3.34}$$

The dimensionless form of Nu_x is produced by the following steps:

$$q_w = -\kappa_{hnf}\Big(1 + \frac{16\sigma^* T_\infty^3}{3k^*\nu_f(\rho C_p)_f}\Big)\Big(\frac{\partial T}{\partial y}\Big)_{y=0}. \tag{3.35}$$

$$\begin{aligned} Nu_x &= -\frac{x\kappa_{hnf}\Big(1 + \frac{16\sigma^* T_\infty^3}{3k^*\nu_f(\rho C_p)_f}\Big)\Big(\frac{\partial T}{\partial y}\Big)_{y=0}}{\kappa_f(T_w - T_\infty)} \\ &= -\frac{x\kappa_{hnf}\Big(1 + \frac{16\sigma^* T_\infty^3}{3k^*\nu_f(\rho C_p)_f}\Big)\frac{cx}{1-\varpi t}\theta'(0)\sqrt{\frac{c}{\nu_f(1-\varpi t)}}}{\kappa_f\frac{cx}{1-\varpi t}} \\ &= -\frac{\kappa_{hnf}\Big(1 + \frac{16\sigma^* T_\infty^3}{3k^*\nu_f(\rho C_p)_f}\Big)\theta'(0)\sqrt{\frac{cx}{\nu_f x(1-\varpi t)}}x}{\kappa_f} \\ &= -\frac{\kappa_{hnf}}{\kappa_f}(1 + Nr)\theta'(0)\sqrt{Re_x}. \\ \Rightarrow \quad Nu_x Re_x^{-\frac{1}{2}} &= -\frac{\kappa_{hnf}}{\kappa_f}(1 + Nr)\theta'(0). \end{aligned} \tag{3.36}$$

Here $Re_x = \frac{U_w c^2}{\nu_f x}$ denotes the Reynolds number.

The entropy generation rate N_G is defined as:

$$N_G = \frac{T_\infty^2 c^2 E_G}{\kappa_f(T_w - T_\infty)^2}. \tag{3.37}$$

The dimensionless form of N_G can be produced through the following steps:

$$E_G = \frac{\kappa_{hnf}}{T_\infty^2}\left(\Big(\frac{\partial T}{\partial y}\Big)^2 + \frac{16}{3}\frac{16\sigma^* T_\infty^3}{3k^*\nu_f(\rho C_p)_f}\Big(\frac{\partial T}{\partial y}\Big)^2\right) + \frac{\mu_{hnf}}{T_\infty}\Big(\frac{\partial u}{\partial y}\Big)^2. \tag{3.38}$$

$$\begin{aligned} \therefore \quad N_G &= \frac{\left(\frac{\kappa_{hnf}}{T_\infty^2}\left(\Big(\frac{\partial T}{\partial y}\Big)^2 + \frac{16}{3}\frac{16\sigma^* T_\infty^3}{3k^*\nu_f(\rho C_p)_f}\Big(\frac{\partial T}{\partial y}\Big)^2\right) + \frac{\mu_{hnf}}{T_\infty}\Big(\frac{\partial u}{\partial y}\Big)^2\right)T_\infty^2 c^2}{\kappa_f(T_w - T_\infty)^2} \\ &= \frac{\left(\frac{P_d\kappa_f}{T_\infty^2}(1 + Nr)\frac{(c^2x^2)}{(1-\varpi t)^2}\frac{c}{\nu_f(1-\varpi t)}\theta'^2 + \frac{\frac{\mu_f}{P_a}}{T_\infty}\frac{(c^2x^2)}{(1-\varpi t)^2}\frac{c}{\nu_f(1-\varpi t)}f''^2\right)T_\infty^2 c^2}{\kappa_f(T_w - T_\infty)^2} \end{aligned}$$

$$= \left(P_d(1+Nr)\theta'^2 + \frac{T_\infty \mu_f}{P_a} \frac{U_w^2}{\kappa_f (T_w - T_\infty)^2} f''^2 \right) \frac{cx}{\nu_f x(1-\varpi t)} c^2$$

$$= \left(P_d(1+Nr)\theta'^2 + \frac{1}{P_a} \frac{T_\infty}{(T_w - T_\infty)} \frac{\mu_f U_w^2}{\kappa_f (T_w - T_\infty)} f''^2 \right) \frac{U_w c^2}{\nu_f x}$$

$$= Re \left(P_d(1+Nr)\theta'^2 + \frac{1}{P_a} \frac{Br}{\Omega} f''^2 \right). \tag{3.39}$$

where $R_e = \frac{U_w c^2}{\nu_f x}$, $Br = \frac{\mu_f U_w^2}{\kappa_f (T_w - T_\infty)}$, and $\Omega = \frac{T_\infty}{(T_w - T_\infty)}$ denote the Reynolds number, Brinkmann number and dimensionless temperature gradient respectively.

3.3 Numerical Method for Solution

The ordinary differential equation (3.28) has been solved numerically by using the shooting technique.

$$f''' = \frac{P_a P_b}{1 + P_a\omega - P_a\omega\Delta f''^2} \left(f'^2 - f f'' + A\left(f' + \frac{\eta}{2} f'' \right) \right). \tag{3.40}$$

The following notations have been taken:

$$f = G_1, \qquad f' = G_1' = G_2, \qquad f'' = G_1'' = G_2' = G_3.$$

The momentum equation is then transformed into the system of first-order ODEs shown below.

$$G_1' = G_2, \qquad G_1(0) = S.$$

$$G_2' = G_3, \qquad G_2(0) = 1 + \frac{\Lambda}{P_a} G_3(0).$$

$$G_3' = \frac{P_a P_b}{1 + P_a\omega - P_a\omega\Delta G_3} \left(G_2 - G_1 G_3 + A\left(G_2 \frac{\eta}{2} G_3 \right) \right), \quad G_3(0) = p.$$

The above IVP will be numerically solved by the Runge-Kutta method of oder 4. The domain of the problem is considered to be bounded i.e. $[0, \eta_\infty]$, where η_∞ is a +ve real number, for which the variation in the solution is ignorable after $\eta = \eta_\infty$.

The missing condition p is to be chosen such that.

$$G_2(\eta_\infty, p) = 0.$$

Newton's method will be used to find p. This method has the following iterative scheme.

$$p_{n+1} = p_n - \frac{G_2(\eta_\infty, p_n)}{(\frac{\partial}{\partial p} G_2(\eta_\infty, p))_{p=p_n}}.$$

We further introduce the following notations:

$$\frac{\partial G_1}{\partial p} = G_4, \quad \frac{\partial G_2}{\partial p} = G_5, \quad \frac{\partial G_3}{\partial p} = G_6.$$

As a result of these new notations, the Newton's iterative scheme gets the form:

$$p_{n+1} = p_n - \frac{G_2(\eta_\infty, p_n)}{G_5(\eta_\infty, p_n)}.$$

Now differentiating the last system of three first order ODEs with respect to p, we get another system of ODEs, as follows.

$$G_4' = G_5, \qquad G_4(0) = 0.$$

$$G_5' = G_6, \qquad G_5(0) = \frac{\Lambda}{P_a}.$$

$$G_6' = \frac{P_a P_b}{1 + P_a\omega - P_a\omega\Delta G_3^2}\left(\frac{2P_a\omega G_3 G_6}{1 + P_a\omega - P_a\omega\Delta G_3^2}\Big(G_2^2 - G_1 G_3 + A\Big(G_2 + \frac{\eta}{2}G_3\Big)\Big)\right.$$
$$\left. + \Big(2G_3 G_5 - G_4 G_3 - G_1 G_6 + A\Big(G_5 + \frac{\eta}{2}G_6\Big)\Big)\right), \qquad G_6(0) = 1.$$

The stopping criteria for the Newton's technique is set as:

$$\mid G_2(\eta_\infty, p) \mid < \epsilon,$$

where $\epsilon > 0$ is a sufficiently small number, which has been considered as 10^{-10}.

The ordinary differential equation (3.29) will be approximated by using the shooting technique and assuming f as a known function.

$$\theta'' = \frac{1}{1+\frac{PrNr}{P_d}}\left(- Pr\frac{P_c}{P_d} \times \left(f\theta' - f'\theta - A\Big(\theta + \frac{\eta}{2}\theta'\Big) + \frac{E^c}{P_aP_c}f''^2\right)\right). \tag{3.41}$$

For this, we utilize the following notions:

$$\theta = H_1, \quad \theta' = H_1' = H_2.$$

The energy equation (3.28) is then transformed into the system of first-order ODEs shown below.

$$\begin{aligned} H_1' &= H_2, & H_1(0) &= q. \\ H_2' &= \frac{1}{1+\frac{PrNr}{P_d}}\left(- Pr\frac{P_c}{P_d} \times \left(G_1H_2 - G_2H_1 - A\Big(H_1 + \frac{\eta}{2}H_2\Big) + \frac{E^c}{P_aP_c}G_3^2\right)\right), \\ & & H_2(0) &= -Bi(1 - H_1(0)). \end{aligned}$$

The above IVP will be numerically solved by Runge-Kutta method of oder 4. The missing condition q is to be chosen such that.

$$H_1(\eta_\infty, q) = 0.$$

The above equation can be solved by using Newton's method with the following iterative formula.

$$q_{n+1} = q_n - \frac{H_1(\eta_\infty, q_n)}{(\frac{\partial}{\partial q}H_1(\eta_\infty, q))_{q=q_n}}.$$

We further introduce the following notations:

$$\frac{\partial H_1}{\partial q} = H_3, \quad \frac{\partial H_2}{\partial q} = H_4.$$

As a result of these new notations, the Newton's iterative scheme gets the form:

$$q_{n+1} = q_n - \frac{H_1(\eta_\infty, q_n)}{H_3(\eta_\infty, q_n)}.$$

Now differentiating the system of two first order ODEs with respect to q, we get another system of ODEs, as follows.

$$\begin{aligned} H_3' &= H_4, & H_3(0) &= 0. \\ H_4' &= \frac{1}{1+\frac{PrNr}{P_d}}\left(- Pr\frac{P_c}{P_d} \times \left(G_1H_4 - G_2H_1 - A\left(H_1 + \frac{\eta}{2}H_2\right) + \frac{E^c}{P_aP_c}G_3^2\right)\right), \\ & & H_4(0) &= -Bi. \end{aligned}$$

The stopping criteria for the Newton's method is set as:

$$\mid H_1(\eta_\infty, q) \mid < 10^{-10}.$$

3.4 Results and Discussion of Graphs and Tables

In this section, the effect of the dimensionless parameters of interest on the skin friction coefficient $Re_x^{\frac{1}{2}}C_f$, Nusselt number $Re_x^{-\frac{1}{2}}Nu_x$ and Entropy generation N_G has been thoroughly discussed through different graphs and tables. In Table 3.2, T_{f_1} and T_{f_2} are the intervals for the choice of missing condition p while computing the of skin friction coefficient for nanofluid and hybrid nanofluid respectively. It is observed that for the computation of Nusselt number, there is great flexibility in the choice of the missing initial condition. Tables 3.3 and 3.4 explain the effect of the material parameters ω and Δ, unsteady parameter A, nanoparticle volume fraction parameters ϕ_1 and ϕ_2, suction/injection parameter Λ, radiation parameter Nr, Eckert number Ec, Biot number Bi with fixed Prandtl number $Pr = 6.2$ and $m = 3$ on the fluid motion, temperature variation and the total volumetric entropy generation of Powell-Eyring nanofluid and hybrid nanofluid. For rising these values, the skin friction coefficient $Re_x^{\frac{1}{2}}C_f$, Nusselt number $Re_x^{-\frac{1}{2}}Nu_x$ increase. Figures 3.2-3.4 represents the value of ω (which describes the effect of

material fluid parameter) on Powell-Eyring nanofluids and hybrid nanofluids. For $\omega = 0.1, 0.3, 0.5$, computations are carried out with nanoparticles volume fraction of $\phi_1 = 0.09$ and $\phi_2 = 0.09$. For different values of ω, Figure 3.2 depicts variation in the velocity profile. For increasing value of ω, an ascending trend in the velocity profile is observed and this enhances the thickness of the momentum boundary layer. As ω is inversely proportional to the base fluid viscosity, an increase in the positive values of ω, enhances the stress rate within the boundary layer and decreases the base fluid viscosity. Consequently, within the boundary layer, the velocity of conventional and hybrid nanofluids, is increased.

In the Table 3.3, the effect of ω on the viscosity of the base fluid can also be seen through difference in values of the skin friction. The skin friction factor at the boundary undertakes a move up trend. Furthermore, for alloted value of $\omega = 0.1$, the thickness of momentum boundary layer for hybrid nanofluid is increased whenever it is collated with the classical nanofluid. A reducing trend is noticed in the temperature profile with an enlargement in the value of the parameter ω as depicted in Figure 3.3. This illustrates a depletion in thickness of the thermal boundary layer and an improvement in the rate of heat transfer inside the boundary layer. In comparison, the thickness of the conventional nanofluid is higher than that for the hybrid nanofluid. Hence, the rate of heat transport at the boundary of $Al_2O_3 - Cu/H_2O$ hybrid nanofluid is higher. For both conventional and hybrid nanofluids increasing trend in Nusselt number is also observed in from Table 3.4.

Figure 3.4 illustrates the influence of the material parameter ω on the volumetric entropy generation of the conventional and hybrid nanofluids. It describes the an increase in the values of the material parameter lessens the entropy of system near the surface but an opposite impact can be seen away from the plate. It shows that the irreversibility of $Cu - H_2O$ nanofluid is less than the $Al_2O_3 - Cu/H_2O$ hybrid nanofluid.

Figures 3.5-3.7 depict the behavior of the fluid motion, temperature distribution and entropy generation due to variation in the non-Newtonian fluid parameter Δ. For the increasing values of Δ, Figures 3.5 and 3.7 show a decreasing trend in the

velocity profile $f'(\eta)$ and entropy generation N_G whereas Figure 3.6 depicts that the temperature profile $\theta(\eta)$ is increased.

Figure 3.8 shows the impact of A. For the increasing values of A, the velocity profile $f'(\eta)$ is decreased. Figures 3.9-3.11 focus on the impact of ϕ. The graphs are produced for velocity, temperature and entropy generation profiles. Computations are carried out for fixed value of $\phi_1 = 0.09$, and analysis is carried for variation in the parameter ϕ_2. For the increasing values of ϕ, Figure 3.9 depicts that initially the velocity profile $f'(\eta)$ decreases due to a rise the value of ϕ. As η increases, the velocity profile increases and asymptotically approach to zero. Figure 3.10 depicts that the temperature profile $\theta(\eta)$ rises due to higher thermal conductivity of solid particles which raises the overall thermal conductivity of the nanofluid. For different value of ϕ, Figure 3.11 depicts the entropy generation N_G increase.

Figures 3.12-3.14 depict a decreasing trend in the fluid motion movement, volumetric entropy generation, and temperature for positive increase in the slip parameter Λ. For the increasing values of Λ, the velocity profile $f'(\eta)$ and temperature profile $\theta(\eta)$ and entropy generation N_G decrease. Figures 3.15-3.16 show the impact of Nr. For the increasing values of Nr, the temperature profile $\theta(\eta)$ and the entropy generation N_G increase. Figures 3.17-3.18 show the impact of Ec. For the increasing values of Ec, the temperature profile $\theta(\eta)$ and the entropy generation N_G increase. Figures 3.19-3.20 show the impact of Bi. For the increasing values of Bi, the temperature profile $\theta(\eta)$ and the entropy generation N_G increase. The shape factor of nanoparticles is an important factor to consider while analysing the system's thermal performance. The shapes of the nanoparticles in the current work include spherical, hexahedron, tetrahedron, column, and lamina. Figures 3.21-3.22 show the impact of m. For the increasing values of m, the temperature profile $\theta(\eta)$ and the entropy generation N_G increase. The effect of Reynolds number Re and Brinkmann number Br on the total volumetric entropy generation rate is depicted in Figures 3.23 and 3.24. In Figure 3.23, it can be observed that the increasing values of Re, the entropy generation N_G increases. In Figure 3.24, it can be observed that the increasing values of Br, the entropy generation

N_G increases.

TABLE 3.2: Missing conditions of $Re_x^{\frac{1}{2}} C_f$ for $Pr = 6.2$, $m = 3$.

ω	Δ	A	ϕ_1	ϕ_2	Λ	T_{f_1}	T_{f_2}
0.1	0.2	0.2	0.03	0	0	[-1.21, -0.80]	- - - -
0.3						[-1.10, -0.78]	[-1.14, -0.75]
0.5						[-1.00, -0.78]	[-1.00, -0.71]
	2.0					[-1.30, -1.00]	[-1.29, -1.10]
	4.0					[-1.50, -1.20]	[-1.46, -1.00]
		0.3				[-1.20, -0.90]	[-1.20, -1.00]
		0.4				[-1.20, -1.00]	[-1.20, -1.10]
			0.06			[-1.20, -0.91]	[-1.26, -0.88]
			0.09			[-1.32, -0.97]	[-1.30, -0.92]
				0.03		- - - -	[-1.21, -0.80]
				0.06		- - - -	[-1.20, -0.79]
				0.09		- - - -	[-1.10, -0.78]
					0.1	[-1.00, -0.72]	[-0.90, -0.70]
					0.3	[-0.81, -0.56]	[-0.79, -0.55]

TABLE 3.3: Results of $Re_x^{\frac{1}{2}} C_f$ for $Pr = 6.2$, $m = 3$.

ω	Δ	A	ϕ_1	ϕ_2	Λ	$Re_x^{\frac{1}{2}} C_f$ *(Cu-H_2O)*	$Re_x^{\frac{1}{2}} C_f$ *(Al_2O_3-Cu/H_2O)*
0.1	0.2	0.2	0.03	0	0	1.3504	- - - -
0.3						1.4521	1.5457
0.5						1.5479	1.6641
	2.0					1.3237	1.4180
	4.0					1.2848	1.3811
		0.3				1.3900	1.4865
		0.4				1.4290	1.5283
			0.06			1.5326	1.6268
			0.09			1.7180	1.8137
				0.03		- - - -	1.4442
				0.06		- - - -	1.5433
				0.09		- - - -	1.6484
					0.1	1.1531	1.2200
					0.3	0.9037	0.9439

TABLE 3.4: Results of $Re_x^{-\frac{1}{2}}Nu_x$ for $Pr = 6.2$, $m = 3$.

ω	Δ	A	ϕ_1	ϕ_2	Λ	Nr	Ec	Bi	$Re_x^{-\frac{1}{2}}Nu_x$ $(Cu\text{-}H_2O)$	$Re_x^{-\frac{1}{2}}Nu_x$ $(Al_2O_3\text{-}Cu/H_2O)$
0.1	0.2	0.2	0.03	0	0	0.2	0.2	0.2	0.2145	- - - -
0.3									0.2174	0.2341
0.5									0.2197	0.2366
	2								0.2132	0.2296
	4								0.2111	0.2324
		0.3							0.2152	0.2317
		0.4							0.2157	0.2324
			0.06						0.2286	0.2460
			0.09						0.2431	0.2615
				0.03					- - - -	0.2309
				0.06					- - - -	0.2480
				0.09					- - - -	0.2658
					0.1				0.2184	0.2358
					0.3				0.2225	0.2408
						0.5			0.2615	0.2818
						0.8			0.3065	0.3305
							0.4		0.1905	0.2030
							0.6		0.1665	0.1750
								0.1	0.1123	0.1210
								0.3	0.3079	0.3311

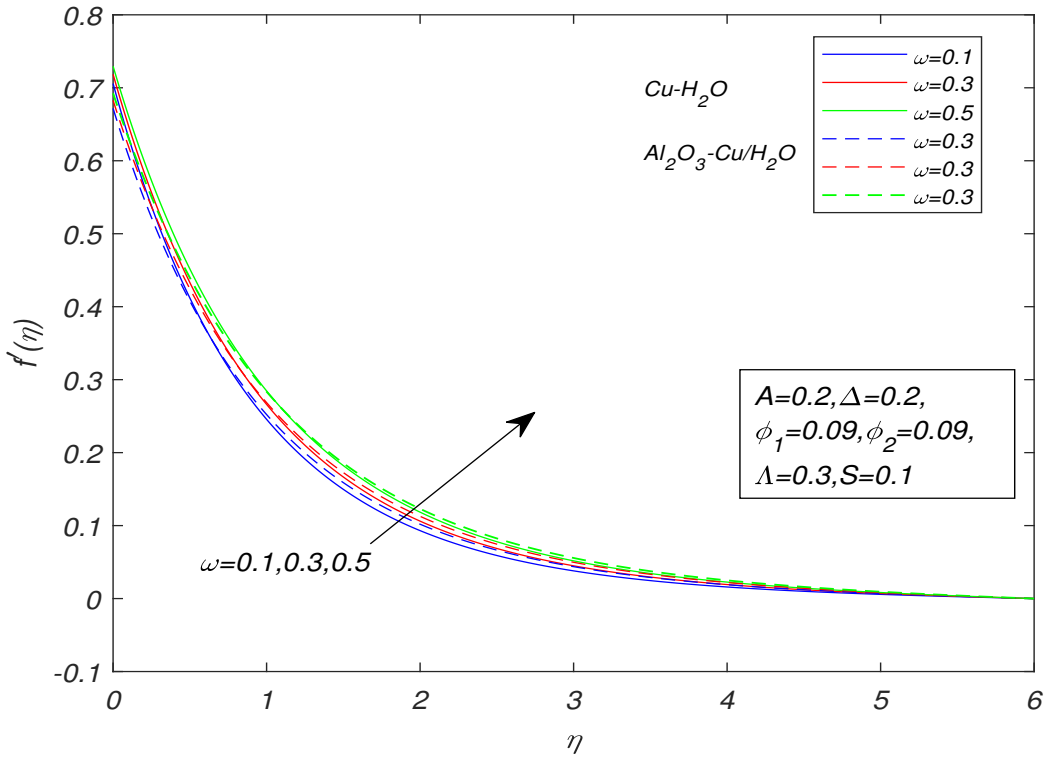

FIGURE 3.2: Velocity profile against ω on $f'(\eta)$ for $Pr = 6.2$.

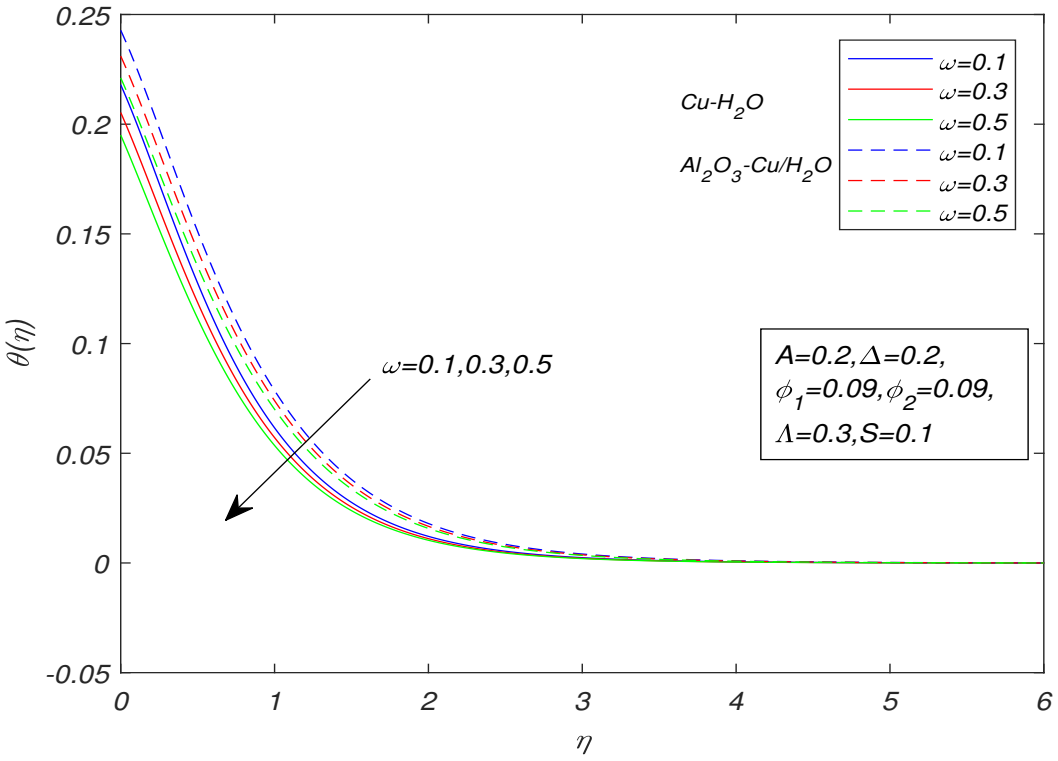

FIGURE 3.3: Temperature profile against ω on $f'(\eta)$ for $Pr = 6.2$.

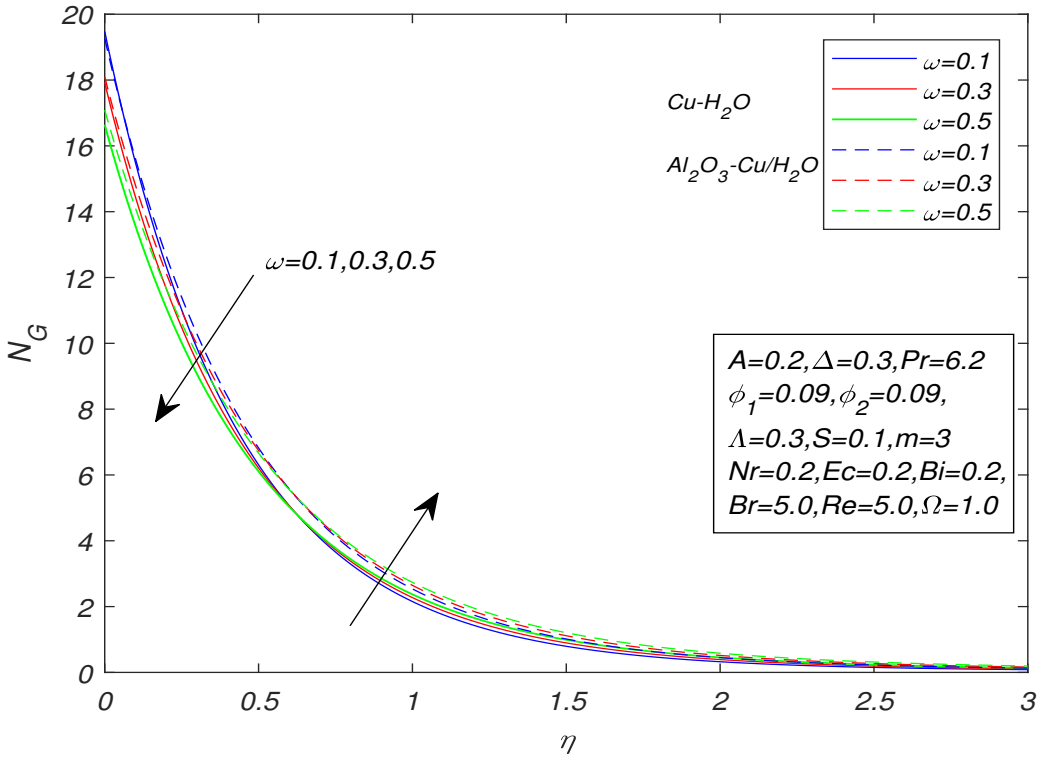

FIGURE 3.4: Entropy profile against ω on N_G for $Pr = 6.2$.

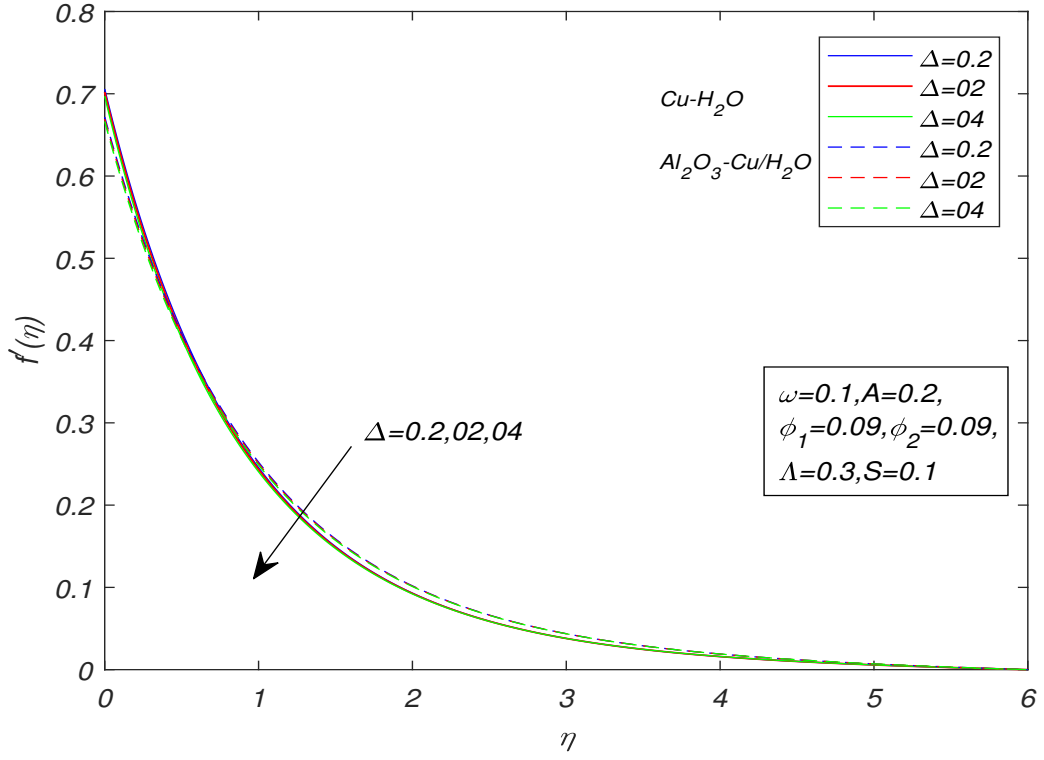

FIGURE 3.5: Velocity profile against Δ on $f'(\eta)$ for $Pr = 6.2$.

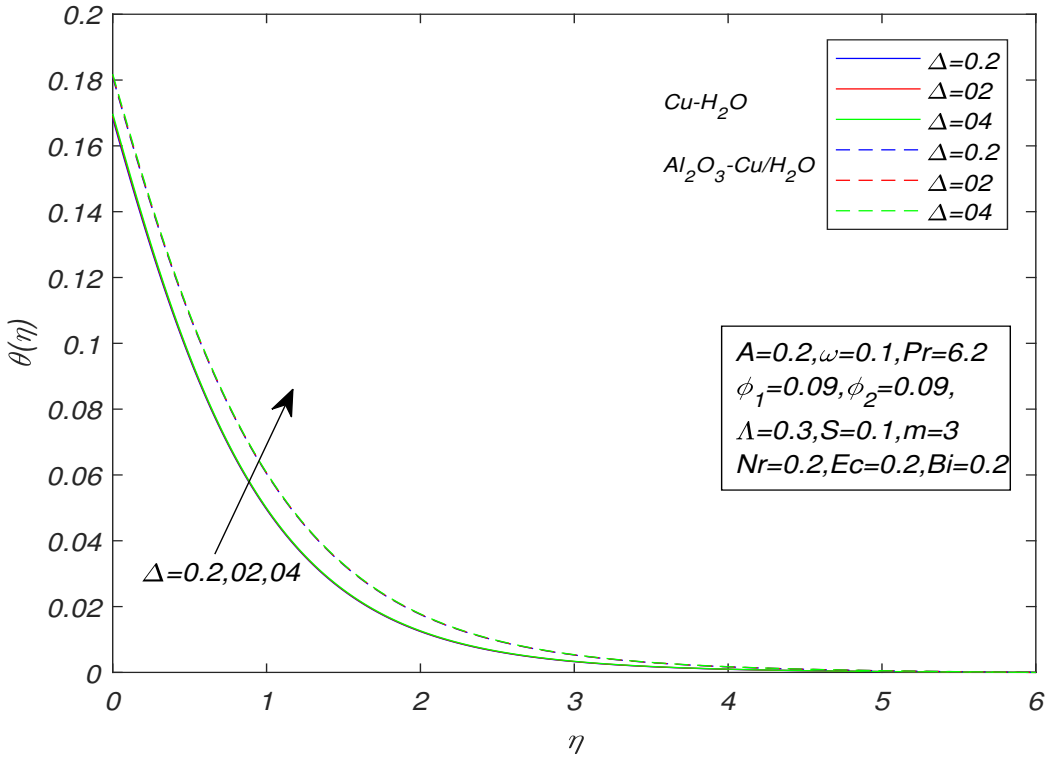

FIGURE 3.6: Temperature profile against Δ on $\theta(\eta)$ for $Pr = 6.2$.

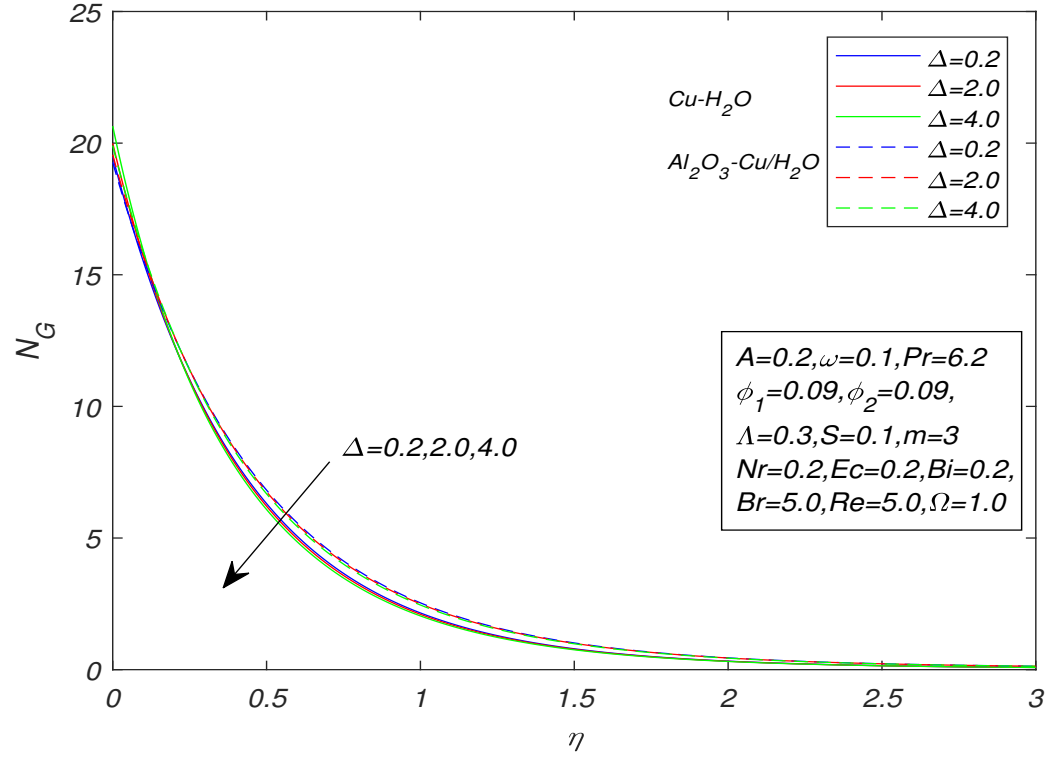

FIGURE 3.7: Entropy profile against Δ on N_G for $Pr = 6.2$.

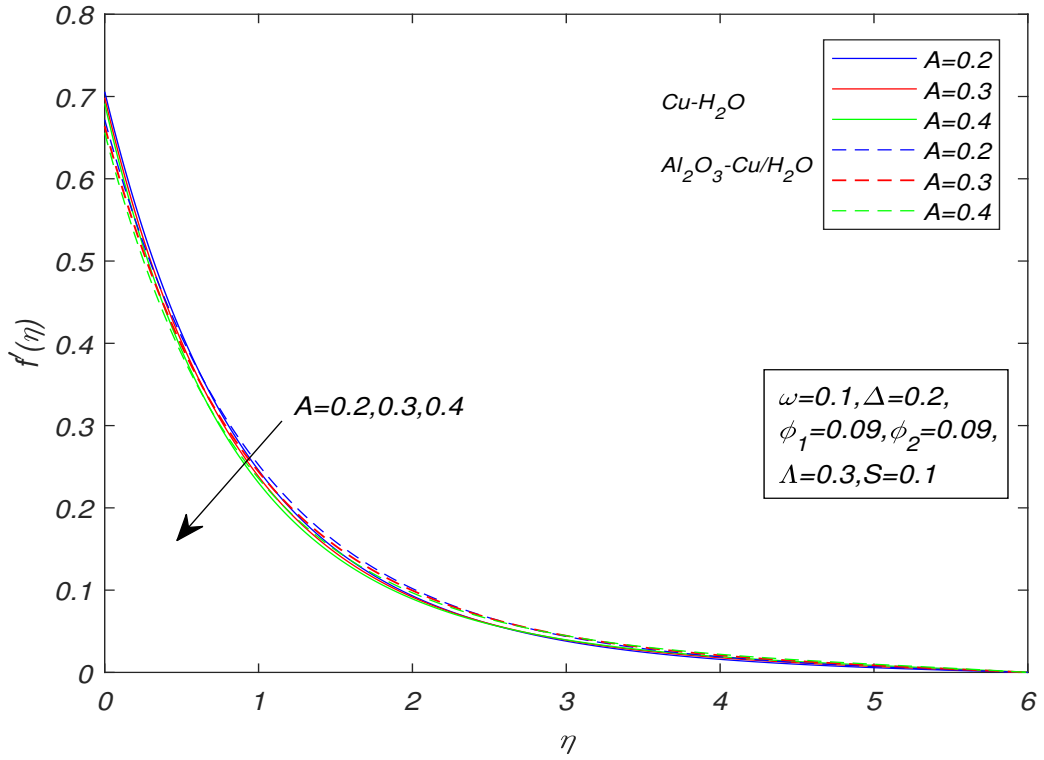

FIGURE 3.8: Velocity profile against A on $f'(\eta)$ for $Pr = 6.2$.

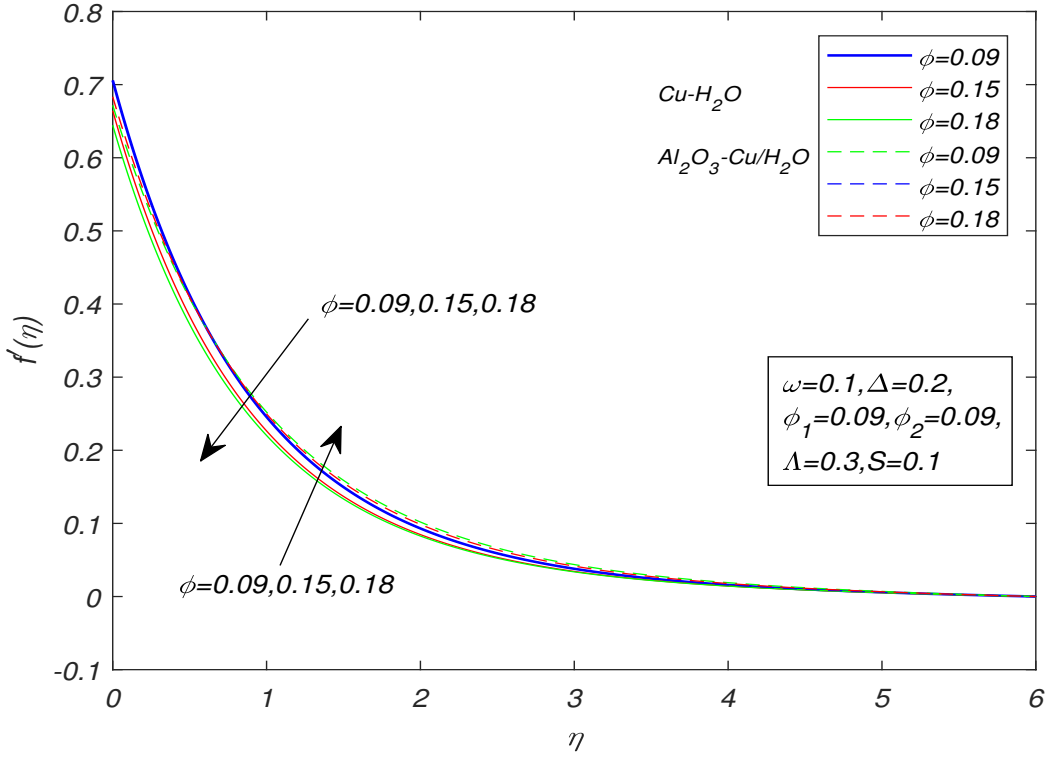

FIGURE 3.9: Velocity profile against ϕ on $f'(\eta)$ for $Pr = 6.2$.

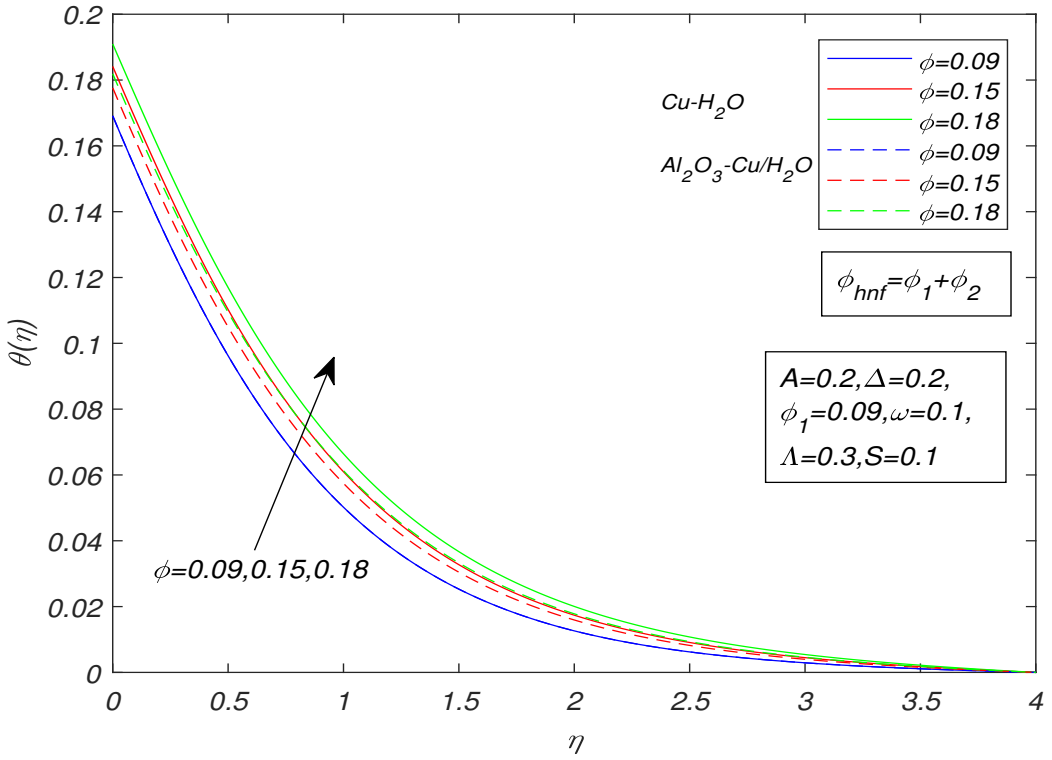

FIGURE 3.10: Temperature profile against ϕ on $\theta(\eta)$ for $Pr = 6.2$.

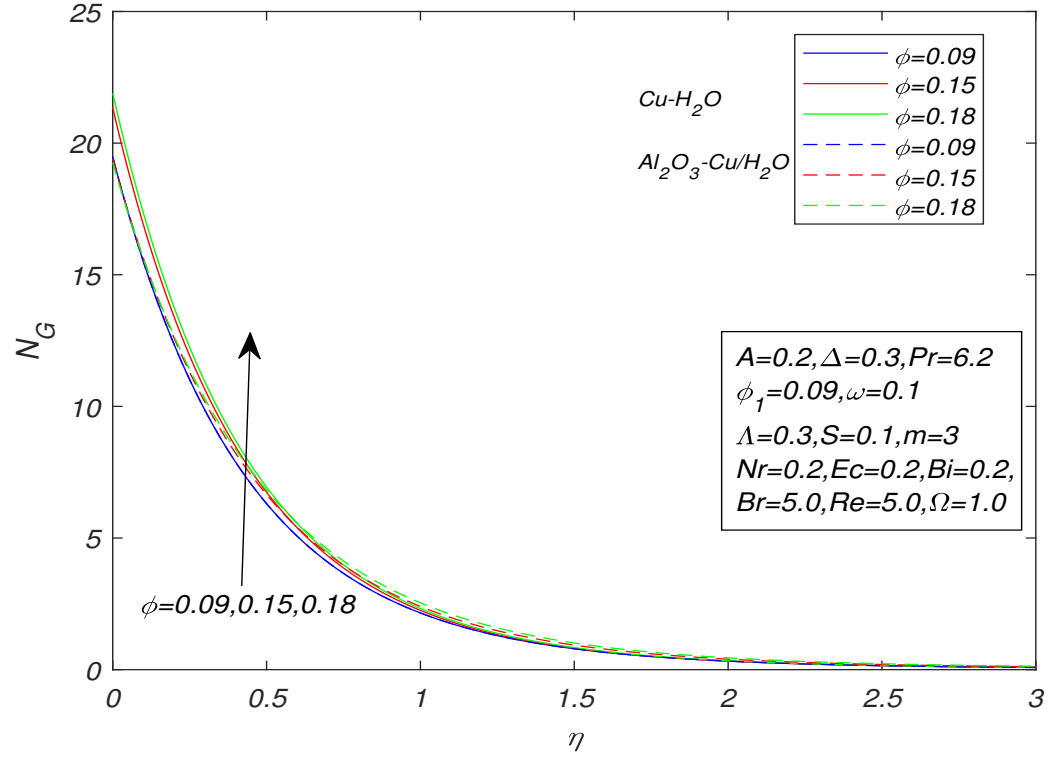

FIGURE 3.11: Entropy profile against ϕ on N_G for $Pr = 6.2$.

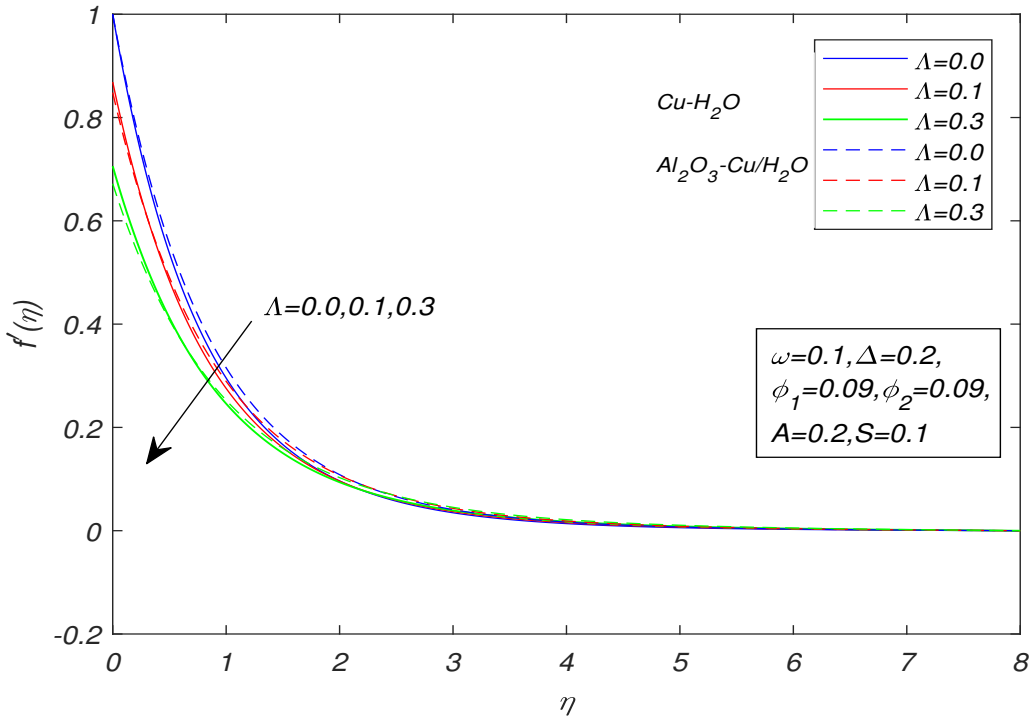

FIGURE 3.12: Velocity profile against Λ on $f'(\eta)$ for $Pr = 6.2$.

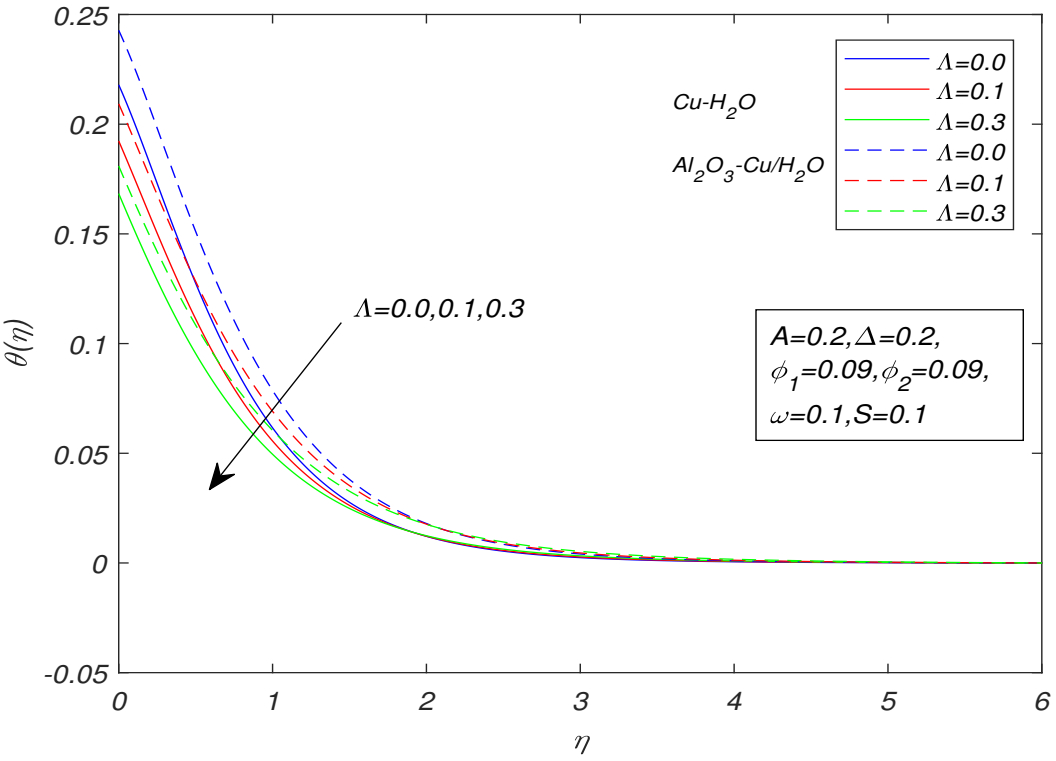

FIGURE 3.13: Temperature profile against Λ on $\theta(\eta)$ for $Pr = 6.2$.

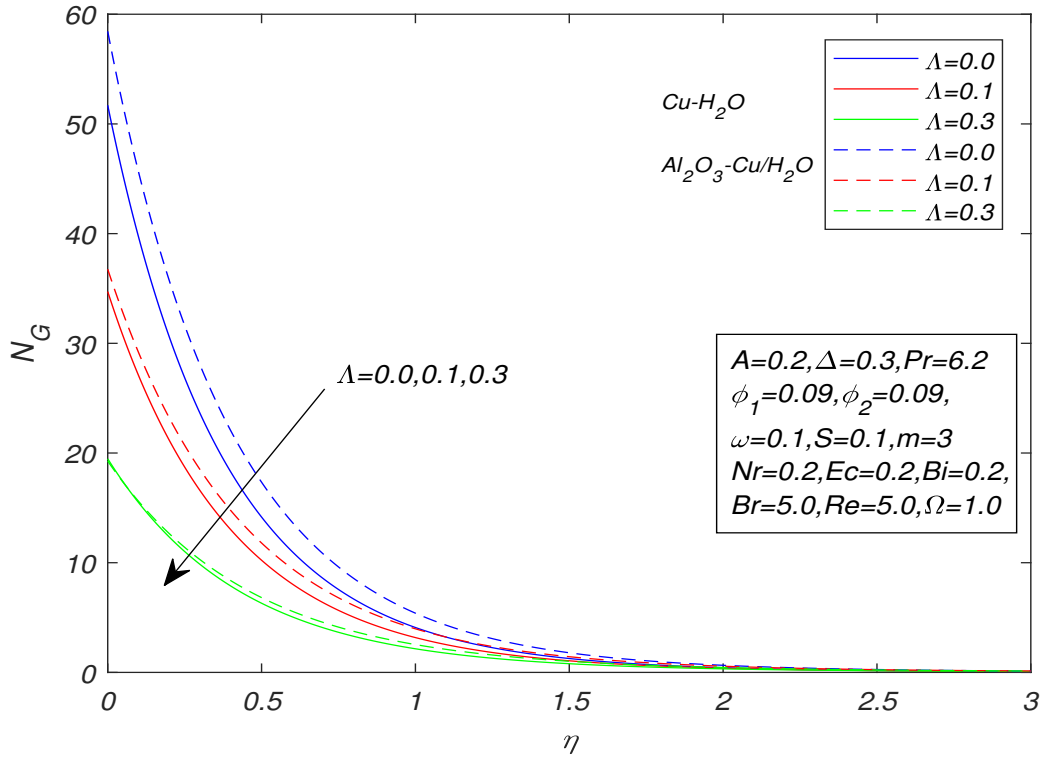

FIGURE 3.14: Entropy profile against Λ on N_G for $Pr = 6.2$.

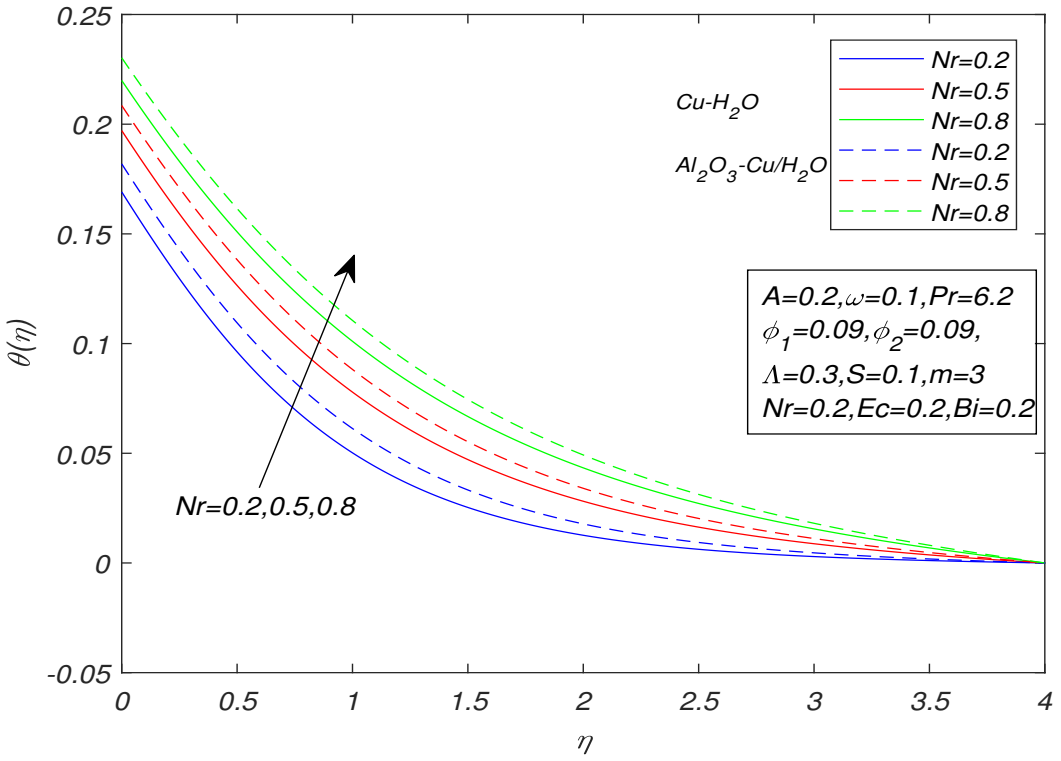

FIGURE 3.15: Temperature profile against Nr on $\theta(\eta)$ for $Pr = 6.2$.

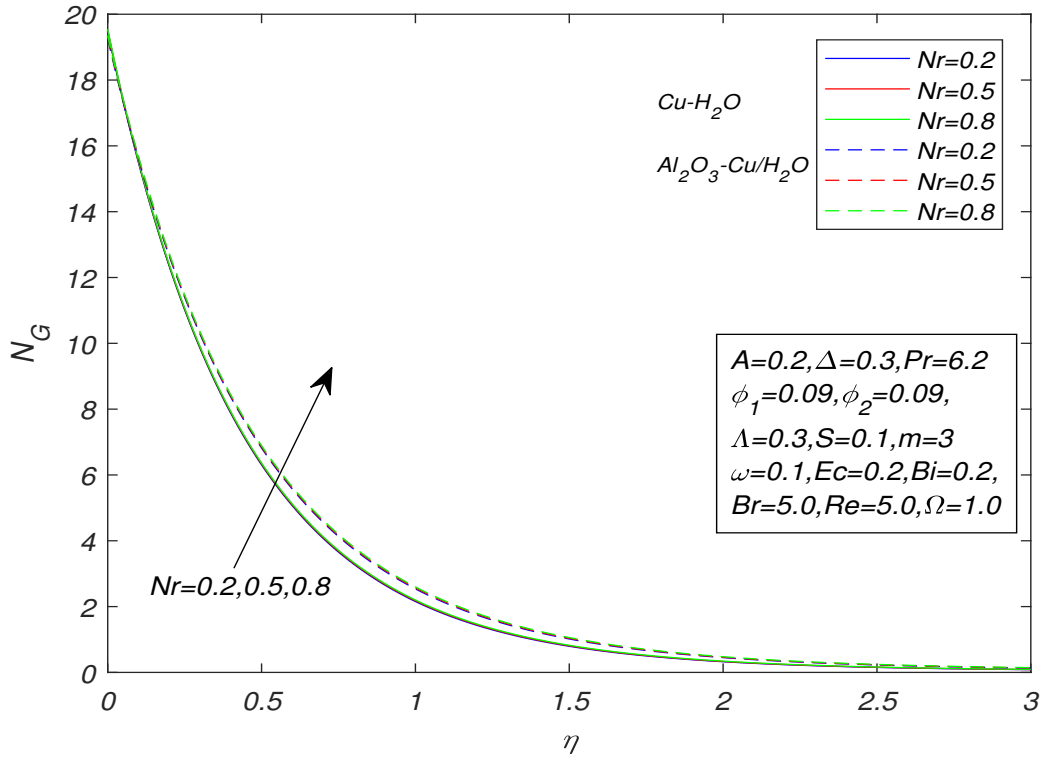

FIGURE 3.16: Entropy profile against Nr on N_G for $Pr = 6.2$.

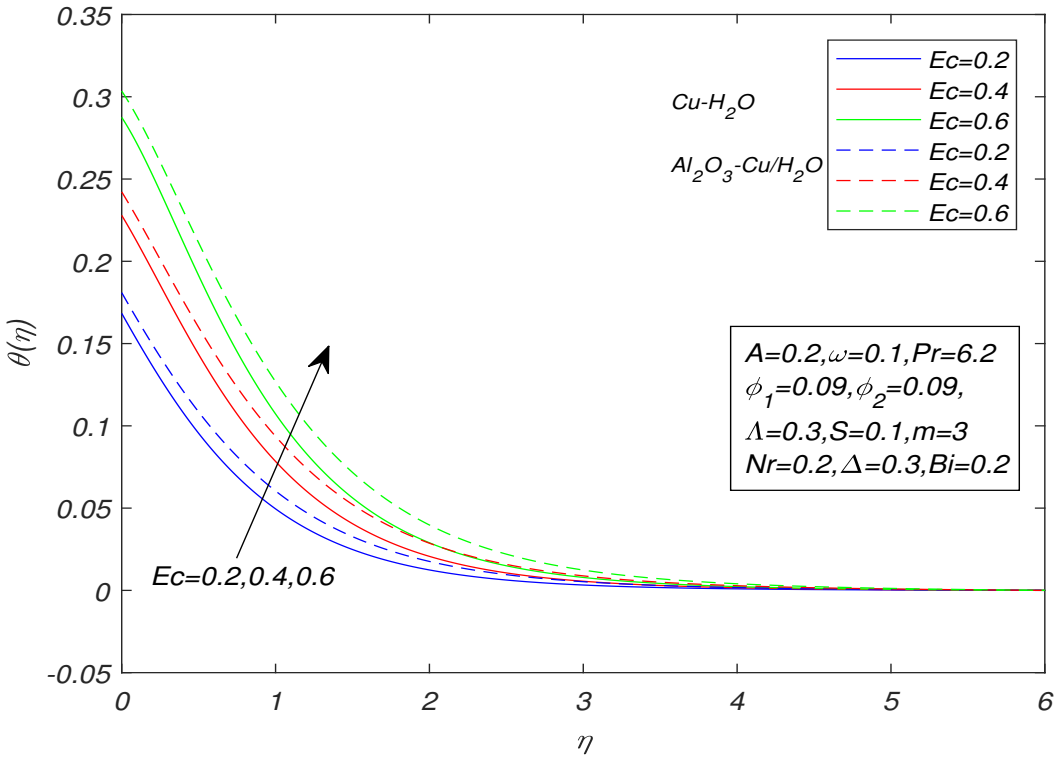

FIGURE 3.17: Temperature profile against Ec on $\theta(\eta)$ for $Pr = 6.2$.

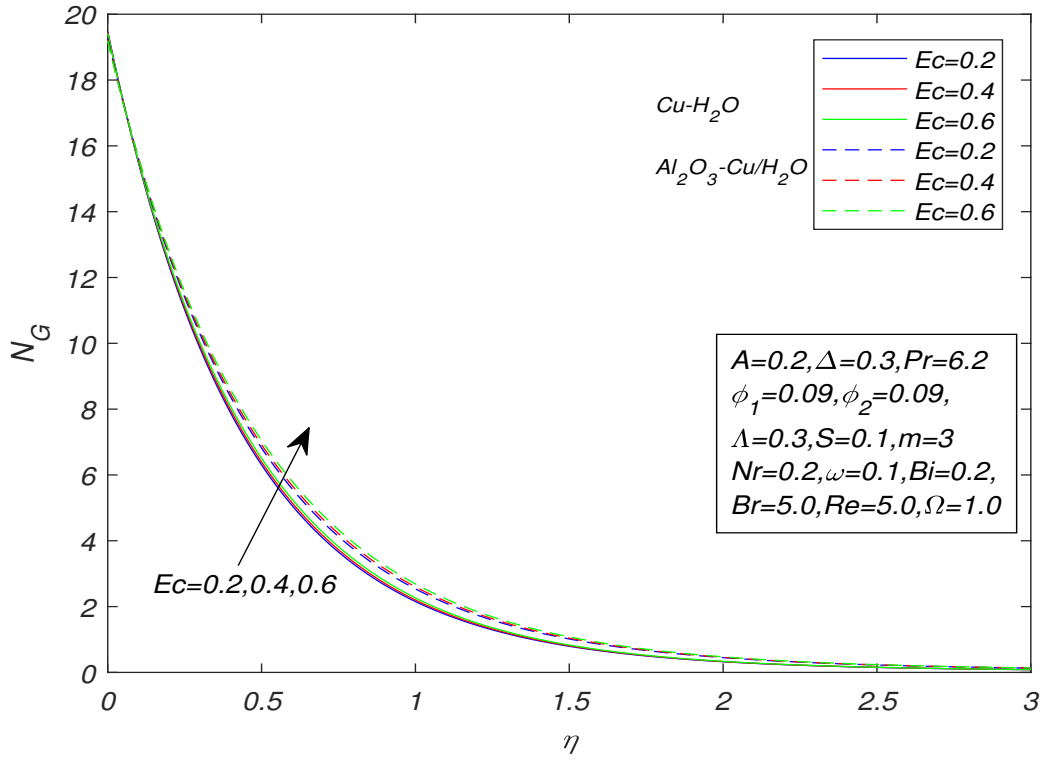

FIGURE 3.18: Entropy profile against Ec on N_G for $Pr = 6.2$.

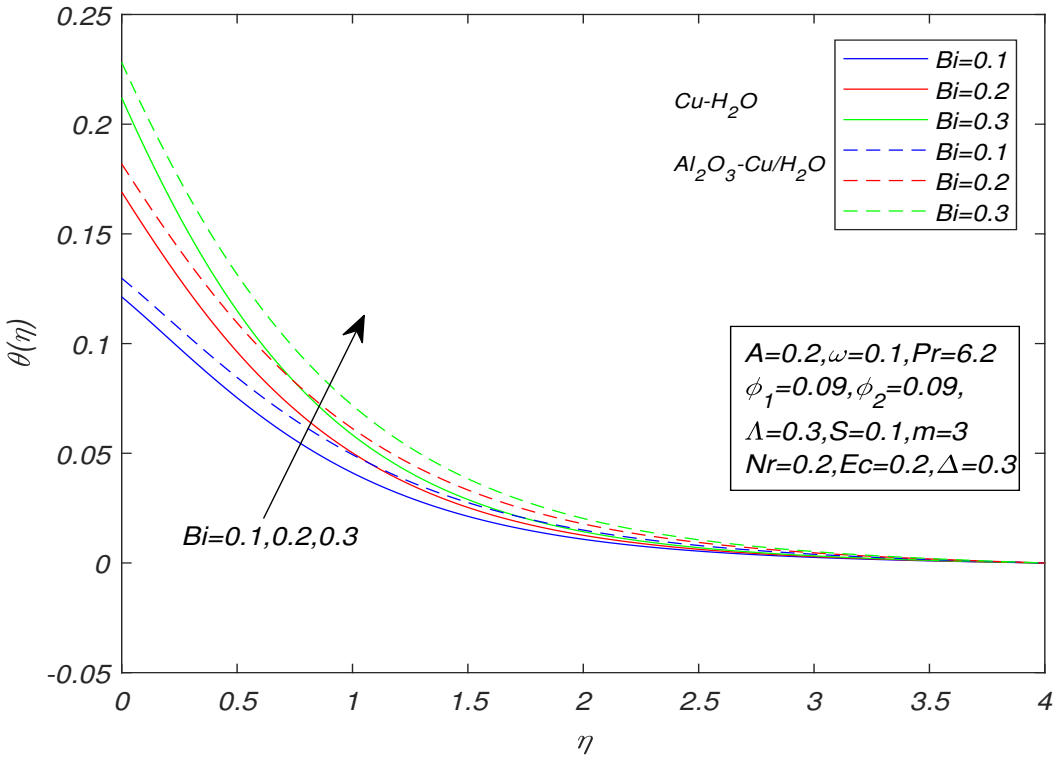

FIGURE 3.19: Temperature profile against Bi on $\theta(\eta)$ for $Pr = 6.2$.

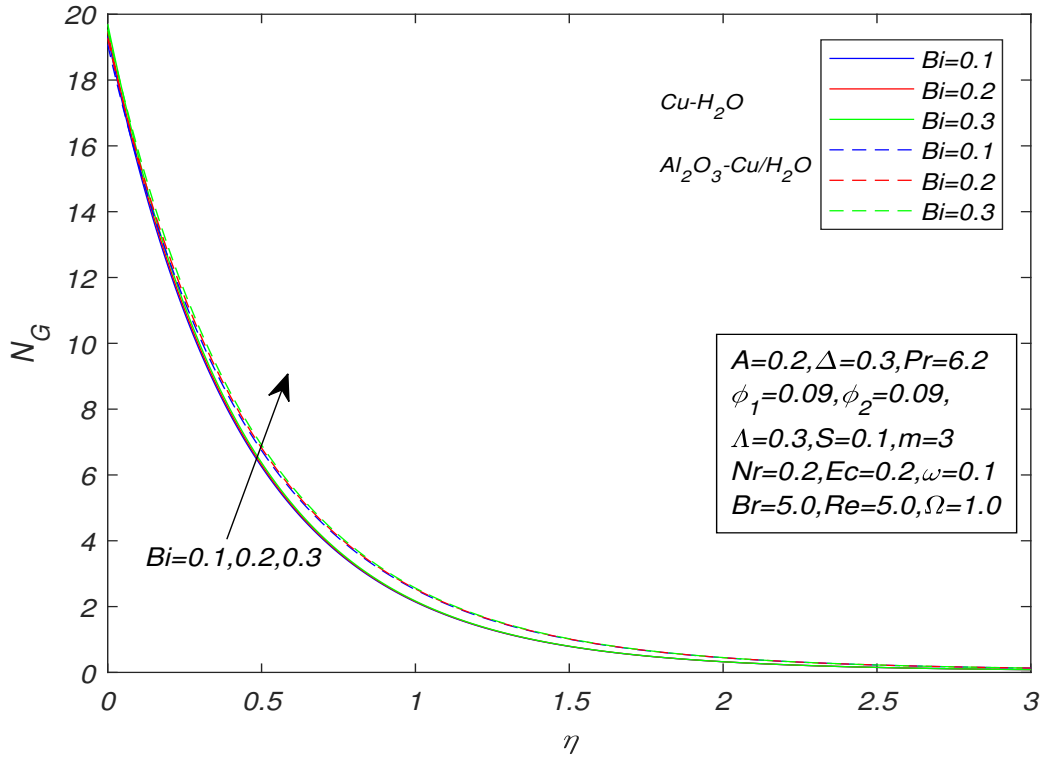

FIGURE 3.20: Entropy profile against Bi on N_G for $Pr = 6.2$.

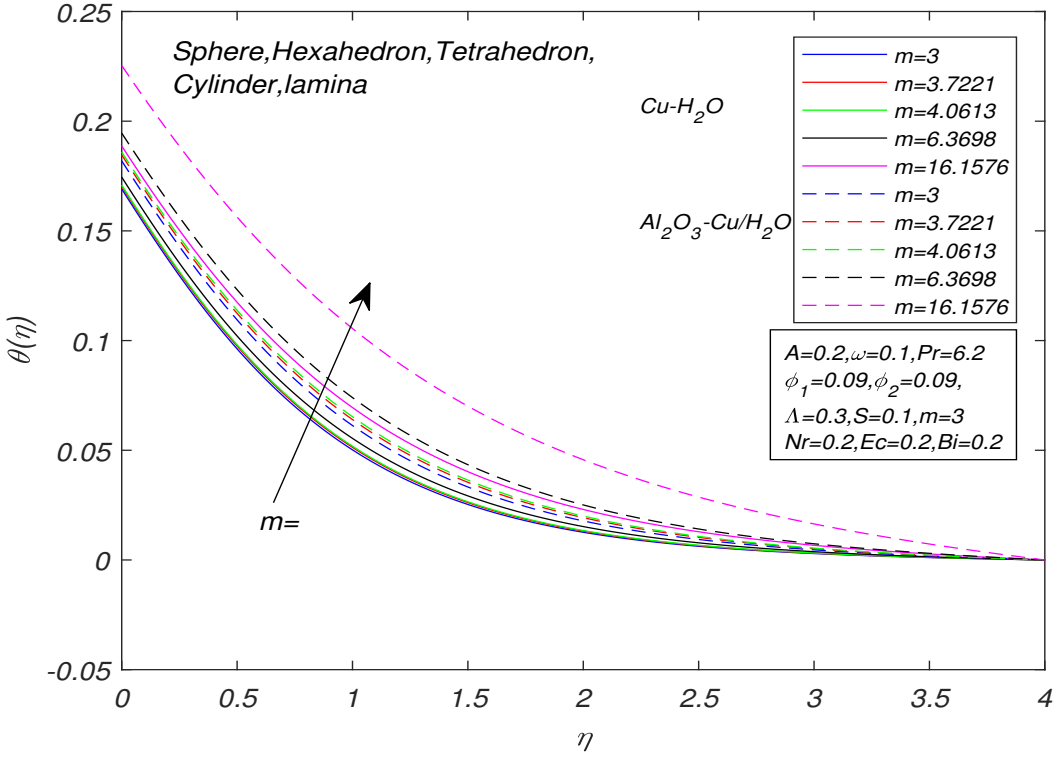

FIGURE 3.21: Temperature profile against m on $\theta(\eta)$ for $Pr = 6.2$.

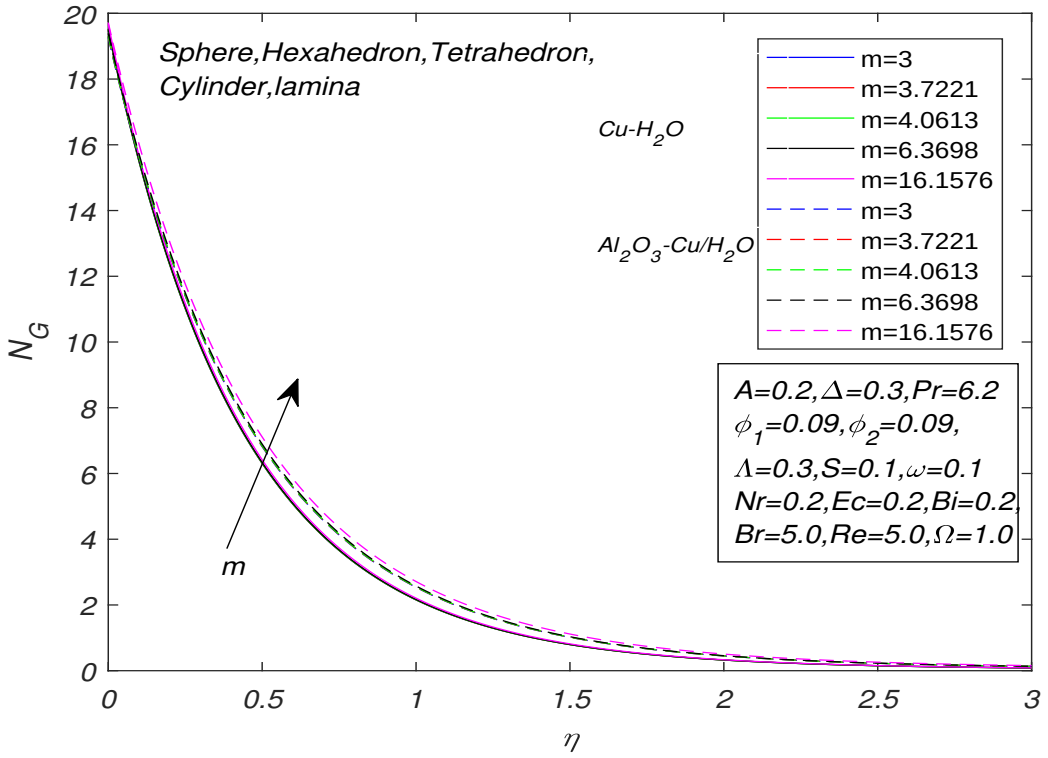

FIGURE 3.22: Entropyprofile against m on N_G for $Pr = 6.2$.

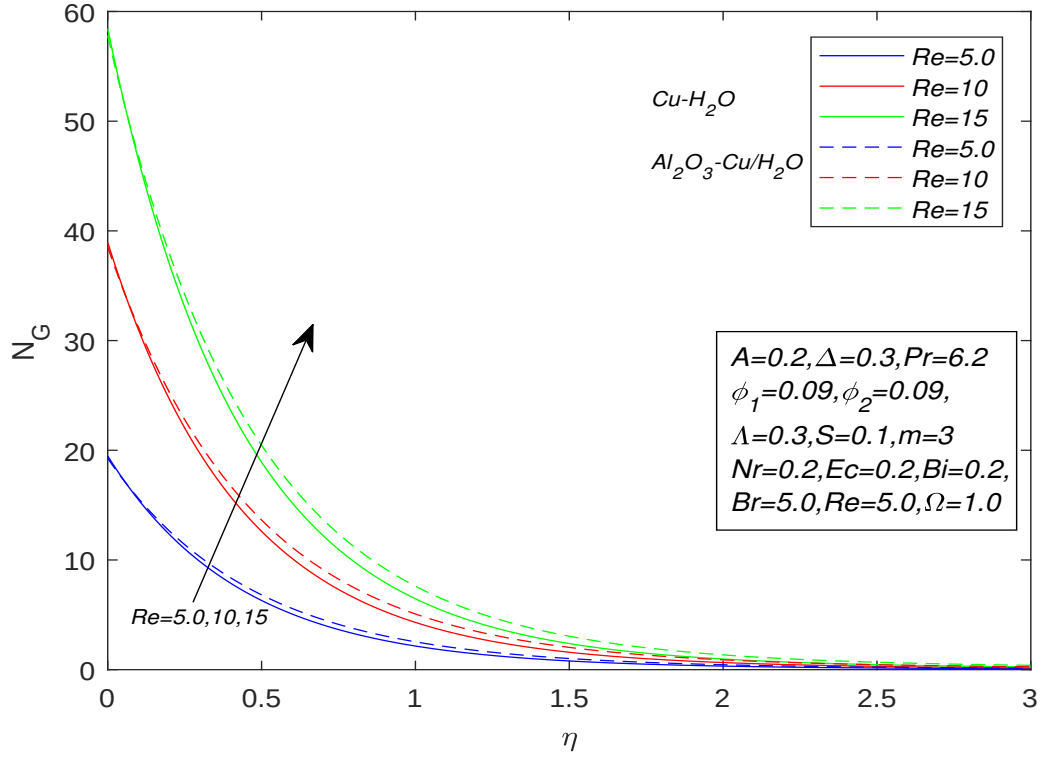

FIGURE 3.23: Entropy profile against Re on N_G for $Pr = 6.2$.

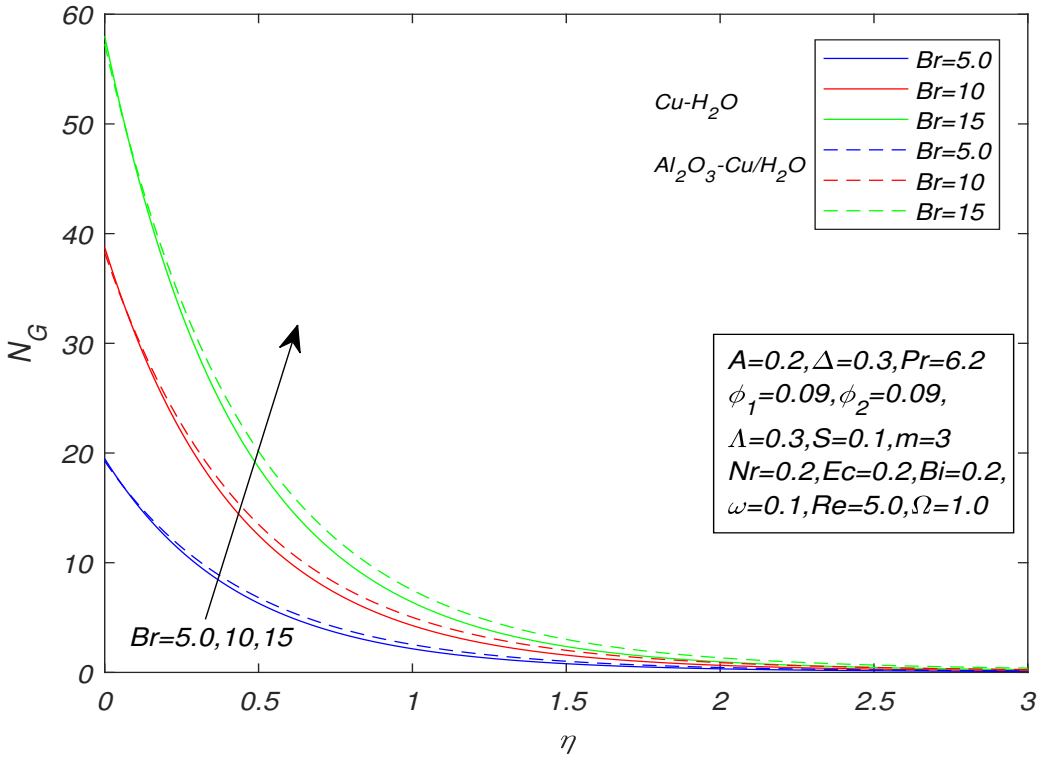

FIGURE 3.24: Entropy profile against Br on N_G for $Pr = 6.2$.

Chapter 4

Cattaneo-Christov based Study of Powell-Eyring Hybrid Nanofluid Including Effect of Magnetic field and Viscous Dissipation

4.1 Introduction

The model analyzed in Chapter 3 has been is expanded in this chapter by taking aligned magnetic field into account in the momentum equation. The temperature equation additionally accounts for the Cattaneo-Christov heat flow. Along with the chemical reaction, the concentration equation is also taken into consideration. In this chapter, we will perform numerical analysis of the flow, heat transfer and total volumetric entropy of the Powell-Eyring hybrid nanofluid. The governing nonlinear partial differential equations are transformed into a system of dimensionless ODEs by utilizing the similarity transformations. The numerical solution of ODEs is obtaind by using numerical method known as shooting technique.

4.2 Mathematical Modeling

Consider an unstable, laminar, two dimensional, boundary layer flow of inviscid optically thick hybrid nanofluid above an infinite penetrable plate. The non-Newtonian Cattaneo-Christov heat flux over Powell-Eyring mathematical model is assumed for hybrid nanofluids. Cartesian dimensional coordinates are assumed with x-axis to have porous surface along it and the y-axis normal to this. In current study, nanofluids are prepared by adding copper (Cu) nanoparticles in pure water with the volume fraction ϕ also alumina (Al_2O_3) and copper (Cu) nanoparticles with volume fractions ϕ_1 and ϕ_2 are dispersed in the pure water to manufacture hybrid nanofluid. The nanoparticle volume concentration of hybrid nanofluid is defined as $\phi_{hnf} = \phi_1 + \phi_2$. The constitutive equations of Powell-Eyring fluid model are derived from the theory of liquids and not from the empirical relationship as in the power-law model. The Powell-Eyring fluid model reduces Newtonian flux at low and high shear rates. The Cauchy stress tensor for Powell-Eyring fluid is given:

$$\tau_{ij} = \mu_{hnf}\left(\frac{\partial u_i}{\partial x_j}\right) + \frac{1}{\tilde{\beta}} Sinh^{-1}\left(\frac{1}{\zeta^*}\frac{\partial u_i}{\partial x_j}\right), \tag{4.1}$$

where μ_{hnf} is the hybrid dynamic viscosity and β, ζ^* are material constants of Powell-Eyring hybrid nanofluid.

A uinform magnetic field of strength is

$$B(t) = \frac{B_0}{\sqrt{1-\varpi t}} \tag{4.2}$$

applied in the transverse direction to the flow and the induced magnetic field is considered negligible. The stretching speed and porous surface temperature are

$$U_w(x,t) = \frac{cx}{1-\varpi t}, \qquad T_w(x,t) = T_\infty + \frac{cx}{1-\varpi t}. \tag{4.3}$$

Here t is the time, c is a +ve constant and T_∞ the ambient temperature.

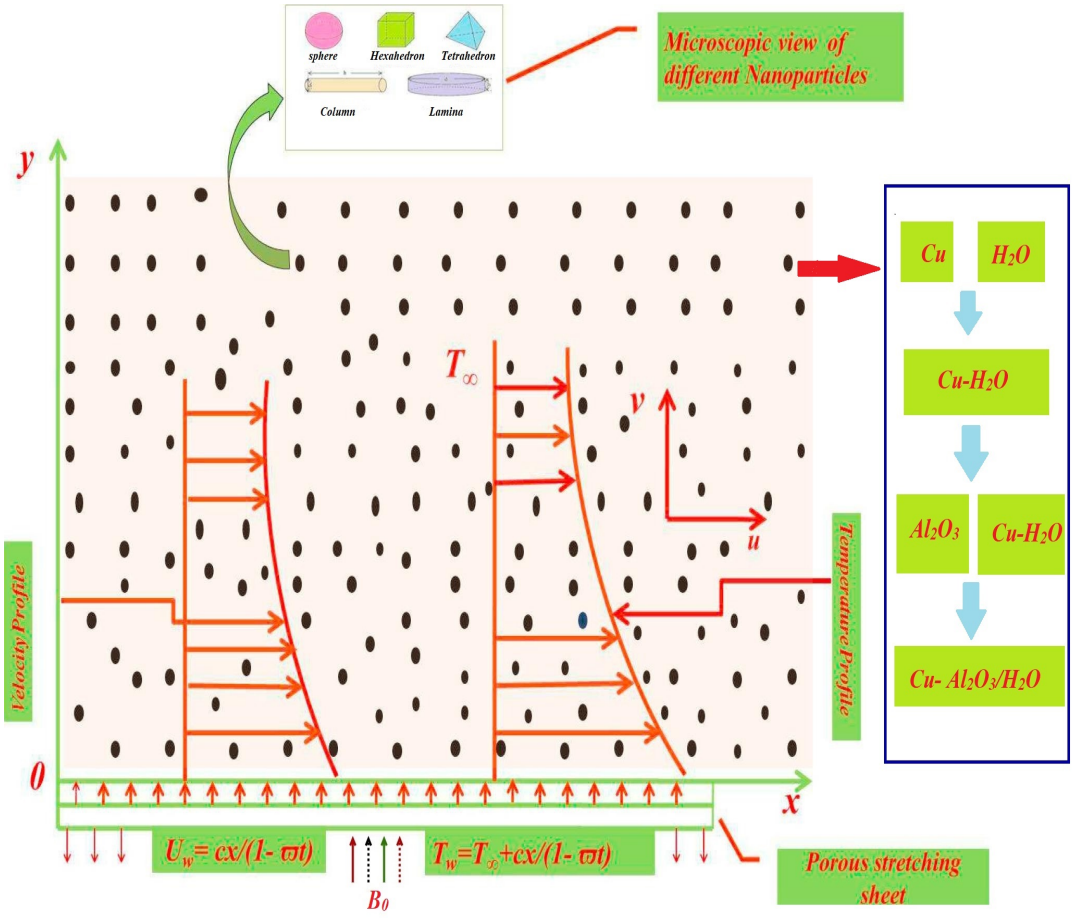

FIGURE 4.1: systematic representation of physical model.

The governing equations of the flow model can be expressed as:

$$\frac{\partial u}{\partial x}+\frac{\partial v}{\partial y}=0, \tag{4.4}$$

$$\frac{\partial u}{\partial t}+u\frac{\partial u}{\partial x}+v\frac{\partial u}{\partial y}=\left(\nu_{hnf}+\frac{1}{\rho_{hnf}\tilde{\beta}\zeta^*}\right)\frac{\partial^2 u}{\partial y^2}-\frac{1}{2\tilde{\beta}\zeta^{*3}\rho_{hnf}}\left(\frac{\partial u}{\partial y}\right)^2\frac{\partial^2 u}{\partial y^2} - \frac{\sigma_{hnf}B^2(t)u}{\rho_{hnf}}, \tag{4.5}$$

$$\frac{\partial T}{\partial t}+u\frac{\partial T}{\partial x}+v\frac{\partial T}{\partial y}=\frac{\kappa_{hnf}}{(\rho C_p)_{hnf}}\left(\frac{\partial^2 T}{\partial y^2}\right)-\frac{1}{(\rho C_p)_{hnf}}\left(\frac{\partial q_r}{\partial y}\right)+\frac{\nu_{hnf}}{(\rho C_p)_{hnf}}\left(\frac{\partial u}{\partial y}\right)^2 - \lambda\left(u\frac{\partial u}{\partial x}\frac{\partial T}{\partial x}+v\frac{\partial v}{\partial y}\frac{\partial T}{\partial y}+u\frac{\partial v}{\partial x}\frac{\partial T}{\partial y}+v\frac{\partial u}{\partial y}\frac{\partial T}{\partial x} + u^2\frac{\partial^2 T}{\partial x^2}+v^2\frac{\partial^2 T}{\partial y^2}+2uv\frac{\partial^2 T}{\partial x\partial y}\right), \tag{4.6}$$

$$u\frac{\partial C}{\partial x}+v\frac{\partial C}{\partial y}=D_{hnf}\frac{\partial^2 C}{\partial y^2}-k_1(C-C_\infty). \tag{4.7}$$

The associated BCs have been taken as.

$$\left.\begin{aligned} &u(x,0) = U_w + \nu_{hnf}\left[\frac{\partial u}{\partial y}\right], \quad v(x,0) = V_w, \\ &-\kappa_f\left[\frac{\partial T}{\partial y}\right] = h_f(T_w - T), \quad C = C_w \quad at \quad y = 0, \\ &u \to 0, \quad C \to C_\infty, \quad T \to T_\infty, \quad as \quad y \to \infty. \end{aligned}\right\} \tag{4.8}$$

For convenience, the following notations have been introduced:

$$P_a = (1-\phi_1)^{2.5}(1-\phi_2)^{2.5}, \tag{4.9}$$

$$P_b = (1-\phi_2)\left((1-\phi_1) + \phi_1\frac{\rho_{p_1}}{\rho_f}\right) + \phi_2\frac{\rho_{p_2}}{\rho_f}, \tag{4.10}$$

$$P_c = (1-\phi_2)\left((1-\phi_1) + \phi_1\frac{(\rho C_p)_{p_1}}{(\rho C_p)_f}\right) + \phi_2\frac{(\rho C_p)_{p_2}}{(\rho C_p)_f}, \tag{4.11}$$

$$P_d = \left[\frac{\kappa_{p_2} + 2\kappa_{nf} - 2\phi_2(\kappa_{nf} - \kappa_{p_2})}{\kappa_{p_2} + 2\kappa_{nf} + \phi_2(\kappa_{nf} - \kappa_{p_2})}\right] \times \left[\frac{\kappa_{p_1} + 2\kappa_f - 2\phi_1(\kappa_{1f} - \kappa_{p_1})}{\kappa_{p_1} + 2\kappa_{1f} + \phi_1(\kappa_f - \kappa_{p_1})}\right], \tag{4.12}$$

$$P_e = \left[1 + \frac{3(\frac{\phi_1\sigma_{p_1} + \phi_2\sigma_{p_2}}{\sigma_f} - (\phi_1 + \phi_2))}{(\frac{\phi_1\sigma_{p_1} + \phi_2\sigma_{p_2}}{(\phi_1+\phi_2)\sigma_f} + 2) - (\frac{\phi_1\sigma_{p_1} + \phi_2\sigma_{p_2}}{\sigma_f} - (\phi_1 + \phi_2))}\right]. \tag{4.13}$$

For the conversion of the mathematical model in the form of partial differential equations (4.4)-(4.7) into the ODEs, the following similarity transformation is used:

$$\left.\begin{aligned} &\eta(t,y) = \sqrt{\frac{c}{\nu_f(1-\varpi t)}}y, \quad \psi(x,y) = \sqrt{\frac{\nu_f c}{(1-\varpi t)}}xf(\eta), \\ &\theta(\eta) = \frac{T - T_\infty}{T_w - T_\infty}, \quad \phi(\eta) = \frac{C - C_\infty}{C_w - C_\infty}, \end{aligned}\right\} \tag{4.14}$$

where ψ denotes the stream function and η is the similarity variable.

The identical satisfaction of (4.4) is already discussed in chapter 3. Now, the procedure for the conversion of (4.5) into the dimensionless form has been presented below. From the previous chapter, we will consider the following expressions:

$$u = \left(\frac{c}{1-\varpi t}\right)xf'. \tag{4.15}$$

$$v = -\sqrt{\frac{\nu_f c}{1-\varpi t}}f(\eta). \tag{4.16}$$

$$\frac{\partial u}{\partial x} = \frac{c}{1-\varpi t} f'(\eta). \tag{4.17}$$

$$\frac{\partial u}{\partial y} = \frac{c}{1-\varpi t}\sqrt{\frac{c}{\nu_f(1-\varpi t)}} x f''. \tag{4.18}$$

$$\frac{\partial^2 u}{\partial y^2} = \frac{c^2}{\nu_f(1-\varpi t)} x f'''. \tag{4.19}$$

$$\frac{\partial v}{\partial x} = 0. \tag{4.20}$$

$$\frac{\partial v}{\partial y} = -\frac{c}{1-\varpi t} f'(\eta). \tag{4.21}$$

$$\frac{\partial u}{\partial t} = \frac{cx}{(1-\varpi t)^2} f' + \frac{1}{2}\frac{c\varpi}{(1-\varpi t)^2}\sqrt{\frac{c}{\nu_f(1-\varpi t)}} xy f''. \tag{4.22}$$

Now, the dimensionless form of the momentum equation (4.5) can be obtained by using equations (4.15)-(4.22) as follows,

$$\frac{\partial u}{\partial t} + u\frac{\partial u}{\partial x} + v\frac{\partial u}{\partial y} = \left(\nu_{hnf} + \frac{1}{\rho_{hnf}\tilde{\beta}\zeta^*}\right)\frac{\partial^2 u}{\partial y^2} - \frac{1}{2\tilde{\beta}\zeta^{*3}\rho_{hnf}}\left(\frac{\partial u}{\partial y}\right)^2 \frac{\partial^2 u}{\partial y^2} - \frac{\sigma_{hnf} B^2(t) u}{\rho_{hnf}}.$$

$$\Rightarrow \frac{cx}{(1-\varpi t)^2} f' + \frac{1}{2}\frac{c\varpi}{(1-\varpi t)^2}\sqrt{\frac{c}{\nu_f(1-\varpi t)}} xy f'' + \left(\frac{c}{1-\varpi t}\right) x f' . \frac{c}{1-\varpi t} f'(\eta) - \sqrt{\frac{\nu_f c}{1-\varpi t}} f(\eta) . \frac{c}{1-\varpi t}\sqrt{\frac{c}{\nu_f(1-\varpi t)}} x f'' = \left(\nu_{hnf} + \frac{1}{\rho_{hnf}\tilde{\beta}\zeta^*}\right) \times \frac{c^2}{\nu_f(1-\varpi t)} x f''' - \frac{1}{2\tilde{\beta}\zeta^{*3}\rho_{hnf}}\left(\frac{c}{1-\varpi t}\sqrt{\frac{c}{\nu_f(1-\varpi t)}} x f''\right)^2 . \frac{c^2}{\nu_f(1-\varpi t)} x f''' - \frac{\sigma_{hnf}}{\rho_{hnf}}\left(\frac{cx}{1-\varpi t} f'\right)\frac{B_0^2}{(\sqrt{1-\varpi t})^2}.$$

$$\Rightarrow \frac{cx}{(1-\varpi t)^2} f' + \frac{1}{2}\frac{c\varpi}{(1-\varpi t)^2}\sqrt{\frac{c}{\nu_f(1-\varpi t)}} xy f'' + \frac{c^2}{(1-\varpi t)^2} x f'^2 - \frac{c^2}{(1-\varpi t)^2} x f f'' = \left(\nu_{hnf} + \frac{1}{\rho_{hnf}\tilde{\beta}\zeta^*}\right)\frac{c^2}{\nu_f(1-\varpi t)} x f''' - \frac{1}{2\tilde{\beta}\zeta^{*3}\rho_{hnf}}\frac{c^5}{\nu_f^2(1-\varpi t)^5} x^3 f''^2 f''' - \frac{\sigma_{hnf}}{\rho_{hnf}}\frac{cx}{(1-\varpi t)^2} B_0^2.$$

$$\Rightarrow \frac{\varpi}{c} f' + \frac{1}{2} . \frac{\varpi}{c} . \sqrt{\frac{c}{\nu_f(1-\varpi t)}} y f'' + f'^2 - f f'' = \left(\nu_{hnf} + \frac{1}{\rho_{hnf}\tilde{\beta}\zeta^*}\right)\frac{1}{\nu_f} f''' - \frac{1}{2}\frac{c^3 x^2}{(1-\varpi t)^3 \rho_{hnf}\nu_f^2\tilde{\beta}\zeta^{*3}} f''^2 f''' - \frac{\sigma_{hnf}}{\rho_{hnf}}\frac{B_0^2}{c} f'.$$

$$\Rightarrow\Big[\frac{\nu_{hnf}}{\nu_f}+\frac{1}{\nu_f\rho_{hnf}\tilde{\beta}\zeta^*}\Big]f'''-\Big[\frac{\frac{c^3x^3}{(1-\varpi t)^3}}{2\nu_f^2\rho_{hnf}\tilde{\beta}\zeta^{*3}x}\Big]f''^2f'''-f'^2+ff''$$
$$-\frac{\varpi}{c}\Big[f'+\frac{1}{2}\sqrt{\frac{c}{\nu_f(1-\varpi t)}}yf''\Big]+\frac{\sigma_{hnf}}{\rho_{hnf}}\frac{B_0^2}{c}f'=0.$$

Since, $\nu=\frac{\mu}{\rho}$, so

$$\left(\frac{\frac{\mu_{hnf}}{\rho_{hnf}}}{\frac{\mu_f}{\rho_f}}+\frac{1}{\frac{\mu_f}{\rho_f}\rho_{hnf}\tilde{\beta}\zeta^*}\right)f'''-\left(\frac{U_w^3}{(2\zeta^{*2}\nu_fx)(\rho_{hnf}\frac{\mu_f}{\rho_f}\tilde{\beta}\zeta^*x)}\right)f''^2f'''-f'^2+ff''$$
$$-\frac{\varpi}{c}\left(f'+\frac{1}{2}\sqrt{\frac{c}{\nu_f(1-\varpi t)}}yf''\right)-\frac{\sigma_{hnf}}{\rho_{hnf}}\frac{B_0^2}{c}f'=0.$$

$$\because\quad\frac{\frac{\mu_{hnf}}{\rho_{hnf}}}{\frac{\mu_f}{\rho_f}}=\frac{\mu_f(1-\phi_1)^{-2.5}(1-\phi_2)^{-2.5}\rho_f}{\mu_f[(1-\phi_2)(1-\phi_1)\rho_f+\phi_1\rho_{p_1}]+\phi_2\rho_{p_2}},$$
$$=\frac{1}{P_aP_b},$$
$$\rho_{hnf}\frac{\mu_f}{\rho_f}=\Big[((1-\phi_2)(1-\phi_1)\rho_f+\phi_1\rho_{p_1})+\phi_2\rho_{p_2}\Big]\times\frac{\mu_f}{\rho_f},$$
$$\sigma_{hnf}=\left[1+\frac{3(\frac{\phi_1\sigma_{p_1}+\phi_2\sigma_{p_2}}{\sigma_f}-(\phi_1+\phi_2))}{(\frac{\phi_1\sigma_{p_1}+\phi_2\sigma_{p_2}}{(\phi_1+\phi_2)\sigma_f}+2)-(\frac{\phi_1\sigma_{p_1}+\phi_2\sigma_{p_2}}{\sigma_f}-(\phi_1+\phi_2))}\right]\times\sigma_f,$$
$$=P_e\sigma_f,$$
$$\therefore\quad\Big(\frac{1}{P_aP_b}+\frac{\omega}{P_b}\Big)f'''+ff''-f'^2-A\Big(f'+\frac{\eta}{2}f''\Big)-\frac{\omega\Delta}{P_b}f''^2f'''-\frac{P_e\sigma_f}{P_b\rho_f}\frac{B_0^2}{c}f'=0.$$

Finally, the dimensionless form of the momentum equation gets the form:

$$\Big(\frac{1}{P_aP_b}+\frac{\omega}{P_b}\Big)f'''+ff''-f'^2-A\Big(f'+\frac{\eta}{2}f''\Big)-\frac{\omega\Delta}{P_b}f''^2f'''-\frac{P_e}{P_b}Mf'=0.\quad(4.23)$$

The following dimensionless parameters are used in equation (4.23):

$$A=\tfrac{\varpi}{c},\qquad\omega=\tfrac{1}{\mu_f\tilde{\beta}\zeta^*},\qquad\Delta=\tfrac{U_w^3}{2\zeta^{*2}\nu_fx},\qquad M=\tfrac{\sigma_fB_0^2}{c\rho_f}.$$

Now, include below the procedure for the conversion of equation (4.6) into the dimensionless form. The following expressions are equations already derived in Chapter 3.

$$\frac{\partial T}{\partial x}=\Big(\frac{c}{1-\varpi t}\Big)\theta(\eta).\quad(4.24)$$

$$\frac{\partial^2 T}{\partial x^2} = 0. \tag{4.25}$$

$$\frac{\partial T}{\partial y} = \left(\frac{cx}{1-\varpi t}\right)\theta' \sqrt{\frac{c}{\nu_f(1-\varpi t)}}. \tag{4.26}$$

$$\frac{\partial^2 T}{\partial y^2} = \left(\frac{c^2 x}{\nu_f(1-\varpi t)^2}\right)\theta''. \tag{4.27}$$

$$\frac{\partial^2 T}{\partial x \partial y} = \frac{c}{1-\varpi t}\sqrt{\frac{c}{\nu_f(1-\varpi t)}}\theta'. \tag{4.28}$$

$$\frac{\partial T}{\partial t} = \frac{cx\varpi}{(1-\varpi t)^2}\theta + \frac{1}{2}\frac{c\ \varpi}{(1-\varpi t)^2}\sqrt{\frac{c}{\nu_f(1-\varpi t)}}xy\theta'. \tag{4.29}$$

$$\frac{\partial q_r}{\partial y} = -\frac{16\sigma^*}{3k^*}T_\infty^3\left(\frac{c^2 x}{\nu_f(1-\varpi t)^2}\right)\theta''. \tag{4.30}$$

The governing equation 4.6 for the conservation of energy is

$$\frac{\partial T}{\partial t} + u\frac{\partial T}{\partial x} + v\frac{\partial T}{\partial y} = \frac{\kappa_{hnf}}{(\rho C_p)_{hnf}}\left(\frac{\partial^2 T}{\partial y^2}\right) - \frac{1}{(\rho C_p)_{hnf}}\left(\frac{\partial q_r}{\partial y}\right) + \frac{\nu_{hnf}}{(\rho C_p)_{hnf}}\left(\frac{\partial u}{\partial y}\right)^2$$
$$- \lambda\left(u\frac{\partial u}{\partial x}\frac{\partial T}{\partial x} + v\frac{\partial v}{\partial y}\frac{\partial T}{\partial y} + u\frac{\partial v}{\partial x}\frac{\partial T}{\partial y} + v\frac{\partial u}{\partial y}\frac{\partial T}{\partial x} + u^2\frac{\partial^2 T}{\partial x^2} + v^2\frac{\partial^2 T}{\partial y^2} + 2uv\frac{\partial^2 T}{\partial x \partial y}\right).$$
$$\Rightarrow \frac{cx\varpi}{(1-\varpi t)^2}\theta + \frac{1}{2}\frac{c\ \varpi}{(1-\varpi t)^2}\sqrt{\frac{c}{\nu_f(1-\varpi t)}}xy\theta' + \left(\frac{cx}{1-\varpi t}f'\right)\left(\frac{c}{1-\varpi t}\right)\theta(\eta)$$
$$+ \left(-\sqrt{\frac{\nu_f c}{1-\varpi t}}f\right)\frac{cx}{1-\varpi t}\theta'\sqrt{\frac{c}{\nu_f(1-\varpi t)}} = \frac{\kappa_{hnf}}{(\rho C_p)_{hnf}}\left(\frac{c^2 x}{\nu_f(1-\varpi t)^2}\right)\theta''$$
$$+ \frac{1}{(\rho C_p)_{hnf}}\left(\frac{16\sigma^* T_\infty^3}{3k^*}\frac{c^2 x}{\nu_f(1-\varpi t)^2}\theta''\right) + \frac{\nu_{hnf}}{(\rho C_p)_{hnf}}\left(\frac{c^2 x^2}{(1-\varpi t)^2}\frac{c}{\nu_f(1-\varpi t)}f''^2\right)$$
$$- \lambda\left(\frac{cx}{1-\varpi t}f'\frac{c}{1-\varpi t}f'\frac{c}{1-\varpi t}\theta + \sqrt{\frac{\nu_f c}{1-\varpi t}}f\frac{c}{1-\varpi t}f'\frac{cx}{1-\varpi t}\theta'\sqrt{\frac{c}{\nu_f(1-\varpi t)}}\right.$$
$$- \sqrt{\frac{\nu_f c}{1-\varpi t}}f.\frac{cx}{1-\varpi t}\sqrt{\frac{c}{\nu_f(1-\varpi t)}}f''.\frac{c}{1-\varpi t}\theta + 0 + \frac{\nu_f c}{1-\varpi t}f^2.\frac{c^2 x}{\nu_f(1-\varpi t)^2}\theta''$$
$$\left. + 2\left(\frac{cx}{1-\varpi t}f'\right).\left(-\sqrt{\frac{\nu_f c}{1-\varpi t}}f\right).\left(\frac{c}{1-\varpi t}\sqrt{\frac{c}{\nu_f(1-\varpi t)}}\theta'\right)\right).$$
$$\Rightarrow \frac{\varpi}{c}\theta + \frac{1}{2}\frac{\varpi}{c}\eta\theta' + f'\theta - f\theta' = \frac{\kappa_{hnf}}{(\rho C_p)_{hnf}}\frac{1}{\nu_f}\theta'' + \frac{16\sigma^*}{3\kappa^*}\frac{1}{(\rho C_p)_{hnf}}\frac{1}{\nu_f}\theta' T_\infty^3$$
$$+ \frac{\nu_{hnf}}{(\rho C_p)_{hnf}}\frac{cx}{\nu_f(1-\varpi t)}f''^2 - \lambda\left(\frac{c}{1-\varpi t}f'^2\theta + \frac{c}{1-\varpi t}ff'\theta' - \frac{c}{1-\varpi t}ff''\theta\right.$$
$$\left. + \frac{c}{1-\varpi t}f^2\theta'' - 2\frac{c}{1-\varpi t}ff'\theta'\right).$$

$$\Rightarrow \frac{\varpi}{c}\theta + \frac{1}{2}\frac{\varpi}{c}\eta\theta' + f'\theta - f\theta' = \frac{\kappa_{hnf}}{(\rho C_p)_{hnf}}\frac{1}{\nu_f}\theta'' + \frac{16\sigma^*}{3\kappa^*}\frac{1}{(\rho C_p)_{hnf}}\frac{1}{\nu_f}\theta' T_\infty^3 + \frac{\nu_{hnf}}{(\rho C_p)_{hnf}}\frac{cx}{\nu_f(1-\varpi t)}f''^2 - \lambda\frac{c}{1-\varpi t}\left(f'^2\theta - ff'\theta' - ff''\theta + f^2\theta''\right).$$

Since

$$\kappa_{hnf} = P_d\kappa_f, \quad (\rho C_p)_{hnf} = P_c(\rho C_p)_f, \quad \lambda = \lambda_0(1-\varpi t),$$

so,

$$A\theta + \frac{1}{2}A\theta' + f'\theta - f\theta' = \frac{P_d}{P_c}\frac{1}{Pr}\theta'' + \frac{Nr}{P_c}\theta' + \frac{E^c}{P_aP_c}f''^2 - \lambda_0 c\left(f'^2\theta - ff'\theta' - ff''\theta + f^2\theta''\right).$$

$$\Rightarrow \quad \left(1 + \frac{PrNr}{P_d}\right)\theta'' + Pr\frac{P_c}{P_d} \times \left(f\theta' - f'\theta - A(\theta + \frac{\eta}{2}\theta') + \frac{E^c}{P_aP_c}f''^2 - \xi\left(f'^2\theta - ff'\theta' - ff''\theta + f^2\theta''\right)\right) = 0. \tag{4.31}$$

The dimensionless parameters used in equation (4.31) are:

$$A = \tfrac{\varpi}{c}, \quad \alpha_f = \tfrac{\kappa_f}{(\rho C_p)_f}, \quad Pr = \tfrac{\nu_f}{\alpha_f}, \quad \xi = \lambda_0 c,$$
$$E^c = \tfrac{U_w^3}{(C_p)_f(T_w - T_\infty)}, \quad Nr = \tfrac{16\sigma^*}{3\kappa^*}\tfrac{T_\infty^3}{\nu_f(\rho C_p)_f}.$$

Now, for the conversion of concentration equation (4.7), the following derivatives are required.

$$\phi(\eta) = \frac{C - C_\infty}{C_w - C_\infty}.$$

$$\Rightarrow \quad C = C_\infty + (C_w - C_\infty)\phi(\eta)$$

$$\frac{\partial C}{\partial x} = 0 \tag{4.32}$$

$$\frac{\partial C}{\partial y} = (C_w - C_\infty)\phi'(\eta)\frac{\partial \eta}{\partial y} = (C_w - C_\infty)\phi'(\eta)\sqrt{\frac{c}{\nu_f(1-\varpi t)}}. \tag{4.33}$$

$$\frac{\partial^2 C}{\partial y^2} = (C_w - C_\infty)\phi''(\eta)\frac{c}{\nu_f(1-\varpi t)}. \tag{4.34}$$

The governing equation (4.7) for the conservation of concentration is

$$
\begin{aligned}
& u\frac{\partial C}{\partial x}+v\frac{\partial C}{\partial y}=D_{hnf}\frac{\partial^2 C}{\partial y^2}-k_1(C-C_\infty).\\
\Rightarrow\quad & -\sqrt{\frac{\nu_f c}{1-\varpi t}}f(\eta)(C_w-C_\infty)\phi'(eta)\sqrt{\frac{c}{\nu_f(1-\varpi t)}}\\
& =D_{hnf}(C_w-C_\infty)\phi''\frac{c}{\nu_f(1-\varpi t)}-k_1(c_\infty+(C_w-C_\infty)\phi(\eta)-C_\infty).\\
\Rightarrow\quad & -(C_w-C_\infty)\frac{c}{1-\varpi t}f(\eta)\phi'=(C_w-C_\infty)\left(D_{hnf}\phi''\frac{c}{\nu_f(1-\varpi t)}+k_1\phi\right).\\
\Rightarrow\quad & -\frac{c}{1-\varpi t}f(\eta)\phi'=D_{hnf}\phi''\frac{c}{\nu_f(1-\varpi t)}+k_1\phi.\\
\Rightarrow\quad & -f(\eta)\phi'=\frac{D_{hnf}}{\nu_f}\phi''+k_1\frac{(1-\varpi t)}{c}\phi.\\
\Rightarrow\quad & \frac{D_{hnf}}{\nu_f}\phi''=k_1\frac{(1-\varpi t)}{c}\phi-f(\eta)\phi'.
\end{aligned}
$$

Since $D_{hnf}=(1-\phi_1)^{2.5}(1-\phi_2)^{2.5}D_f$, so

$$
\begin{aligned}
& \frac{D_f P_a}{\nu_f}\phi''=\frac{k_1(1-\varpi t)}{c}\phi-f(\eta)\phi'.\\
\Rightarrow\quad & \phi''=\frac{\nu_f}{D_f P_a}\frac{k_1(1-\varpi t)}{c}\phi-\frac{\nu_f}{D_f P_a}f(\eta)\phi'.\\
\Rightarrow\quad & \phi''=\frac{Sc}{P_a}K_1\phi-\frac{Sc}{P_a}f(\eta)\phi'.
\end{aligned}
$$

Therefore, the dimensionless form of the concentration equation gets the form:

$$\phi''+\frac{Sc}{P_a}f(\eta)\phi'-\frac{Sc}{P_a}K_1\phi=0. \tag{4.35}$$

The following dimensionless parameters are used in equation (4.35):

$$Sc=\tfrac{\nu_f}{D_f},\quad K_1=\tfrac{k_1(1-\varpi t)}{c}.$$

The related BCs are converted into the dimensionless form by the following procedure.

$$v(x,0)=V_w, \qquad at \quad y=0.$$

$$\Rightarrow \quad -\sqrt{\frac{\nu_f c}{1-\varpi t}} f(\eta) = V_w, \qquad at \quad \eta = 0.$$

$$\Rightarrow \quad f(\eta) = -\sqrt{\frac{1-\varpi t}{\nu_f c}}, \qquad at \quad \eta = 0.$$

$$\Rightarrow \quad f(0) = S$$

$$u(x,0) = U_w(x) + \mu_{hnf}\Big[\frac{\partial u}{\partial y}\Big], \qquad at \quad y = 0.$$

$$\Rightarrow \quad \frac{cx}{1-\varpi t} f'(\eta) = \frac{cx}{1-\varpi t} + \frac{cx}{1-\varpi t}\sqrt{\frac{c}{\nu_f(1-\varpi t)}}\frac{\mu_f}{P_a} f''(\eta), \qquad at \quad \eta = 0.$$

$$\Rightarrow \quad \frac{cx}{1-\varpi t} f'(\eta) = \frac{cx}{1-\varpi t}\Big[1 + \sqrt{\frac{c}{\nu_f(1-\varpi t)}}\mu_f\Big] f'', \qquad at \quad \eta = 0.$$

$$\Rightarrow \quad f'(\eta) = 1 + \frac{\Lambda}{P_a} f''(\eta), \qquad at \quad \eta = 0.$$

$$\Rightarrow \quad f'(0) = 1 + \frac{\Lambda}{P_a} f''(0).$$

$$-\kappa_f\Big[\frac{\partial T}{\partial y}\Big] = h_f(T_w - T), \qquad at \quad y = 0.$$

$$\Rightarrow \quad -\kappa_f \frac{cx}{1-\varpi t}\sqrt{\frac{c}{\nu_f(1-\varpi t)}}\theta' = h_f\Big(T_\infty + \frac{cx}{1-\varpi t} - T\Big), \qquad at \quad \eta = 0.$$

$$\Rightarrow \quad \frac{cx}{1-\varpi t}\theta'(\eta) = \frac{-h_f}{\kappa_f}\sqrt{\frac{\nu_f(1-\varpi t)}{c}}\Big(\frac{cx}{1-\varpi t} - (T - T_w)\Big), \qquad at \quad \eta = 0.$$

$$\Rightarrow \quad \frac{cx}{1-\varpi t}\theta'(\eta) = -\frac{h_f}{\kappa_f}\sqrt{\frac{\nu_f(1-\varpi t)}{c}}\Big(\frac{cx}{1-\varpi t} - \frac{cx}{1-\varpi t}\theta(\eta)\Big), \qquad at \quad \eta = 0.$$

$$\Rightarrow \quad \theta'(\eta) = -Bi(1-\theta(\eta)), \qquad at \quad \eta = 0.$$

$$\Rightarrow \quad \theta'(0) = -Bi(1-\theta(0)).$$

$$C = C_w, \qquad at \quad y = 0.$$

$$\Rightarrow \quad C = C_\infty + (C_w - C_\infty)\phi(\eta), \qquad at \quad \eta = 0.$$

$$\Rightarrow \quad \phi(\eta) = \frac{C_w - C_\infty}{C_w - C_\infty}, \qquad at \quad \eta = 0.$$

$$\Rightarrow \quad \phi(\eta) = 1, \qquad at \quad \eta = 0.$$

$$\Rightarrow \quad \phi'(0) = 1.$$

Similarly,

$$u \to 0, \qquad as \quad y \to \infty.$$

$$\Rightarrow \quad f'(\eta) \to 0, \qquad as \quad \eta \to \infty.$$

$$
\begin{aligned}
\Rightarrow \quad & f'(\infty) \to 0, && as \quad \eta \to \infty. \\
& T \to T_\infty, && as \quad y \to \infty. \\
\Rightarrow \quad & \theta(\eta) \to 0, && as \quad \eta \to \infty. \\
\Rightarrow \quad & \theta(\infty) \to 0, && as \quad \eta \to \infty. \\
& C \to C_\infty, && as \quad y \to \infty. \\
\Rightarrow \quad & \phi(\eta) \to 0, && as \quad \eta \to \infty. \\
\Rightarrow \quad & \phi(\infty) \to 0, && as \quad \eta \to \infty.
\end{aligned}
$$

The final dimensionless form of the governing model, is

$$\Big(\frac{1}{P_a P_b} + \frac{\omega}{P_b}\Big) f''' + f f'' - f'^2 - A\Big(f' + \frac{\eta}{2} f''\Big) - \frac{\omega\Delta}{P_b} f''^2 f''' - \frac{P_e}{P_b} M f' = 0. \quad (4.36)$$

$$\Big(1 + \frac{PrNr}{P_d}\Big)\theta'' + Pr\frac{P_c}{P_d} \times \Big(f\theta' - f'\theta - A\Big(\theta + \frac{\eta}{2}\theta'\Big) + \frac{E^c}{P_a P_c} f''^2 - \xi\Big(f'^2\theta - f f'\theta' - f f''\theta + f^2\theta''\Big)\Big) = 0. \quad (4.37)$$

$$\phi'' + \frac{Sc}{P_a} f(\eta)\phi' - \frac{Sc}{P_a} K_1 \phi = 0. \quad (4.38)$$

The associated BCs (4.8) in the dimensionless form are:

$$\left.\begin{aligned}
& f(0) = S, \quad f'(0) = 1 + \frac{\Lambda}{P_a} f''(0), \quad f'(\eta) \to 0. \\
& \theta'(0) = -Bi(1 - \theta(0)), \quad \theta(\eta) \to 0. \\
& \phi'(0) = 1, \quad \phi(\eta) \to 0.
\end{aligned}\right\} \quad (4.39)$$

The skin friction coefficient and Local Nusselt numbers are the same as discussed in Chapter 3. So,

$$C_f Re_{x^{\frac{1}{2}}} = -\left(\Big(\frac{1}{P_a} + \omega\Big) f''(0) - \frac{\omega\Delta}{3} f'''^3(0)\right), \quad (4.40)$$

$$Nu_x Re_x^{-\frac{1}{2}} = -\frac{\kappa_{hnf}}{\kappa_f}(1 + Nr)\theta'(0) \quad (4.41)$$

The local Sherwood number is defined as:

$$Sh_x = \frac{xq_m}{D_{hnf}(C_w - C_\infty)}. \tag{4.42}$$

The dimensionless form of Nu_x can be produced through the following steps:

$$\begin{aligned}
q_m &= -D_{hnf}\left(\frac{\partial C}{\partial y}\right)_{y=0}. \\
\therefore \quad Sh_x &= -\frac{xD_{hnf}(C_w - C_\infty)\sqrt{\frac{c}{\nu_f(1-\varpi t)}}\phi'(0)}{D_{hnf}(C_w - C_\infty)} \\
&= -\sqrt{\frac{c}{\nu_f(1-\varpi t)}}x\phi'(0) \\
&= -\sqrt{\frac{cx}{\nu_f x(1-\varpi t)}}x\phi'(0) \\
&= -\sqrt{\frac{U_w}{\nu_f x}}x\phi'(0) \\
&= -\sqrt{\frac{U_w x}{\nu_f}}\phi'(0) \\
&= -Re_x^{\frac{1}{2}}\phi'(0) \\
\Rightarrow \quad Sh_x Re_x^{\frac{1}{2}} &= -\phi'(0).
\end{aligned} \tag{4.43}$$

Here $Re_x = \frac{U_w c^2}{\nu_f x}$ denotes the Reynolds number.

The entropy generation rate N_G is defined as:

$$N_G = \frac{T_\infty^2 c^2 E_G}{\kappa_f (T_w - T_\infty)^2} \tag{4.44}$$

The dimensionless form of N_G can be produced through the following steps:

$$\begin{aligned}
E_G &= \frac{\kappa_{hnf}}{T_\infty^2}\left(\left(\frac{\partial T}{\partial y}\right)^2 + \frac{16}{3}\frac{16\sigma^* T_\infty^3}{3k^*\nu_f(\rho C_p)_f}\left(\frac{\partial T}{\partial y}\right)^2\right) + \frac{\mu_{hnf}}{T_\infty}\left(\frac{\partial u}{\partial y}\right)^2 \\
&\quad + \frac{\sigma_{hnf}B^2(t)u^2}{T_\infty}. \\
\therefore \quad N_G &= \frac{\left(\frac{\kappa_{hnf}}{T_\infty^2}\left(\left(\frac{\partial T}{\partial y}\right)^2 + \frac{16}{3}\frac{16\sigma^* T_\infty^3}{3k^*\nu_f(\rho C_p)_f}\left(\frac{\partial T}{\partial y}\right)^2\right) + \frac{\mu_{hnf}}{T_\infty}\left(\frac{\partial u}{\partial y}\right)^2 + \frac{\sigma_{hnf}B^2(t)u^2}{T_\infty}\right)T_\infty^2 c^2}{\kappa_f(T_w - T_\infty)^2}
\end{aligned}$$

$$
\begin{aligned}
&= \left(\frac{P_d \kappa_f}{T_\infty^2}(1+Nr)\frac{(c^2x^2)}{(1-\varpi t)^2}\frac{c}{\nu_f(1-\varpi t)}\theta'^2 + \frac{\frac{\mu_f}{P_a}}{T_\infty}\frac{(c^2x^2)}{(1-\varpi t)^2}\frac{c}{\nu_f(1-\varpi t)}f''^2 \right. \\
&\quad \left. + \frac{P_e \sigma_f B_0^2 u^2}{T_\infty(\sqrt{1-\varpi t})^2}\frac{c^2x^2}{(1-\varpi t)^2}f'^2 \right) T_\infty^2 c^2 \times \frac{1}{\kappa_f(T_w - T_\infty)^2} \\
&= \left(P_d(1+Nr)\theta'^2 + \frac{T_\infty \mu_f}{P_a}\frac{U_w^2}{\kappa_f(T_w-T_\infty)^2}f''^2 \right)\frac{cx}{\nu_f x(1-\varpi t)}c^2 \\
&\quad + \frac{T_\infty c^2 P_e \sigma_f B_0^2}{\kappa_f(T_w-T_\infty)^2(1-\varpi t)}\frac{c^2x^2}{(1-\varpi t)^2}f'^2 \\
&= \left(P_d(1+Nr)\theta'^2 + \frac{1}{P_a}\frac{T_\infty}{(T_w-T_\infty)}\frac{\mu_f U_w^2}{\kappa_f(T_w-T_\infty)}f''^2 \right)\frac{U_w c^2}{\nu_f x} \\
&\quad + \frac{T_\infty}{(T_w-T_\infty)}\frac{\sigma_f B_0^2}{\rho_f c}\frac{\mu_f U_w^2}{\kappa_f(T_w-T_\infty)} \times \frac{U_w c^2}{\nu_f}f'^2 \\
\Rightarrow \quad N_G &= Re\left(P_d(1+Nr)\theta'^2 + \frac{1}{P_a}\frac{Br}{\Omega}f''^2 + \frac{BrP_eM}{\Omega}f'^2 \right), \qquad (4.45)
\end{aligned}
$$

where $R_e = \frac{U_w c^2}{\nu_f x}$, $Br = \frac{\mu_f U_w^2}{\kappa_f(T_w - T_\infty)}$, $\Omega = \frac{T_\infty}{(T_w - T_\infty)}$ denote the Reynolds number, Brinkmann number and dimensionless temperature gradient respectively and $M = \frac{\sigma_f B_0^2}{c\rho_f}$ is the magnetic parameter.

4.3 Numerical Method for Solution

The ordinary differential equation (4.36) has been sloved numerically by using the shooting technique.

$$
f''' = \frac{P_a P_b}{1 + P_a\omega - P_a\omega\Delta f''^2}\left(f'^2 - ff'' + A\left(f' + \frac{\eta}{2}f'' \right) + \frac{P_e}{P_b}Mf' \right). \qquad (4.46)
$$

The following notations have been taken:

$$
\begin{aligned}
f &= G_1, \\
f' &= G_1' = G_2, \\
f'' &= G_1'' = G_2' = G_3.
\end{aligned}
$$

The momentum equation (4.46) is then transformed into the system of first-order ODEs shown below.

$$G_1' = G_2, \qquad G_1(0) = S.$$
$$G_2' = G_3, \qquad G_2(0) = 1 + \frac{\Lambda}{P_a} G_3(0).$$
$$G_3' = \frac{P_a P_b}{1 + P_a\omega - P_a\omega\Delta G_3^2}\left(G_2^2 - G_1 G_3 + A\Big(G_2 + \frac{\eta}{2}G_3\Big) + \frac{P_e}{P_b} M G_2\right), \quad G_3(0) = p.$$

The above IVP will be numerically solved by the Runge-Kutta method of oder 4.

The domain of the problem is considered to be bounded i.e. $[0,\, \eta_\infty]$, where η_∞ is a +ve real number, for which the variation in the solution is ignorable after $\eta = \eta_\infty$. The missing condition p is to be chosen such that.

$$G_2(\eta_\infty, p) = 0.$$

Newton's method will be used to find p. This method has the following iterative scheme.

$$p_{n+1} = p_n - \frac{G_2(\eta_\infty, p_n)}{(\frac{\partial}{\partial p_n} G_2(\eta_\infty, p))_{p=p_n}}.$$

We further introduce the following notations:

$$\frac{\partial G_1}{\partial p} = G_4, \qquad \frac{\partial G_2}{\partial p} = G_5, \qquad \frac{\partial G_3}{\partial p} = G_6.$$

As a result of these new notations, the Newton's iterative scheme gets the form:

$$p_{n+1} = p_n - \frac{G_2(\eta_\infty, p_n)}{G_5(\eta_\infty, p_n)}.$$

Now differentiating the last system of three first order ODEs with respect to p, we

get another system of ODEs, as follows.

$$G_4' = G_5, \qquad G_4(0) = 0.$$

$$G_5' = G_6, \qquad G_5(0) = \frac{\Lambda}{P_a}.$$

$$G_6' = \frac{P_a P_b}{1 + P_a\omega - P_a\omega\Delta G_3^2}\Bigg(\frac{2P_a\omega G_3 G_6}{1 + P_a\omega - P_a\omega\Delta G_3^2}\Big(G_2^2 - G_1G_3 + A\Big(G_2 + \frac{\eta}{2}G_3\Big) + \frac{P_e}{P_b}MG_2\Big) + 2G_2G_5 - G_4G_3 - G_1G_6 + A\Big(G_5 + \frac{\eta}{2}G_6\Big) + \frac{P_e}{P_b}MG_5\Bigg), \qquad G_6(0) = 1.$$

The stopping criteria for the Newton's technique is set as:

$$\mid G_2(\eta_\infty, p) \mid < \epsilon,$$

where $\epsilon > 0$ is a sufficiently small number, which has been considered as 10^{-10}. The ordinary differential equation (4.37) will be approximated by using the shooting technique and assuming f as a known function.

$$\theta'' = \frac{1}{1 + \frac{PrNr}{P_d} - \xi Pr\frac{P_c}{P_d}f^2}\Bigg(-Pr\frac{P_c}{P_d} \times \Big(f\theta' - f'\theta - A\Big(\theta + \frac{\eta}{2}\theta'\Big) + \frac{E^c}{P_aP_c}f''^2 - \xi(f'^2\theta - ff'\theta' - ff''\theta)\Big)\Bigg). \tag{4.47}$$

For this, we utilize the following notions:

$$\theta = H_1, \quad \theta' = H_1' = H_2.$$

The energy equation (4.47) is then transformed into a system of first-order ODEs as shown below.

$$H_1' = H_2, \qquad H_1(0) = q.$$

$$H_2' = \frac{1}{1 + \frac{PrNr}{P_d} - \xi Pr\frac{P_c}{P_d}G_1^2}\Bigg(-Pr\frac{P_c}{P_d} \times \Big(G_1H_2 - G_2H_1 - A\Big(H_1 + \frac{\eta}{2}H_2\Big) + \frac{E^c}{P_aP_c}G_3^2 - \xi(G_2^2H_1 - G_1G_2H_2 - G_1G_3H_1)\Big)\Bigg), \quad H_2(0) = -Bi(1 - H_1(0)).$$

The above IVP will be numerically solved by Runge-Kutta method of oder 4. The missing condition q is to be chosen such that.

$$H_1(\eta_\infty, q) = 0.$$

The above equation can be solved by using Newton's method with the following iterative formula.

$$q_{n+1} = q_n - \frac{H_1(\eta_\infty, q_n)}{(\frac{\partial}{\partial q} H_1(\eta_\infty, q))_{q=q_n}}.$$

We further introduce the following notations:

$$\frac{\partial H_1}{\partial q} = H_3, \quad \frac{\partial H_2}{\partial q} = H_4.$$

As a result of these new notations, the Newton's iterative scheme gets the form:

$$q_{n+1} = q_n - \frac{H_1(\eta_\infty, q_n)}{H_3(\eta_\infty, q_n)}.$$

Now differentiating the system of two first order ODEs with respect to q, we get another system of ODEs, as follows.

$$\begin{aligned}
&H_3' = H_4, && H_3(0) = 0.\\
&H_4' = \frac{1}{1 + \frac{PrNr}{P_d} - \xi Pr \frac{P_c}{P_d} G_1^2}\Bigg(- Pr\frac{P_c}{P_d} \times \Big(G_1 H_4 - G_2 H_3 - A\Big(H_3 + \frac{\eta}{2} H_4\Big)\\
&\quad - \xi(G_2^2 H_3 - G_1 G_2 H_4 - G_1 G_3 H_3)\Big)\Bigg), && H_4(0) = -Bi.
\end{aligned}$$

The stopping criteria for the Newton's method is set as:

$$\mid H_1(\eta_\infty, q) \mid < 10^{-10}.$$

The ordinary differential equation (4.38) will be approximated by using the shooting technique assuming f as a known function.

$$\phi'' = \frac{Sc}{P_a}\Big(K_1\phi - f\phi'\Big). \tag{4.48}$$

For this, we utilize the following notions:

$$\phi = Y_1, \quad \phi' = Y_1' = Y_2.$$

The concentration equation (4.48) is then transformed into the system of first-order ODEs shown below.

$$\begin{aligned} Y_1' &= Y_2, & Y_1(0) &= 1. \\ Y_2' &= \frac{Sc}{P_a}\Big(K_1 Y_1 - G_1 Y_2\Big), & Y_2(0) &= r. \end{aligned}$$

The above IVP will be numerically solved by Runge-Kutta method of oder 4. The missing condition r is to be chosen such that.

$$Y_1(\eta_\infty, r) = 0.$$

The above equation can be solved by using Newton's method with the following iterative formula.

$$r_{n+1} = r_n - \frac{Y_1(\eta_\infty, r_n)}{(\frac{\partial}{\partial r} Y_1(\eta_\infty, r))_{r=r_n}}.$$

We further introduce the following notations:

$$\frac{\partial Y_1}{\partial r} = Y_3, \qquad \frac{\partial Y_2}{\partial r} = Y_4.$$

As a result of these new notations, the Newton's iterative scheme gets the form:

$$r_{n+1} = r_n - \frac{Y_1(\eta_\infty, r_n)}{Y_3(\eta_{\infty,n}\, r)}.$$

Now differentiating the system of two first order ODEs with respect to r, we get another system of ODEs, as follows.

$$\begin{aligned} Y_3' &= Y_4, & Y_3(0) &= 0. \\ Y_4' &= \frac{Sc}{P_a}\Big(K1 Y_3 - G_1 Y_4\Big), & Y_4(0) &= 1. \end{aligned}$$

The stopping criteria for the Newton's technique is set as:

$$| Y_1(\eta_\infty, r) | < \epsilon.$$

where $\epsilon > 0$ is a sufficiently small number, which has been considered as 10^{-10}.

4.4 Representation of Graphs and Tables

In this section, the effect of the dimensionless parameters of interest on the skin friction coefficient $Re_x^{\frac{1}{2}} C_f$, Nusselt number $Re_x^{-\frac{1}{2}} Nu_x$, Sherwood number Sh and Entropy generation N_G has been thoroughly discussed in the graphs and tables. In Table 4.1, T_{f_1} and T_{f_2} are the intervals for the choice of missing condition q while computing the skin friction coefficient for nanofluid and hybrid nanofluid respectively. It is observed that for the computation of Nusselt number and Sherwood number, there is a great flexibility in the choice of the missing initial condition. Tables 4.2, 4.3 and 4.4 explain the effect of the material parameters ω and Δ, unsteady parameter A, nanoparticle volume fraction parameters ϕ_1 and ϕ_2, suction/injection parameter Λ, magnetic parameter M, relaxation time parameter ξ, radiation parameter Nr, Eckert number Ec, Biot number Bi, Schmidt number Sc and chemical reaction parameter K_1 with fixed Prandtl number $Pr = 6.2$ and shape factor $m = 3$ on fluid motion, temperature variation, mass concentration and the total volumetric entropy generation of Powell-Eyring nanofluid and hybrid nanofluid.

For rising these values the skin friction coefficient $Re_x^{\frac{1}{2}} C_f$, Nusselt number $Re_x^{\frac{-1}{2}} Nu_x$ and Sherwood number Sh increase. Figures 4.2 -4.4, show the impect of ω on velocity profile $f'(\eta)$, temperature profile $\theta(\eta)$ and entropy profile N_G respectively. For $\omega = 0.1, 0.3, 0.5$, computations are carried out with nanoparticles volume fraction of $\phi_1 = 0.09$ and $\phi_2 = 0.09$. For different values of ω, Figure 4.2 depicts variation in the velocity profile. For increasing value of ω, an ascending trend in the velocity profile is observed and this enhances the thickness of the momentum

boundary layer. As ω is inversely proportional to the base fluid viscosity, an increase in the positive values of ω, enhances the stress rate within the boundary layer and decreases the base fluid viscosity. Consequently, within the boundary layer, the velocity of the conventional and hybrid nanofluids, is increased.

In Table 4.2, the effect of ω on the viscosity of the base fluid can also be seen through difference in values of the skin friction. The skin friction factor at the boundary undertakes a move up trend. Furthermore, for alloted value of $\omega = 0.1$, the thickness of momentum boundary layer for hybrid nanofluid is increased whenever it is collated with the classical nanofluid. A reducing trend is noticed in the temperature profile with an enlargement in the value of the parameter ω as depicted in Figure 4.3. This illustrates a depletion in thickness of the thermal boundary layer and an improvement in the rate of heat transfer inside the boundary layer. In comparison, the thickness of the conventional nanofluid is higher than that for the hybrid nanofluid. Hence, the rate of heat transport at the boundary of $Al_2O_3 - Cu/H_2O$ hybrid nanofluid is higher. For both conventional and hybrid nanofluids increasing trend in Nusselt number is also observed in from Table 4.3.

Figure 4.4 illustrates the influence of the material parameter ω on the volumetric entropy generation of the conventional and hybrid nanofluids. It describes the an increase in the values of the material parameter lessens the entropy of system near the surface but an opposite impact can be seen away from the plate. It shows that the irreversibility of $Cu - H_2O$ nanofluid is less than the $Al_2O_3 - Cu/H_2O$ hybrid nanofluid.

Figures 4.5-4.7 depict the behavior of the fluid motion, temperature distribution and entropy generation due to variation in the non-Newtonian fluid parameter Δ. For the increasing values of Δ, Figures 4.5 and 4.7 show a decreasing trend in the velocity profile $f'(\eta)$ and entropy generation N_G whereas in Figure 4.6, it can be observed that the increasing values of Δ, initially the entropy profile N_G increases. As η increases, the entropy profile decreases and asymptotically approach to zero.

Figures 4.8-4.10 focus on the impact of ϕ. The graphs are produced for velocity, temperature and entropy generation profiles. Computations are carried out for

fixed value of $\phi_1 = 0.09$, and analysis is carried for variation in the parameter ϕ_2. In Figure 4.8, it can be observed that the increasing values of ϕ, initially the velocity profile $f'(\eta)$ decreases due to a rise the value of ϕ. As η increases, the velocity profile increases and asymptotically approach to zero. Figure 4.9 depicts that the temperature profile $\theta(\eta)$ rises due to higher thermal conductivity of solid particles which raises the overall thermal conductivity of the nanofluid. In Figure 4.10, it can be observed that the increasing values of ϕ, the entropy generation N_G increases.

Figures 4.11-4.13 depict a decreasing trend in the fluid motion movement, volumetric entropy generation, and temperature for positive increase in the slip parameter Λ. For the increasing values of Λ, the velocity profile $f'(\eta)$ and temperature profile $\theta(\eta)$ and entropy generation N_G decrease. Figures 4.14 -4.16 show the impact of M. For the increasing values of M, the velocity profile $f'(\eta)$ decreases and temperature profile $\theta(\eta)$ and entropy profile N_G increases. Figures 4.17 ,4.18 show the impact of ξ. For the increasing values of ξ, the temperature profile $\theta(\eta)$ is decreases and entropy profile N_G is increases.

Figures 4.19-4.20 show the impact of Nr. For the increasing values of Nr, the temperature profile $\theta(\eta)$ and the entropy generation N_G increase. Figures 4.21-4.22 show the impact of Ec. For the increasing values of Ec, the temperature profile $\theta(\eta)$ and the entropy generation N_G increase. Figures 4.23-4.24 show the impact of Bi. For the increasing values of Bi, the temperature profile $\theta(\eta)$ and the entropy generation N_G increase. The shape factor of nanoparticles is an important factor to consider while analysing the system's thermal performance. The shapes of the nanoparticles in the current work include spherical, hexahedron, tetrahedron, column, and lamina. Figures 4.25-4.26 show the impact of m. For the increasing values of m, the temperature profile $\theta(\eta)$ and the entropy generation N_G increase. The effect of Reynolds number Re and Brinkmann number Br on the total volumetric entropy generation rate is depicted in Figures 4.27 and 4.28. In Figure 4.27, it can be observed that the increasing values of Re, the entropy generation N_G increases. Figure 4.28 shows the impact of Re. For the increasing values of Br, the entropy generation N_G increases.

In Figure 4.29, it can be observed that the increasing values of Sc, the increasing values of Sc the concentration profile is decreased. In Figure 4.30, it can be observed that the increasing values of K_1, the increasing values of K_1 the concentration profile is decreased.

TABLE 4.1: Missing conditions of $Re_x^{\frac{1}{2}} C_f$ for $Pr = 6.2$, $m = 3$.

ω	Δ	A	ϕ_1	ϕ_2	Λ	M	T_{f_1}	T_{f_2}
0.1	0.2	0.2	0.03	0	0	0.1	[-1.2, -1.0]	- - - -
0.3							[-1.1, -1.0]	[-1.1, -0.9]
0.5							[-1.1, -0.8]	[-1.1, -0.9]
	2.0						[-1.3, -1.1]	[-1.3, -1.1]
	4.0						[-1.6, -1.3]	[-1.5, -1.3]
		0.3					[-1.2, -1.1]	[-1.2, -1.0]
		0.4					[-1.2, -1.1]	[-1.3, -1.2]
			0.06				[-1.3, -1.0]	[-1.3, -1.0]
			0.09				[-1.3, -1.0]	[-1.3, -1.1]
				0.03			- - - -	[-1.2, -0.9]
				0.06			- - - -	[-1.2, -0.9]
				0.09			- - - -	[-1.2, -0.9]
					0.1		[-1.0, -0.8]	[-1.0, -0.8]
					0.3		[-0.8, -0.7]	[-0.8, -0.6]
						0.2	[-1.3, -1.0]	[-1.3, -1.0]
						0.3	[-1.3, -1.1]	[-1.3, -1.0]

TABLE 4.2: Results of $Re_x^{\frac{1}{2}} C_f$ for $Pr = 6.2$, $m = 3$

ω	Δ	A	ϕ_1	ϕ_2	Λ	M	$Re_x^{\frac{1}{2}} C_f$ $(Cu\text{-}H_2O)$	$Re_x^{\frac{1}{2}} C_f$ $(Al_2O_3\text{-}Cu/H_2O)$
0.1	0.2	0.2	0.03	0	0	0.1	1.3995	- - - -
0.3							1.5047	1.6031
0.5							1.6039	1.7026
	2						1.3698	1.4686
	4						1.3242	1.4259
		0.3					1.4378	1.5388
		0.4					1.4756	1.5792
			0.06				1.5836	1.6828
			0.09				1.7715	1.8728
				0.03			- - - -	1.4979
				0.06			- - - -	1.6021
				0.09			- - - -	1.7129
					0.1		1.1531	1.2624
					0.3		0.9037	0.9738
						0.2	0.9037	1.5496
						0.3	0.9037	1.5995

TABLE 4.3: Results of $Re_x^{-\frac{1}{2}}Nu_x$ for $Pr = 6.2$, $m = 3$

ω	Δ	A	ϕ_1	ϕ_2	Λ	M	ξ	Nr	Ec	Bi	$Re_x^{-\frac{1}{2}}Nu_x$ *(Cu-H_2O)*	$Re_x^{-\frac{1}{2}}Nu_x$ *(Al_2O_3-Cu/H_2O)*
0.1	0.2	0.2	0.03	0	0	0.1	0.01	0.2	0.2	0.2	0.2129	- - - -
0.3											0.2159	0.2323
0.5											0.2183	0.2349
	2										0.2114	0.2274
	4										0.2087	0.2248
		0.3									0.2136	0.2298
		0.4									0.2142	0.2306
			0.06								0.2266	0.2437
			0.09								0.2408	0.2589
				0.03							- - - -	0.2289
				0.06							- - - -	0.2457
				0.09							- - - -	0.2631
					0.1						0.2171	0.2343
					0.3						0.2215	0.2396
						0.2					0.2113	0.2272
						0.3					0.2099	0.2254
							0.2				0.2096	0.2252
							0.3				0.2078	0.2231
								0.5			0.2596	0.2796
								0.8			0.3042	0.3278
									0.4		0.1873	0.1992
									0.6		0.1617	0.1694
										0.1	0.1114	0.1200
										0.3	0.3054	0.3282

TABLE 4.4: Results of Sh for $Pr = 6.2$, $m = 3$

ω	Δ	A	ϕ_1	ϕ_2	Λ	M	Sc	K_1	Sh $(Cu\text{-}H_2O)$	Sh $(Al_2O_3\text{-}Cu/H_2O)$
0.1	0.2	0.2	0.03	0	0	0.2	0.2	0.2	0.5955	- - - -
0.3									0.6065	0.6368
0.5									0.6160	0.6461
	2								0.5920	0.6228
	4								0.5867	0.6178
		0.3							0.5933	0.6238
		0.4							0.5910	0.6214
			0.06						0.6191	0.6524
			0.09						0.6472	0.6832
				0.03					- - - -	0.6161
				0.06					- - - -	0.6600
				0.09					- - - -	0.6975
					0.1				0.5729	0.6004
					0.3				0.5410	0.5648
						0.5			0.5903	0.6207
						0.8			0.5855	0.6155
							0.4		0.9813	1.0316
							0.6		1.3649	1.4336
								0.1	0.8332	0.8706
								0.3	1.2894	1.3428

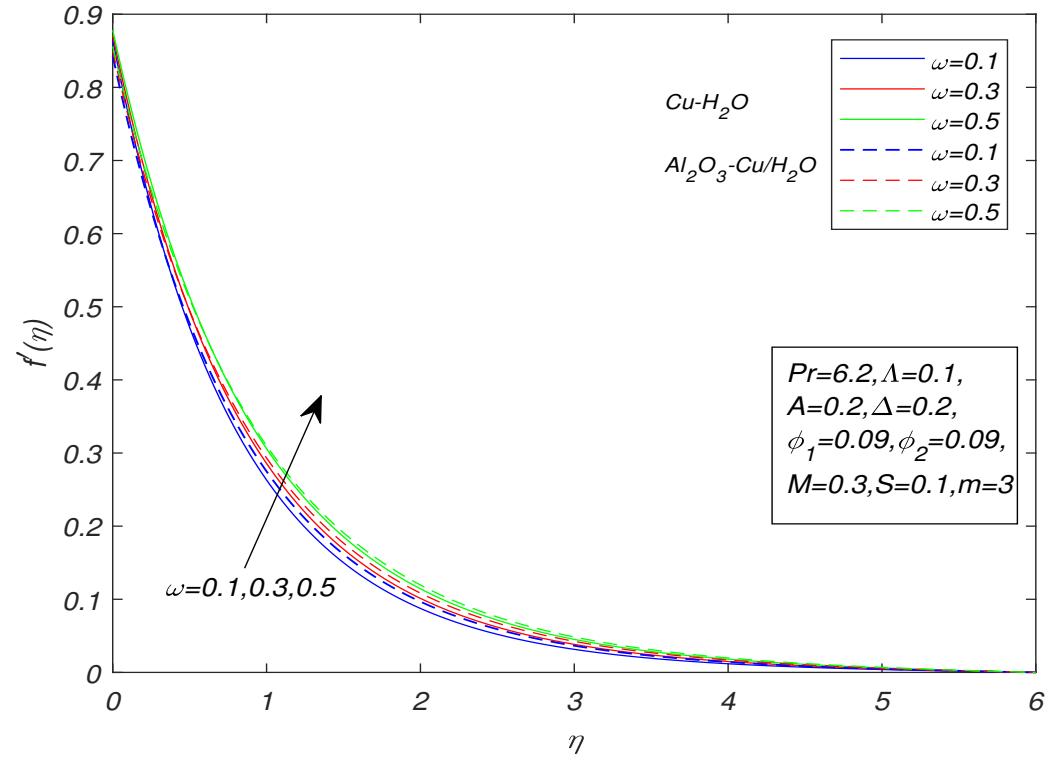

FIGURE 4.2: Velocity profile against ω on $f'(\eta)$ for $Pr = 6.2$.

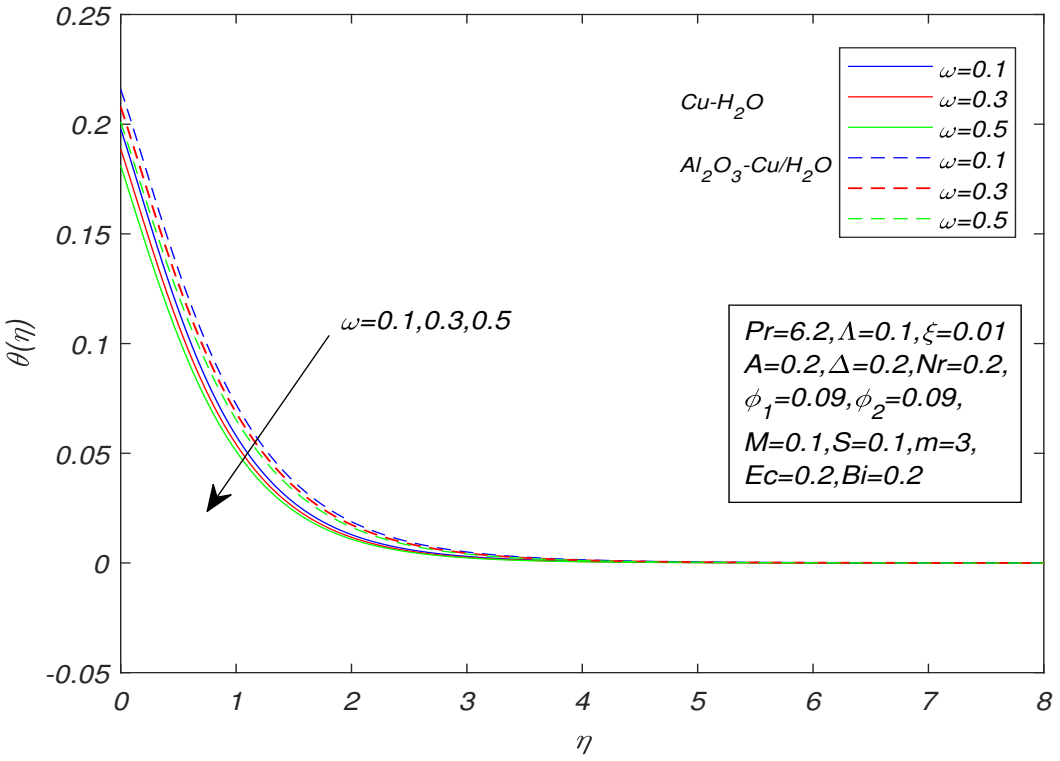

FIGURE 4.3: Temperature profile against ω on $\theta(\eta)$ for $Pr = 6.2$.

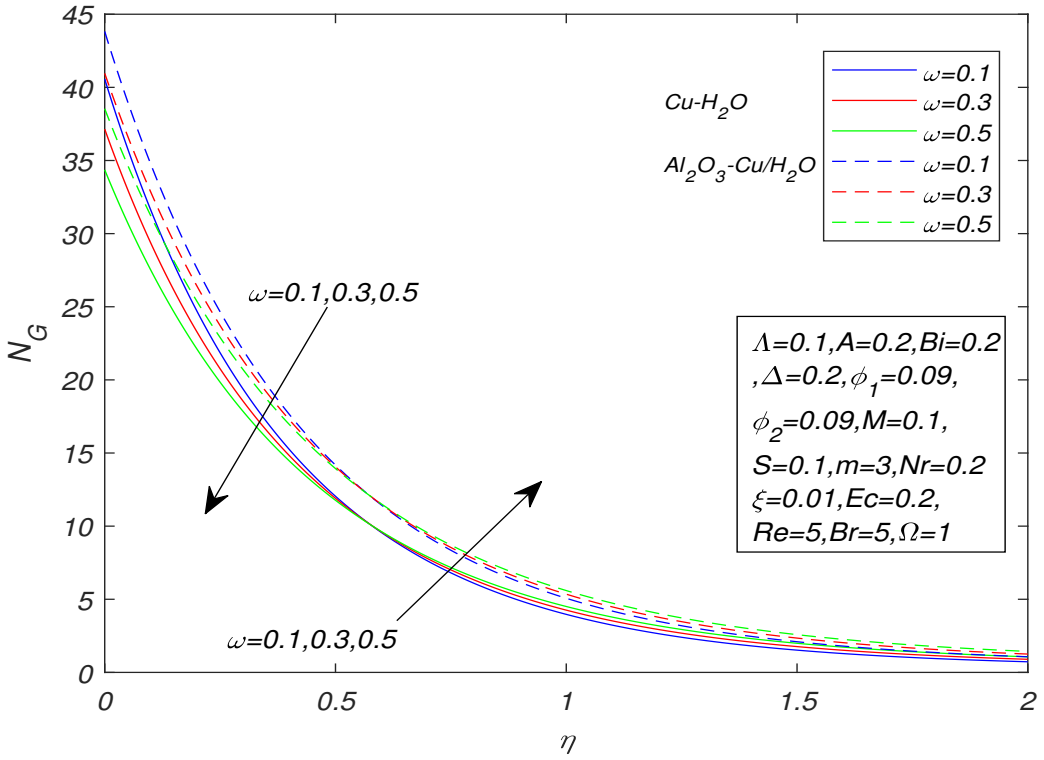

FIGURE 4.4: Entropy profile against ω on N_G for $Pr = 6.2$.

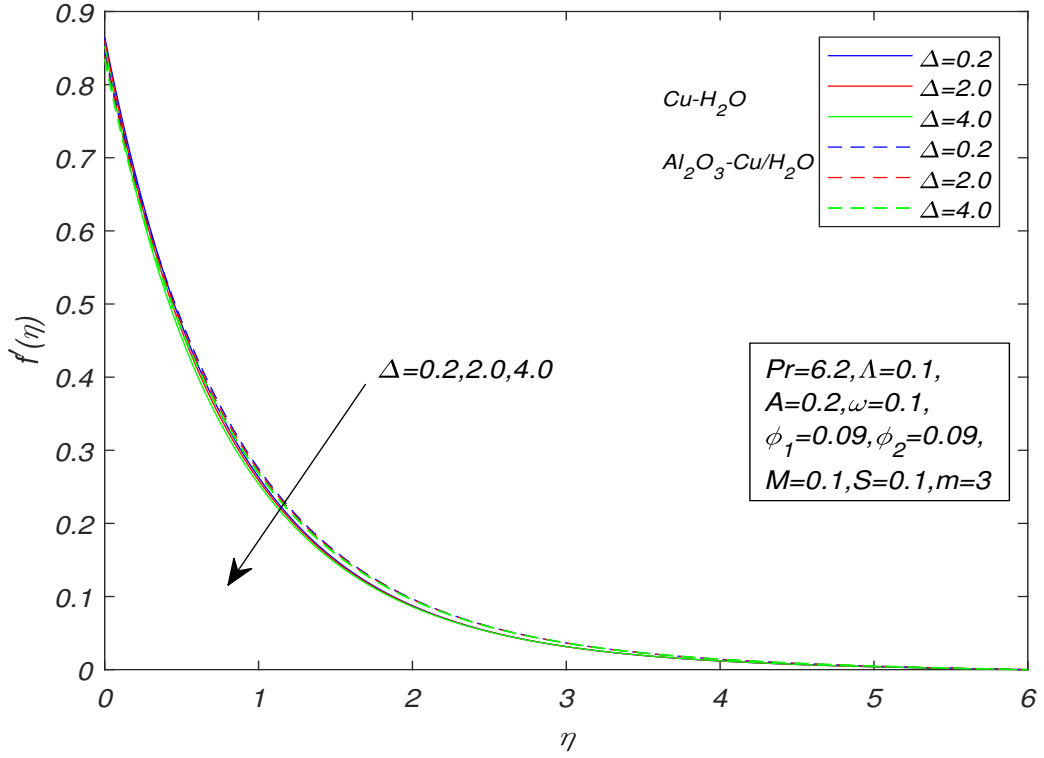

FIGURE 4.5: Velocity profile against Δ on $f'(\eta)$ for $Pr = 6.2$.

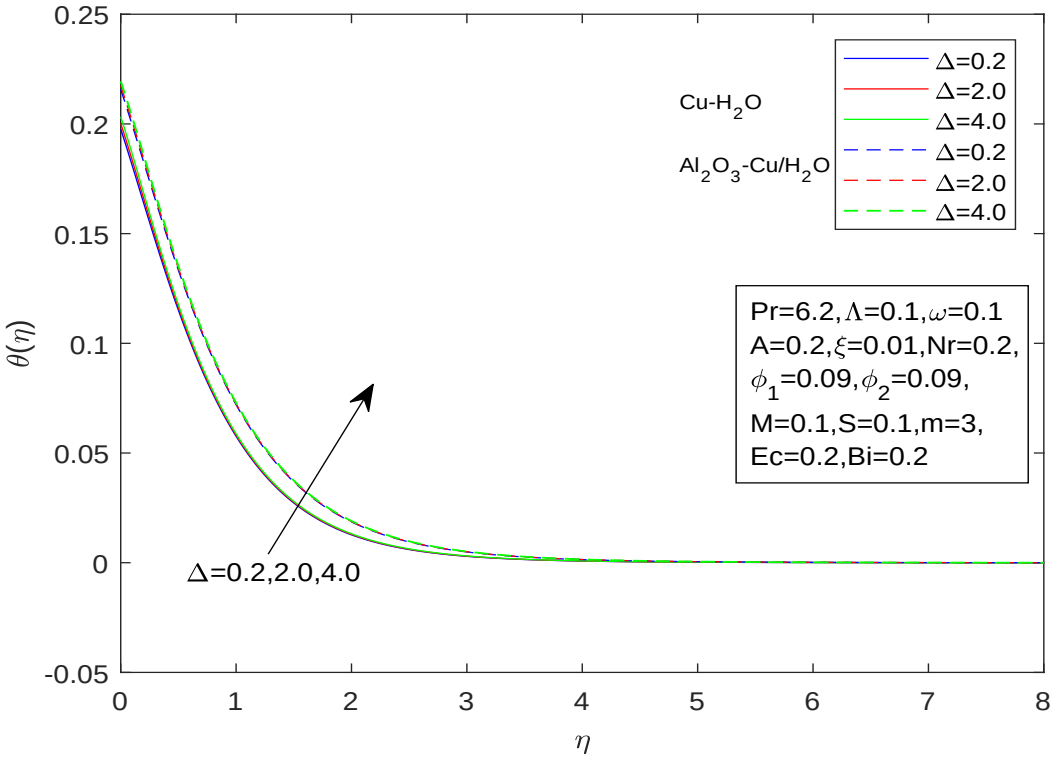

FIGURE 4.6: Temperature profile against Δ on $\theta(\eta)$ for $Pr = 6.2$.

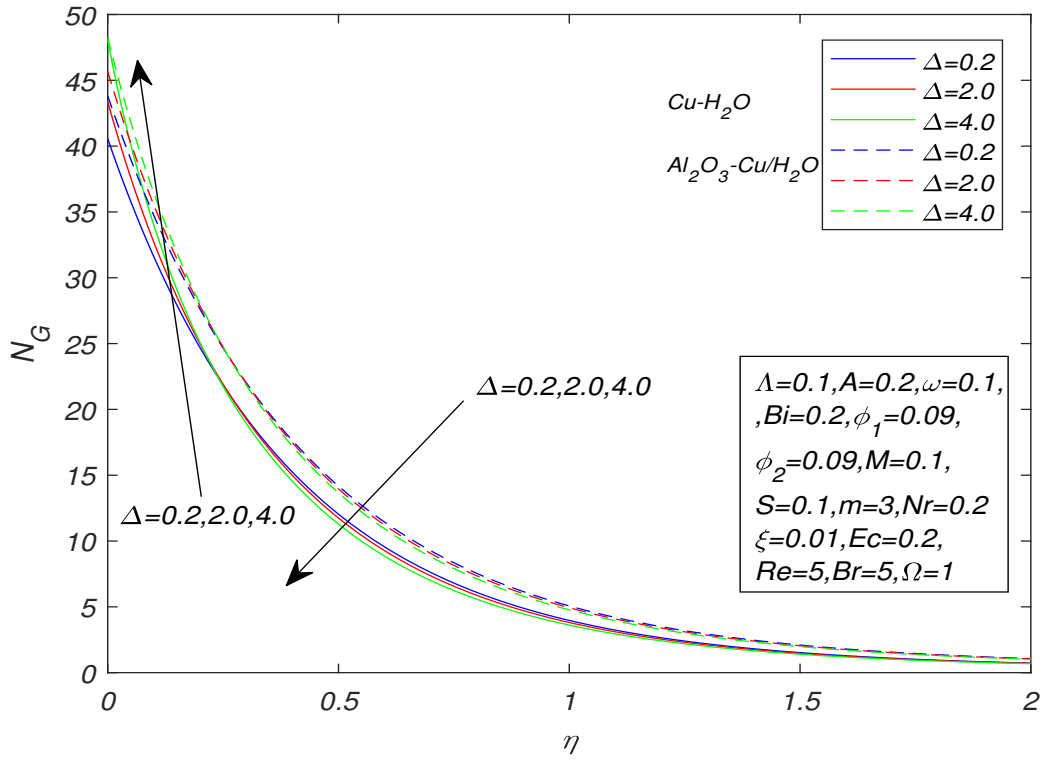

FIGURE 4.7: Entropy profile against Δ on N_G for $Pr = 6.2$.

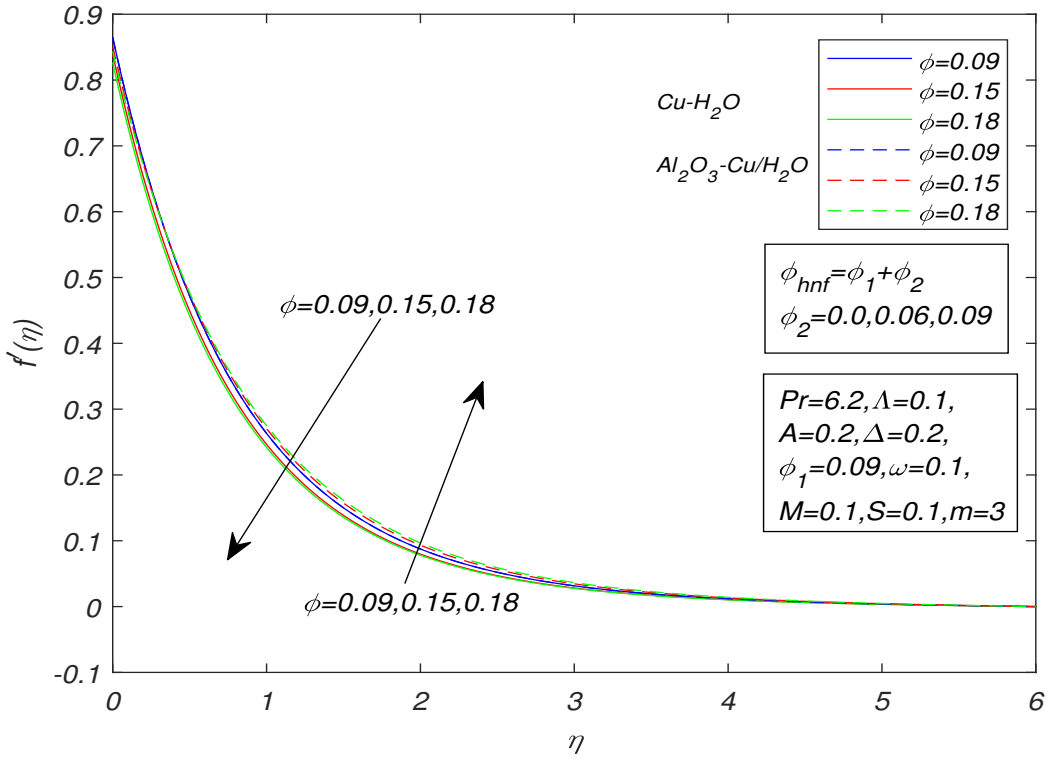

FIGURE 4.8: Velocity profile against ϕ on $f'(\eta)$ for $Pr = 6.2$.

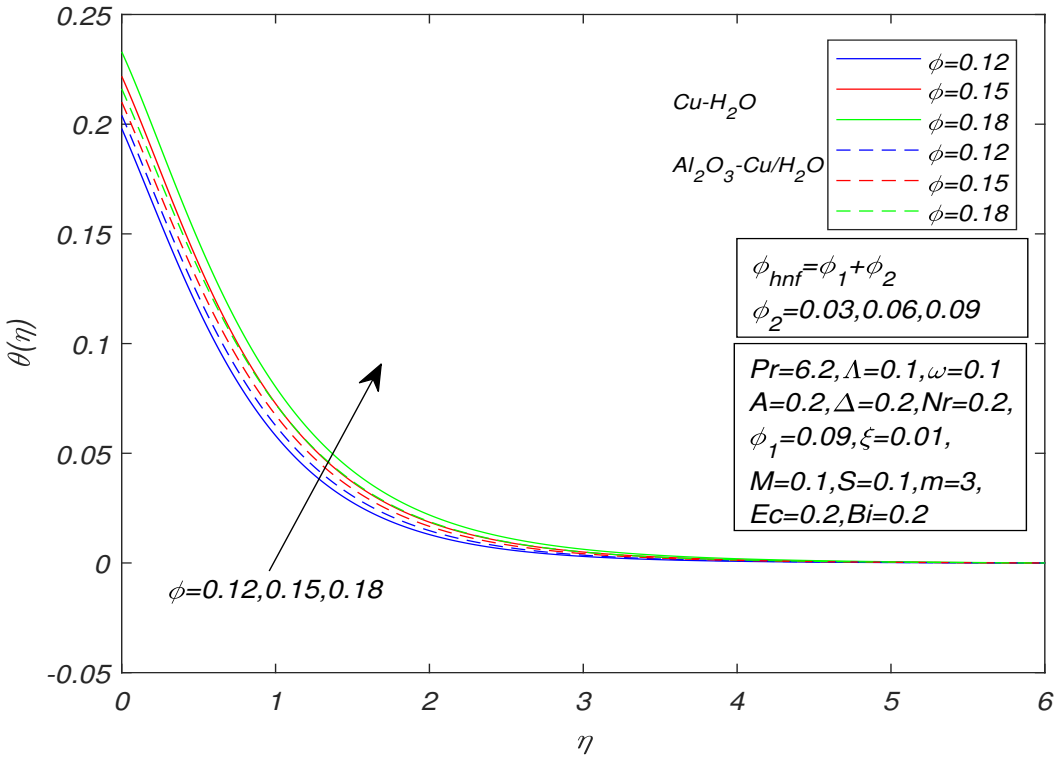

FIGURE 4.9: Temperature profile against ϕ on $\theta(\eta)$ for $Pr = 6.2$.

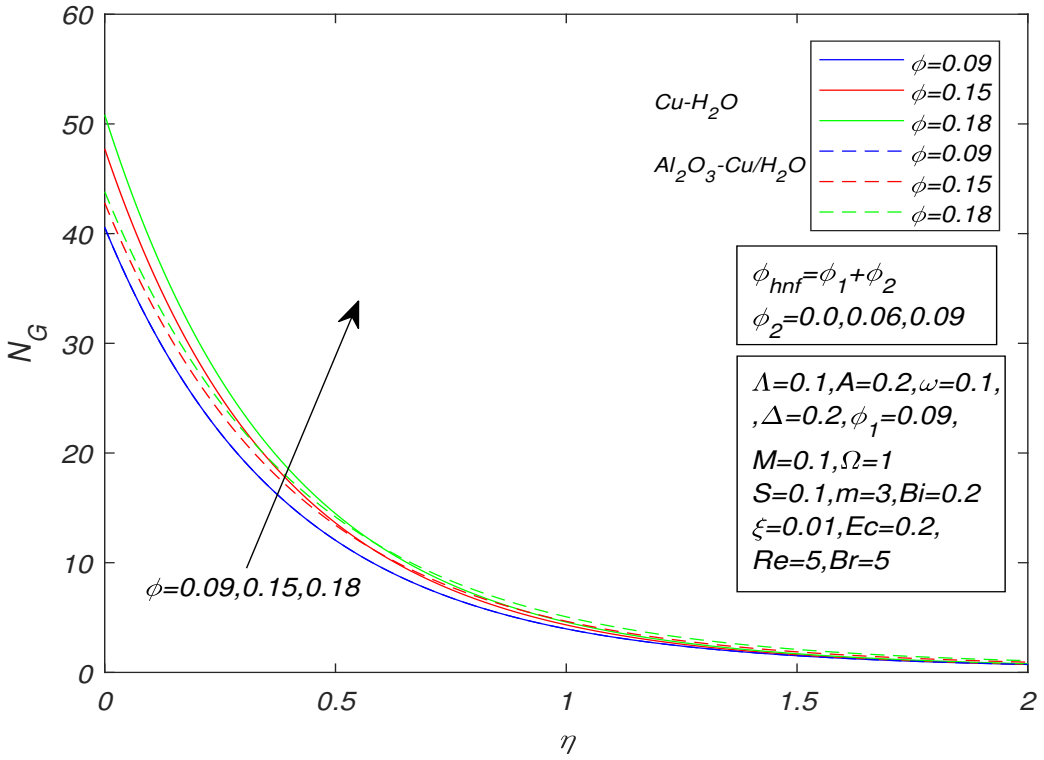

FIGURE 4.10: Entropy profile against ϕ on N_G for $Pr = 6.2$.

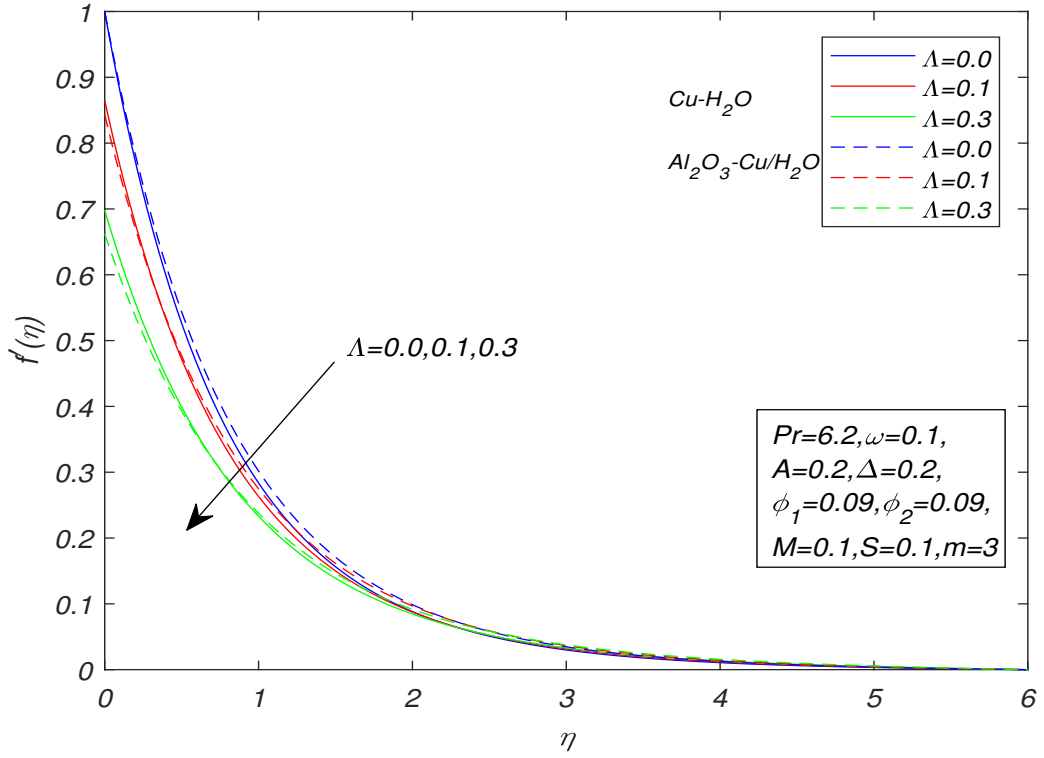

FIGURE 4.11: Velocity profile against Λ on $f'(\eta)$ for $Pr = 6.2$.

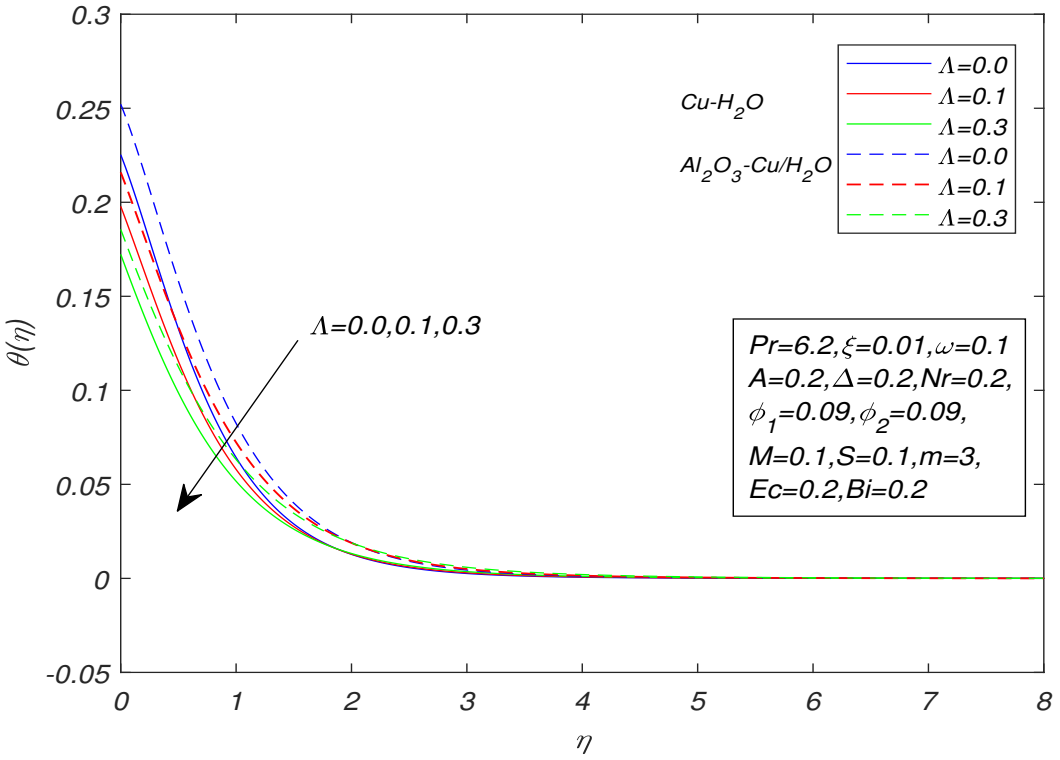

FIGURE 4.12: Temperature profile against Λ on $\theta(\eta)$ for $Pr = 6.2$.

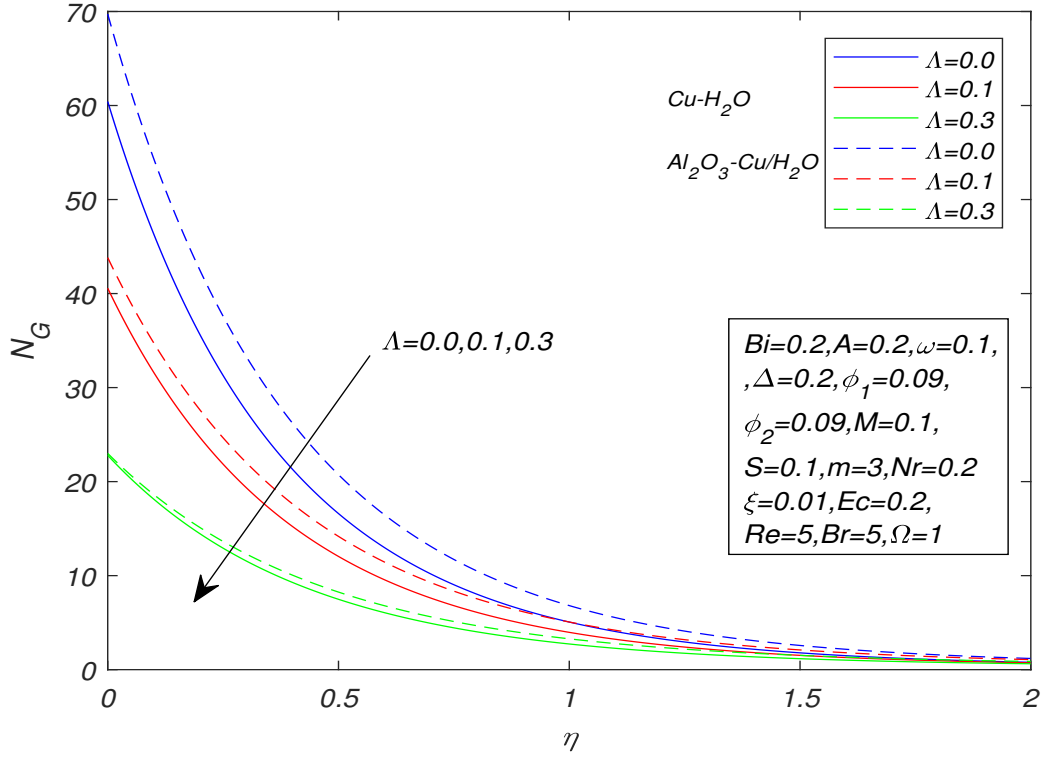

FIGURE 4.13: Entropy profile against Λ on N_G for $Pr = 6.2$.

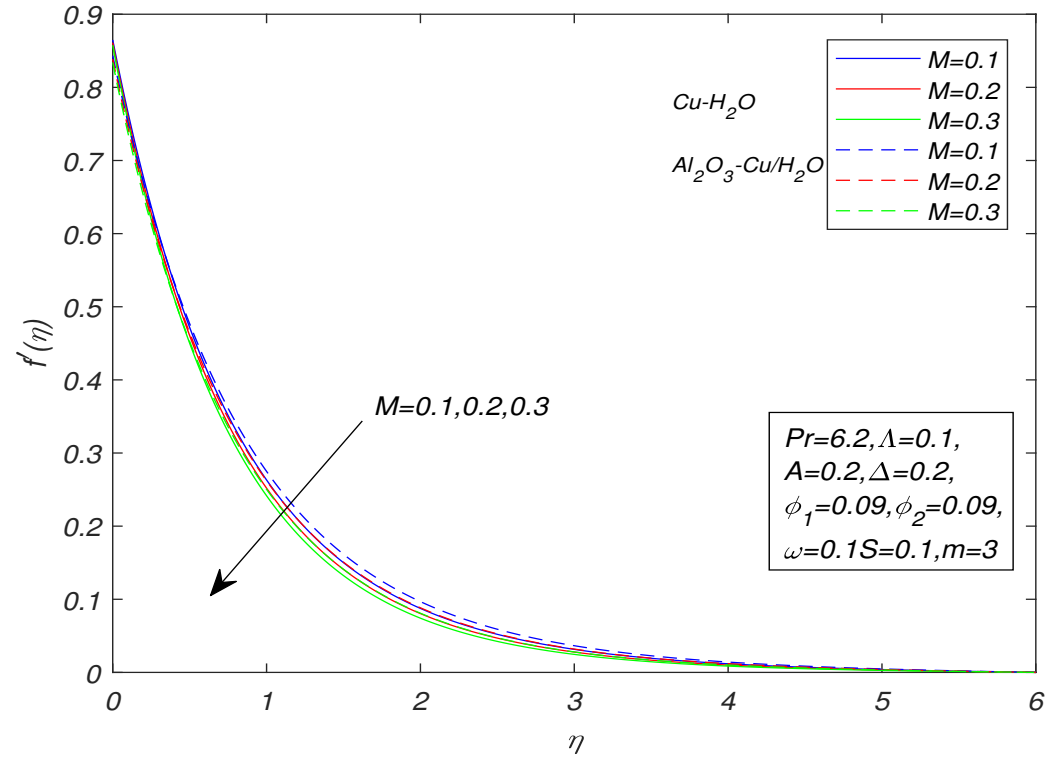

FIGURE 4.14: Velocity profile against M on $f'(\eta)$ for $Pr = 6.2$.

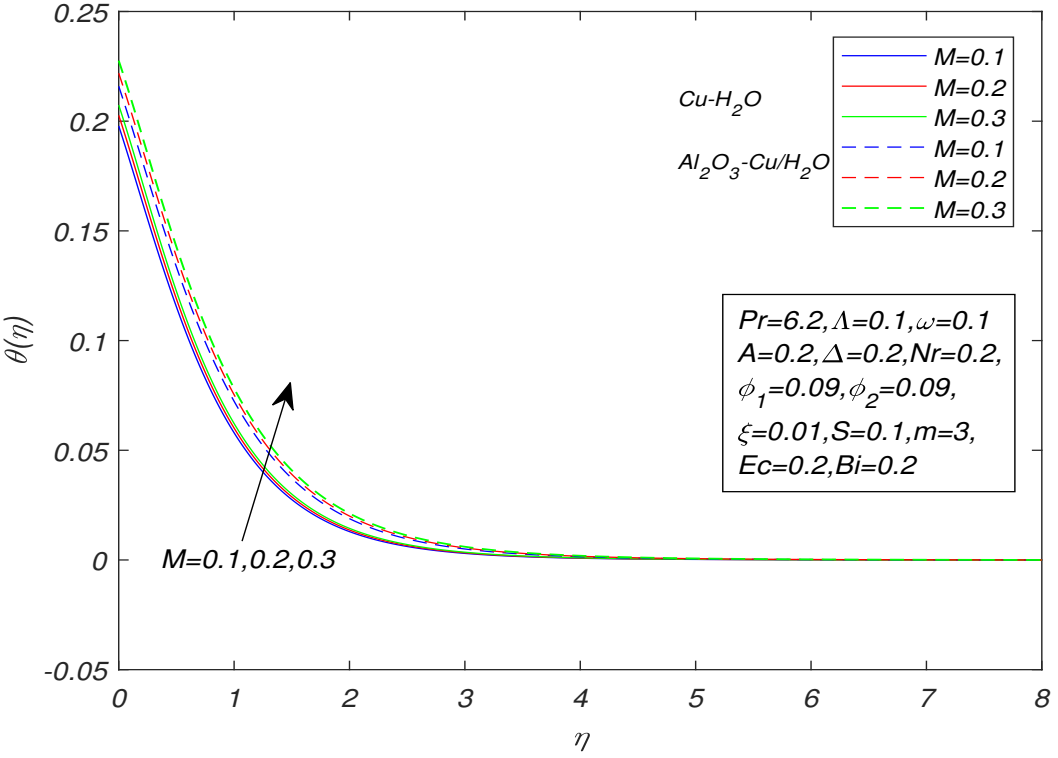

FIGURE 4.15: Temperature profile against M on $\theta(\eta)$ for $Pr = 6.2$.

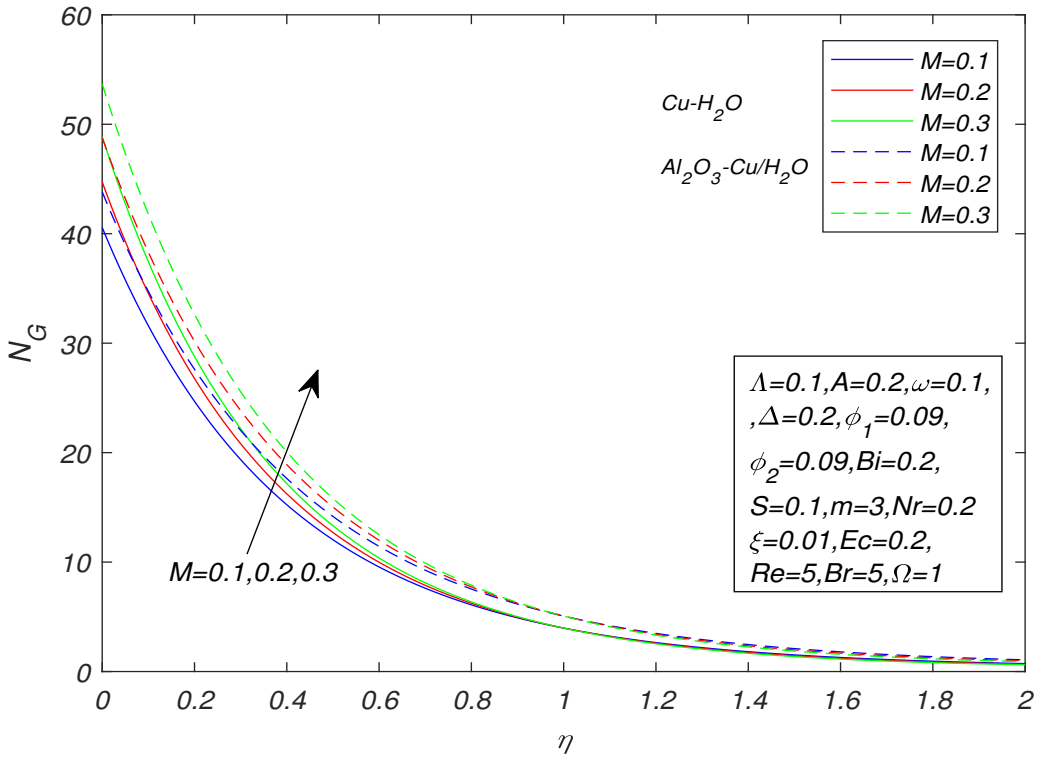

FIGURE 4.16: Entropy profile against M on N_G for $Pr = 6.2$.

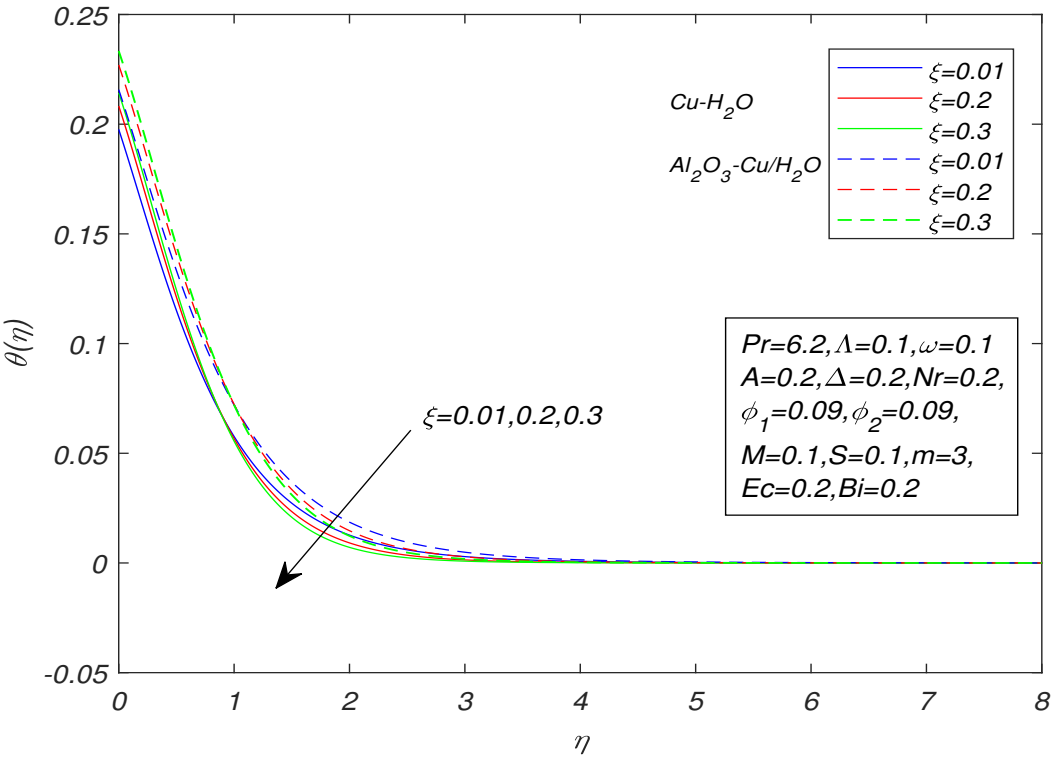

FIGURE 4.17: Temperature profile against ξ on $\theta(\eta)$ for $Pr = 6.2$.

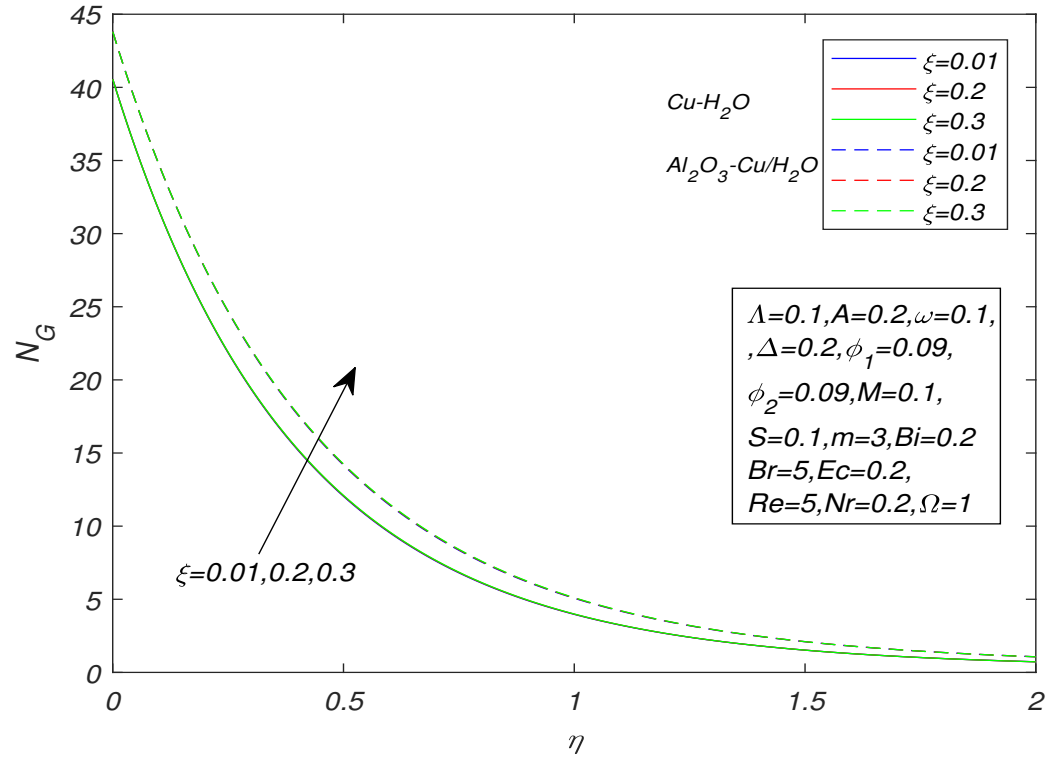

FIGURE 4.18: Entropy profile against ξ on N_G for $Pr = 6.2$.

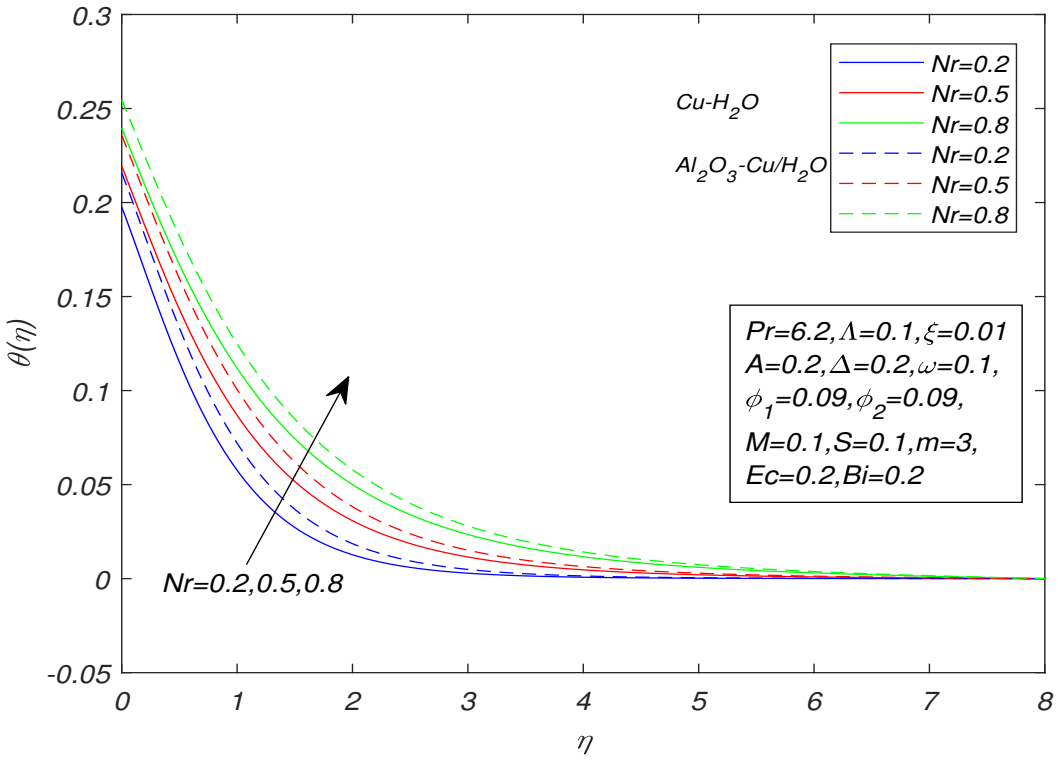

FIGURE 4.19: Temperature profile against Nr on $\theta(\eta)$ for $Pr = 6.2$.

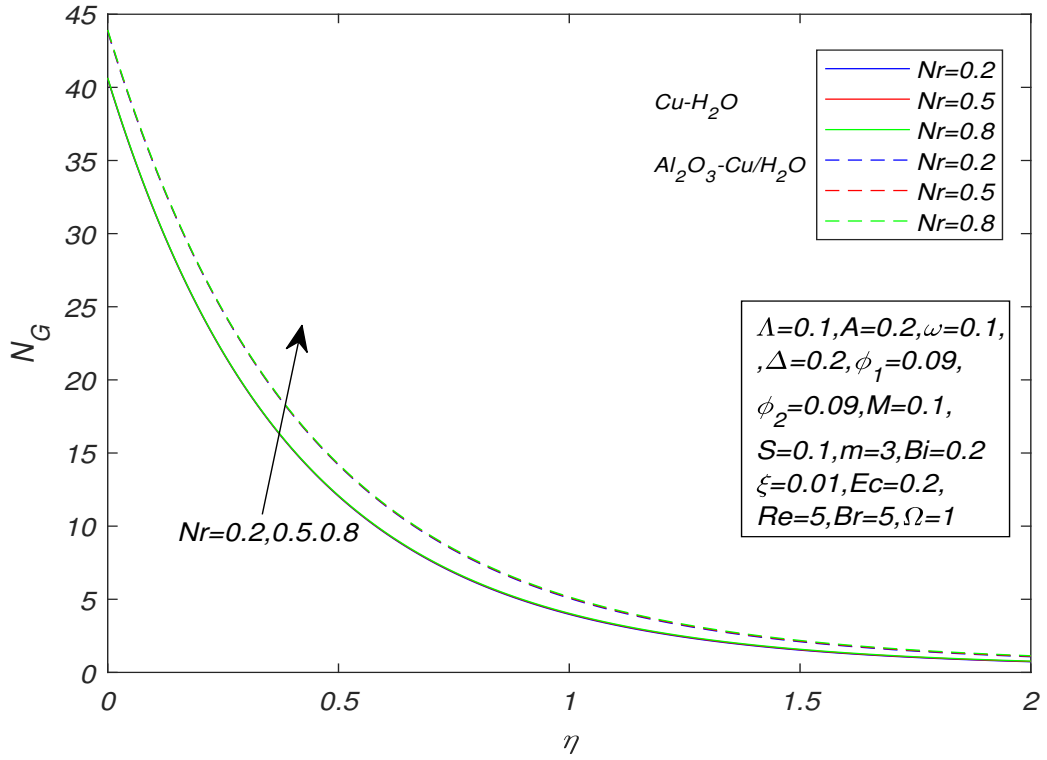

FIGURE 4.20: Entropy profile against Nr on N_G for $Pr = 6.2$.

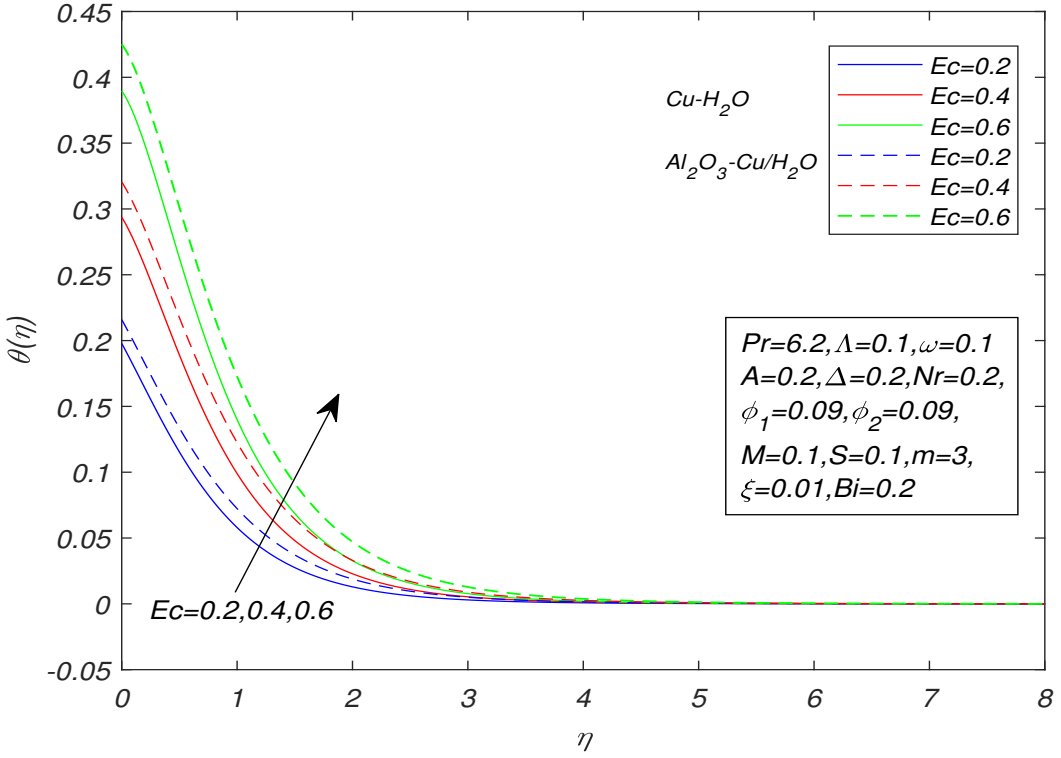

FIGURE 4.21: Temperature profile against Ec on $\theta(\eta)$ for $Pr = 6.2$.

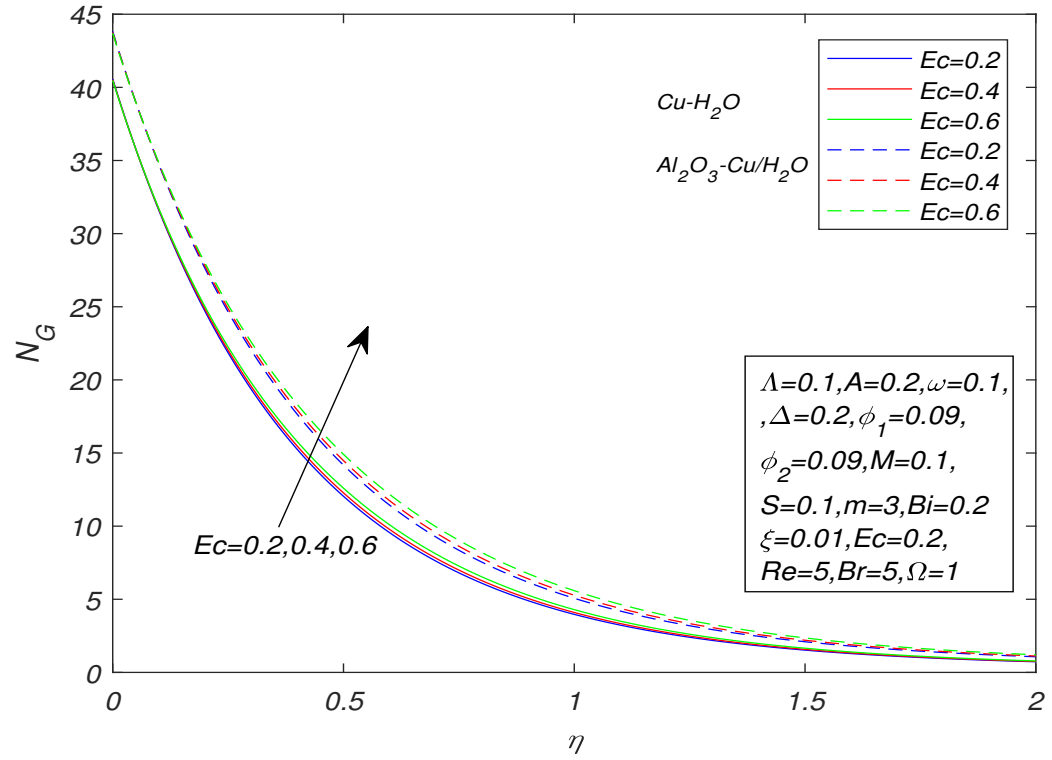

FIGURE 4.22: Entropy profile against Ec on N_G for $Pr = 6.2$.

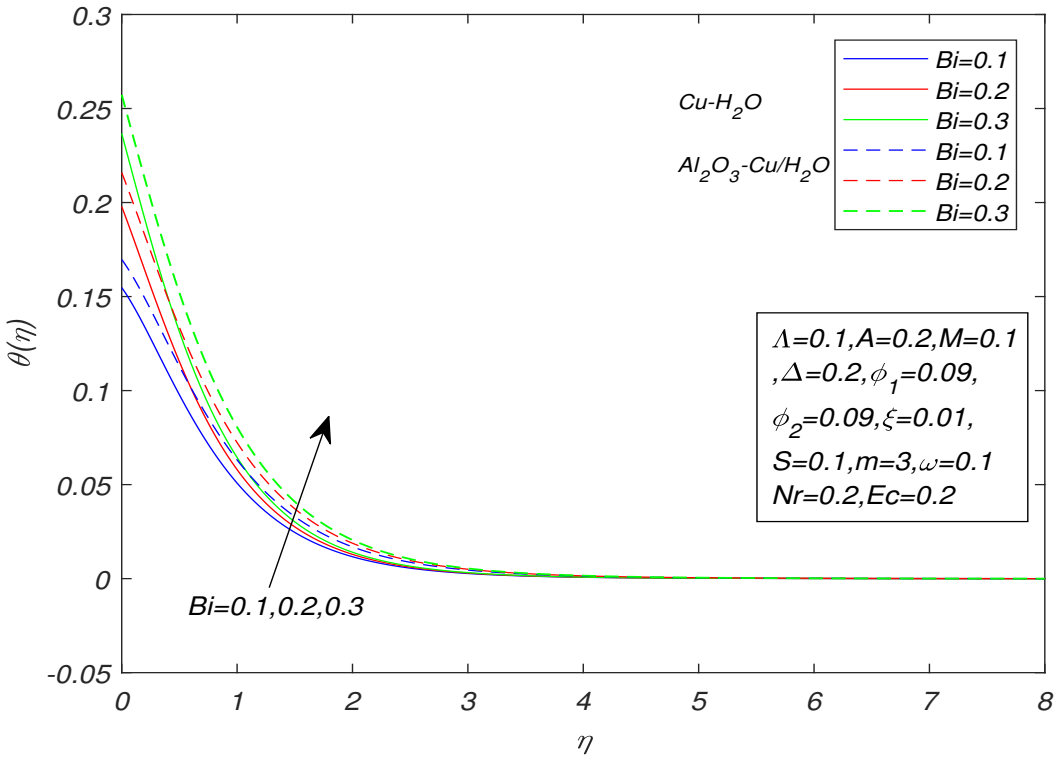

FIGURE 4.23: Temperature profile against Bi on $\theta(\eta)$ for $Pr = 6.2$.

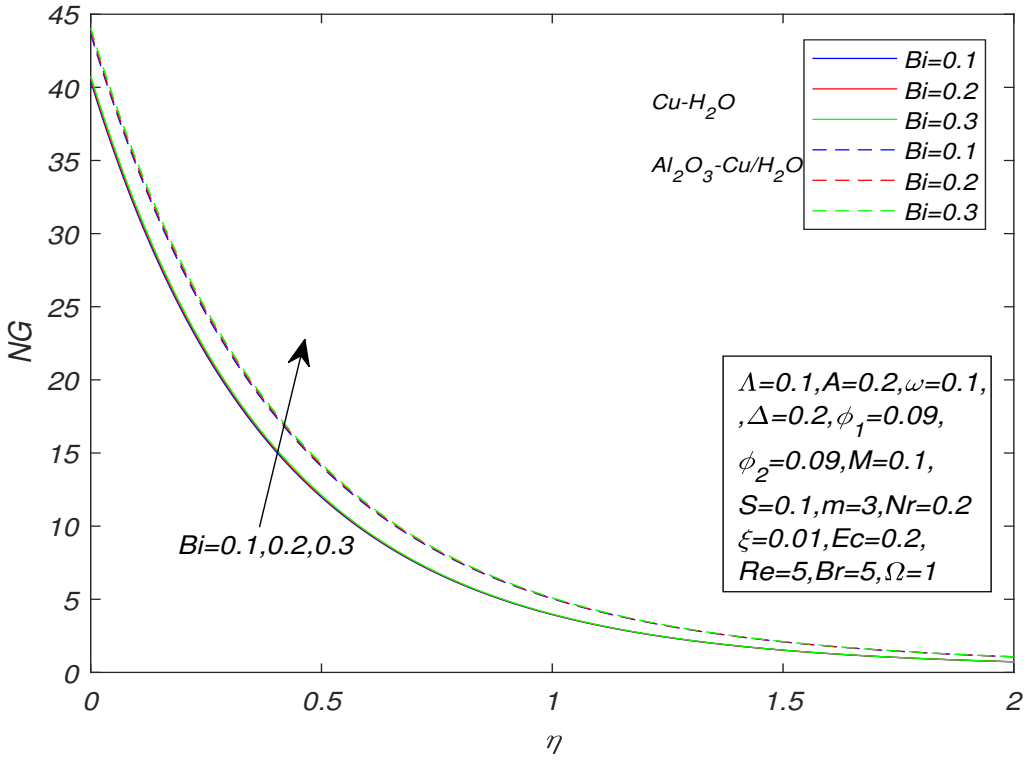

FIGURE 4.24: Entropy profile against Bi on N_G for $Pr = 6.2$.

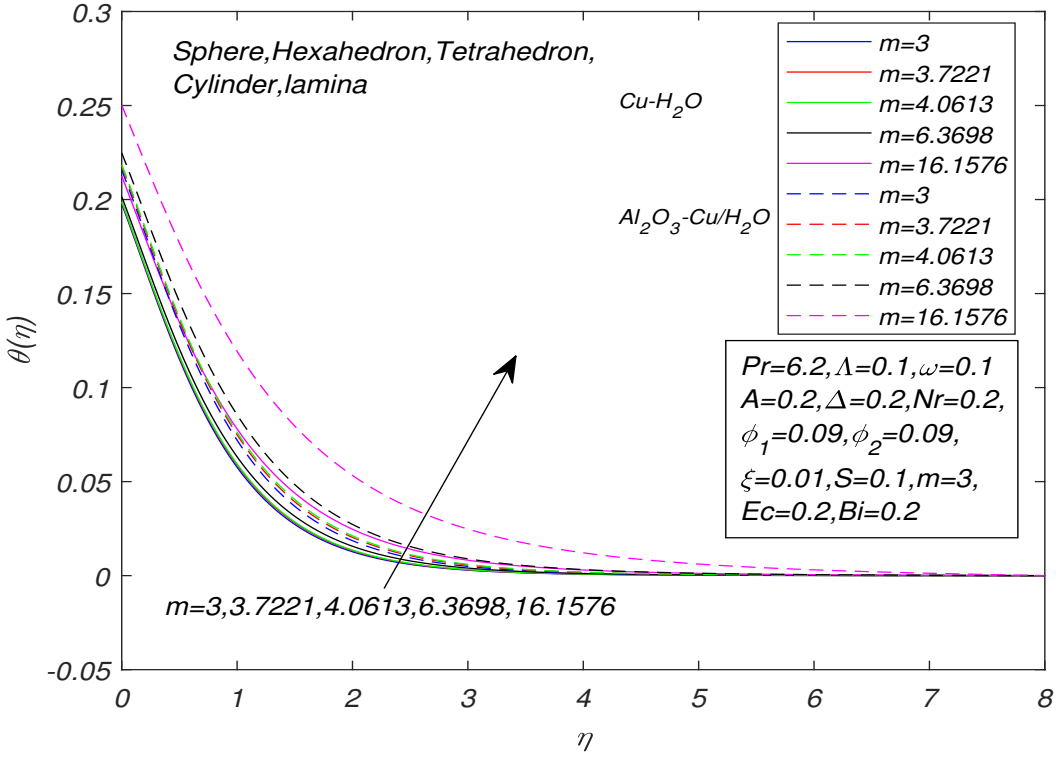

FIGURE 4.25: Temperature profile against m on $\theta(\eta)$ for $Pr = 6.2$.

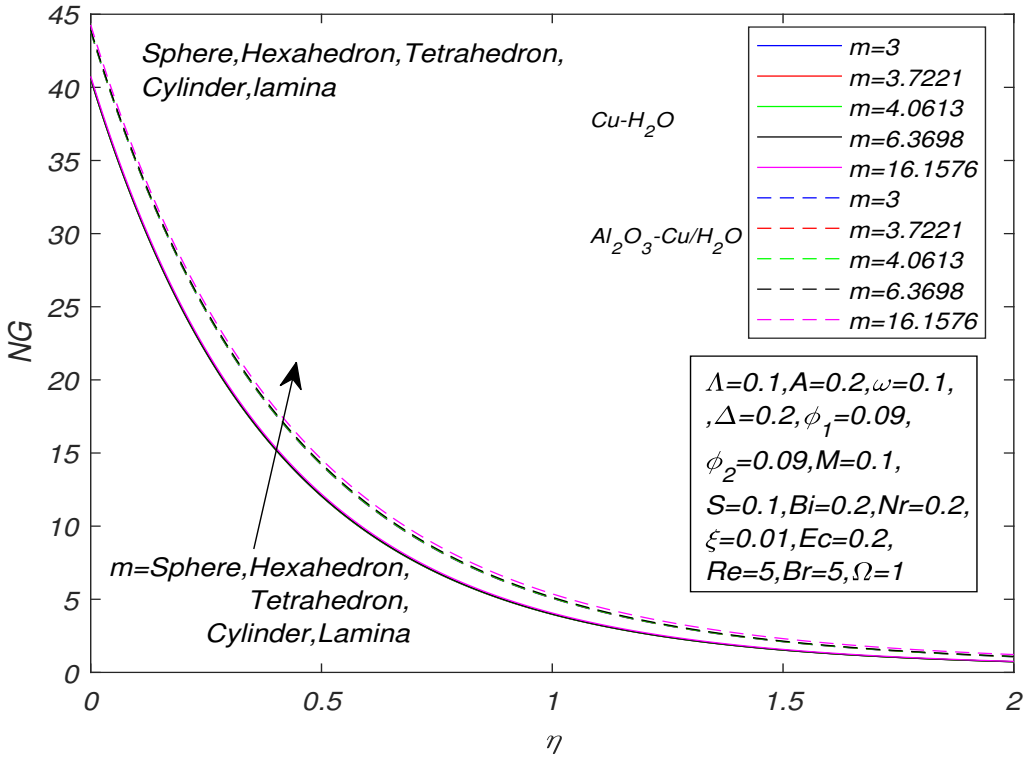

FIGURE 4.26: Entropy profile against m on N_G for $Pr = 6.2$.

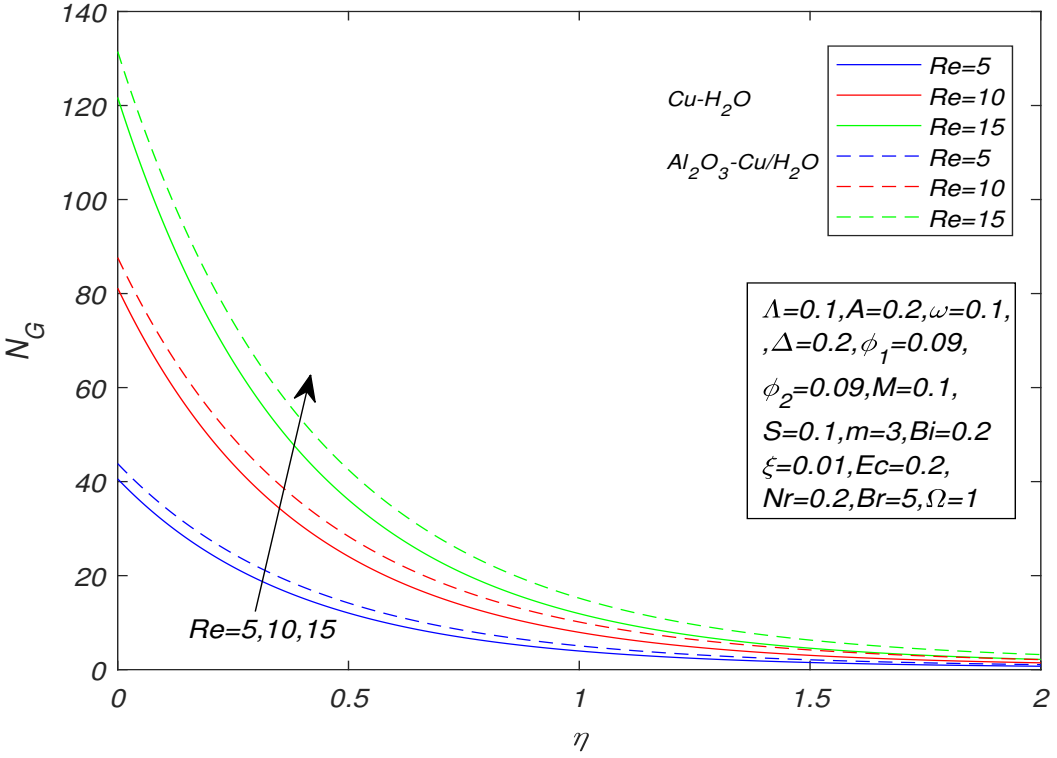

FIGURE 4.27: Entropy profile against Re on N_G for $Pr = 6.2$.

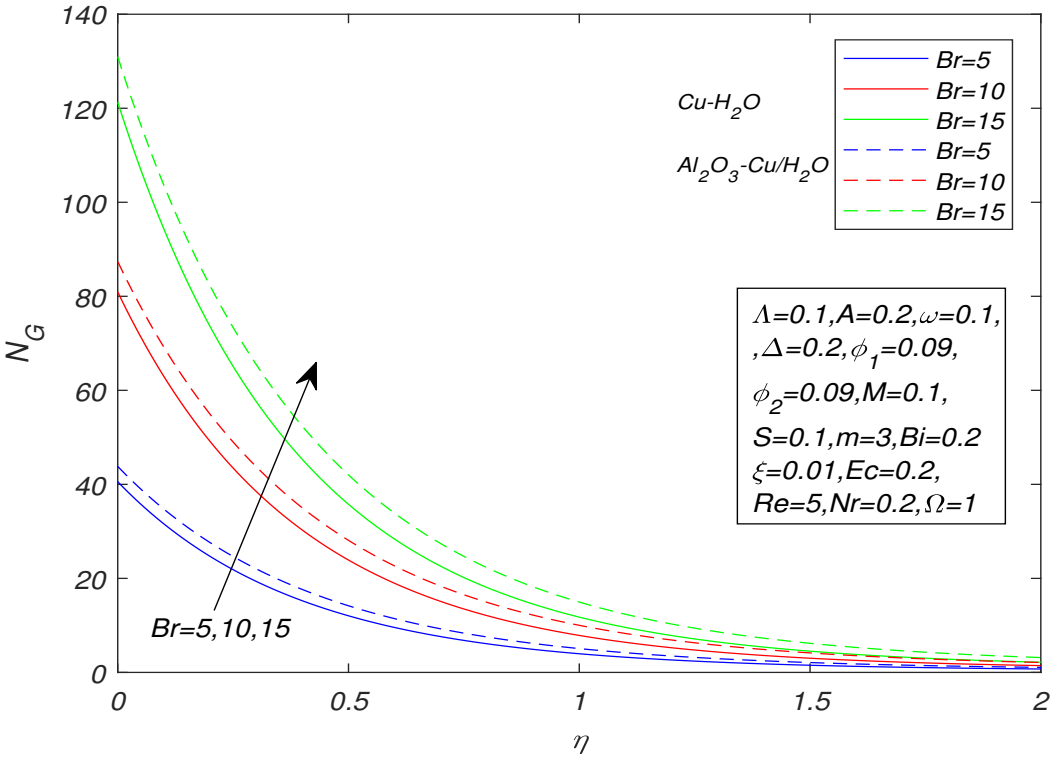

FIGURE 4.28: Entropy profile against Re on N_G for $Pr = 6.2$.

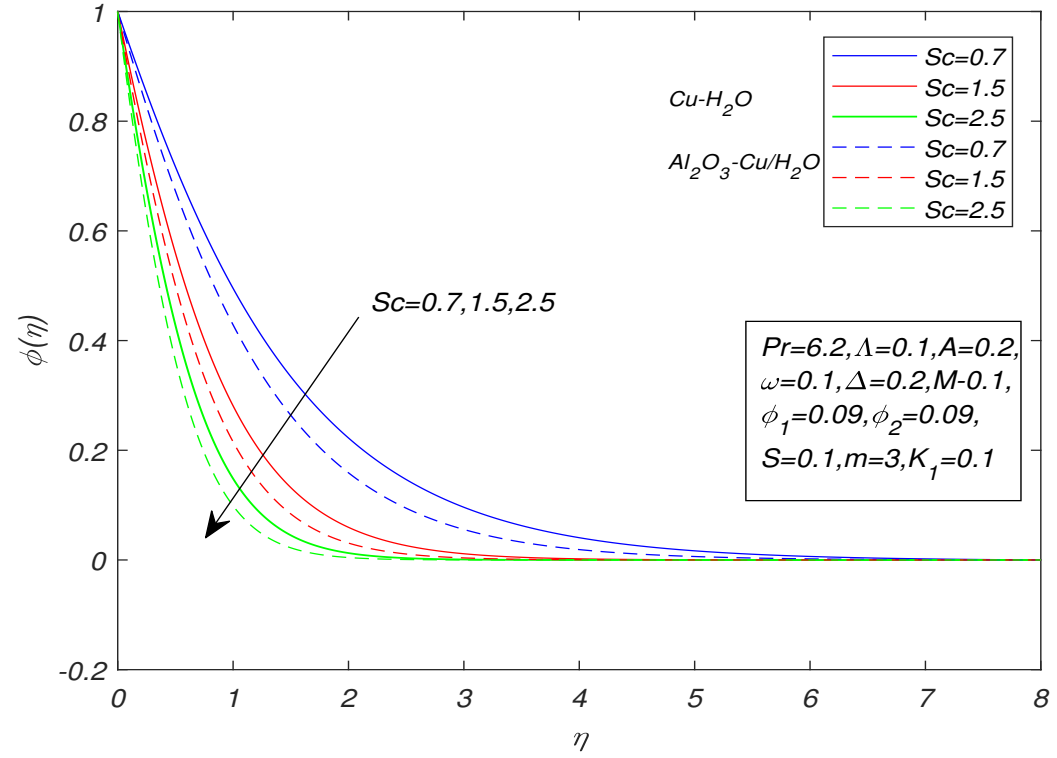

FIGURE 4.29: Concentration profile against Sc on $\phi(\eta)$ for $Pr = 6.2$.

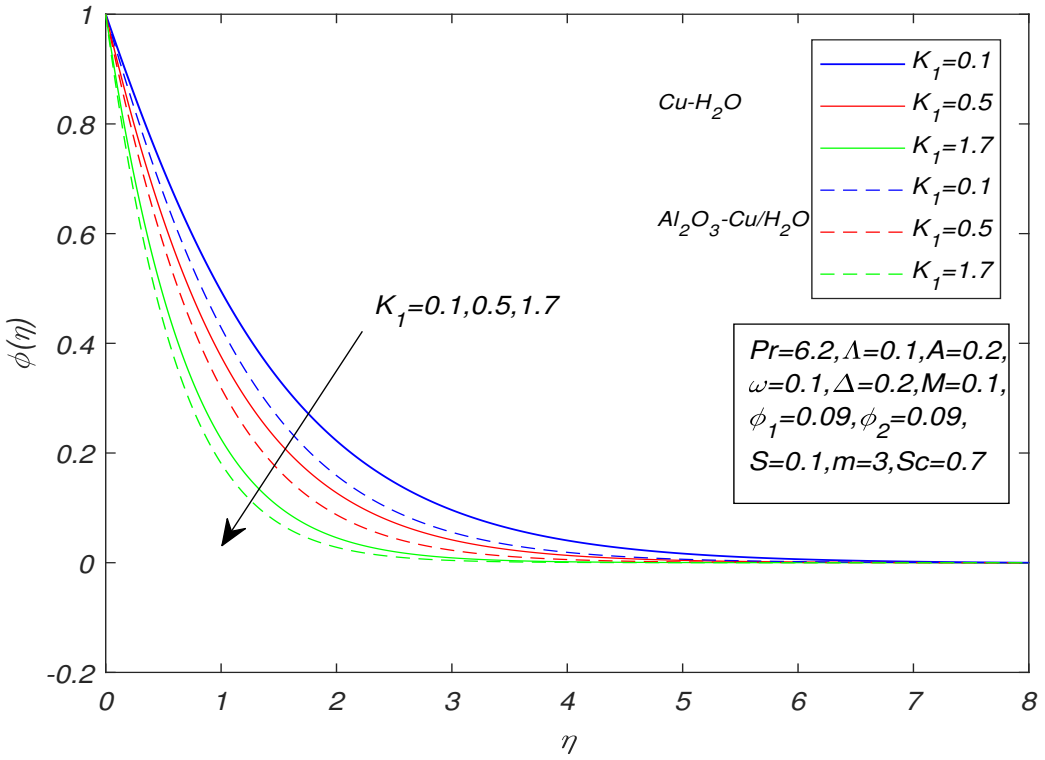

FIGURE 4.30: Concentration profile against K_1 on $\phi(\eta)$ for $Pr = 6.2$.

Chapter 5

Conclusion

In the current study, computational results for entropy generation and heat transfer resulting from Powell-Eyring hybrid nanofluid flow are reported. The nanofluid occupies the space over an infinite porous stretching surface. The boundary layer region is included in the mathematical model along with the effects of viscous dissipation, boundary slip, nanoparticle form, magnetic effects and thermal radiation. Numerical computations are carried for copper water Cu-H_2O nanofluid and aluminacopper water Al_2O_3-Cu/H_2O hybrid nanofluids. To the best of researcher's knowledge, no studies on entropy analysis due to Cattaneo-Christov based study of Powell-Eyring hybrid nanofluid flow have been published so far. The model under consideration here uses a physical mechanism to examine the impact of diffusivity on non-Newtonian hybrid nanofluid flows. The following are the key results of the current work:

- It has been shown that the hybrid Powell-Eyring nanofluid Al_2O_3-Cu/H_2O conducts heat more effectively than the traditional Powell-Eyring nanofluid Cu-H_2O .
- The heat transfer rate rises with the higher concentration of nanoparticles.
- Entropy of the system is observed to rise and fall with a rise in the values of the material parameters ω and Δ.

- Entropy of the system is examined to increase with an increase in the nanoparticle volumetric concentration parameter ϕ and ϕ_{hnf}, relaxation time parameter ξ, magnetic parameter M, thermal radiation parameter Nr, local Eckert number Ec, Biot number Bi, Brinkman number Br and Reynolds number Re but reduces with an increase in the velocity slip parameter Λ.

- The heat transfer rate rises for the larger shape factor m in the boundary layer.

- An increment is noticed in the temperature distribution by rising the values of Eckert number Ec.

- The highest temperature in the boundary layer is found for lamina-shaped particles, whereas the lowest temperature is found for spherical nanoparticles.

- Mass concentration of the system is observed decline with a rise in the values of Schmidt number Sc and chemical reaction number K_1

Bibliography

[1] H. I. Andersson, J. B. Aarseth, and B. S. Dandapat, "Heat transfer in a liquid film on an unsteady stretching surface," *International Journal of Heat and Mass Transfer*, vol. 43, no. 1, pp. 69–74, 2000.

[2] R. Cortell, "Combined effect of viscous dissipation and thermal radiation on fluid flows over a non-linearly stretched permeable wall," *Meccanica*, vol. 47, no. 3, pp. 769–781, 2012.

[3] H. M. Ali, M. M. Janjua, U. Sajjad, and W.-M. Yan, "A critical review on heat transfer augmentation of phase change materials embedded with porous materials/foams," *International Journal of Heat and Mass Transfer*, vol. 135, pp. 649–673, 2019.

[4] S. Ghadikolaei, K. Hosseinzadeh, M. Yassari, H. Sadeghi, and D. Ganji, "Analytical and numerical solution of non-newtonian second-grade fluid flow on a stretching sheet," *Thermal Science and Engineering Progress*, vol. 5, pp. 309–316, 2018.

[5] A. Rasheed and M. S. Anwar, "Simulations of variable concentration aspects in a fractional nonlinear viscoelastic fluid flow," *Communications in Nonlinear Science and Numerical Simulation*, vol. 65, pp. 216–230, 2018.

[6] A. R. Rahmati, O. A. Akbari, A. Marzban, D. Toghraie, R. Karimi, and F. Pourfattah, "Simultaneous investigations the effects of non-newtonian nanofluid flow in different volume fractions of solid nanoparticles with slip and no-slip boundary conditions," *Thermal Science and Engineering Progress*, vol. 5, pp. 263–277, 2018.

[7] H. M. Ali, A. Saieed, W. Pao, and M. Ali, "Copper foam/pcms based heat sinks: an experimental study for electronic cooling systems," *International Journal of Heat and Mass Transfer*, vol. 127, pp. 381–393, 2018.

[8] A. Rasheed and M. S. Anwar, "Interplay of chemical reacting species in a fractional viscoelastic fluid flow," *Journal of Molecular Liquids*, vol. 273, pp. 576–588, 2019.

[9] M. Sajawal, T.-U. Rehman, H. M. Ali, U. Sajjad, A. Raza, and M. S. Bhatti, "Experimental thermal performance analysis of finned tube-phase change material based double pass solar air heater," *Case Studies in Thermal Engineering*, vol. 15, p. 100543, 2019.

[10] T.-U. Rehman and H. M. Ali, "Thermal performance analysis of metallic foam-based heat sinks embedded with RT-54HC paraffin: an experimental investigation for electronic cooling," *Journal of Thermal Analysis and Calorimetry*, vol. 140, no. 3, pp. 979–990, 2020.

[11] H. M. Ali, "Experimental study on the thermal behavior of RT-35HC paraffin within Copper and Iron-Nickel open cell foams: energy storage for thermal management of electronics," *International Journal of Heat and Mass Transfer*, vol. 146, p. 118852, 2020.

[12] S. U. Choi and J. A. Eastman, "Enhancing thermal conductivity of fluids with nanoparticles," tech. rep., Argonne National Lab.(ANL), Argonne, IL (United States), 1995.

[13] J. Qing, M. M. Bhatti, M. A. Abbas, M. M. Rashidi, and M. E.-S. Ali, "Entropy generation on MHD Casson nanofluid flow over a porous stretching/shrinking surface," *Entropy*, vol. 18, no. 4, p. 123, 2016.

[14] T. Aziz, A. Aziz, and C. Khalique, "Exact solutions for stokes flow of a non-newtonian nanofluid model: a lie similarity approach," *Zeitschrift für Naturforschung A*, vol. 71, no. 7, pp. 621–630, 2016.

[15] D. MD Tausif, K. Das, and P. K. Kundu, "Presence of different shapes of ZrO_2 nanoparticles in the melting heat transfer of a Casson flow," *The European Physical Journal Plus*, vol. 132, no. 10, pp. 1–14, 2017.

[16] M. M. Bhatti, T. Abbas, M. M. Rashidi, M. E.-S. Ali, and Z. Yang, "Entropy generation on MHD Powell-Eyring nanofluid through a permeable stretching surface," *Entropy*, vol. 18, no. 6, p. 224, 2016.

[17] O. Koriko, I. Animasaun, M. G. Reddy, and N. Sandeep, "Scrutinization of thermal stratification, nonlinear thermal radiation and quartic autocatalytic chemical reaction effects on the flow of three-dimensional Powell-Eyring Alumina-Water nanofluid," *Multidiscipline Modeling in Materials and Structures*, 2017.

[18] A. Aziz and W. Jamshed, "Unsteady mhd slip flow of non-newtonian power-law nanofluid over a moving surface with temperature dependent thermal conductivity," *Discrete & Continuous Dynamical Systems-S*, vol. 11, no. 4, p. 617, 2018.

[19] S. Qayyum, T. Hayat, and A. Alsaedi, "Thermal radiation and heat generation/absorption aspects in third grade magneto-nanofluid over a slendering stretching sheet with newtonian conditions," *Physica B: Condensed Matter*, vol. 537, pp. 139–149, 2018.

[20] N. Justh, B. Berke, K. László, and I. M. Szilágyi, "Thermal analysis of the improved hummers synthesis of graphene oxide," *Journal of Thermal Analysis and Calorimetry*, vol. 131, no. 3, pp. 2267–2272, 2018.

[21] F. Selimefendigil and A. J. Chamkha, "Magnetohydrodynamics mixed convection in a power law nanofluid-filled triangular cavity with an opening using tiwari and das nanofluid model," *Journal of Thermal Analysis and Calorimetry*, vol. 135, no. 1, pp. 419–436, 2019.

[22] A. Aziz, W. Jamshed, T. Aziz, H. Bahaidarah, and K. Ur Rehman, "Entropy analysis of Powell–Eyring hybrid nanofluid including effect of linear

thermal radiation and viscous dissipation," *Journal of Thermal Analysis and Calorimetry*, vol. 143, no. 2, pp. 1331–1343, 2021.

[23] N. Akram, R. Sadri, S. Kazi, M. N. M. Zubir, M. Ridha, W. Ahmed, M. E. M. Soudagar, and M. Arzpeyma, "A comprehensive review on nanofluid operated solar flat plate collectors," *Journal of Thermal Analysis and Calorimetry*, vol. 139, no. 2, pp. 1309–1343, 2020.

[24] S. Suresh, K. Venkitaraj, P. Selvakumar, and M. Chandrasekar, "Experimental investigation of mixed convection with synthesis of Al_2O_3-Water hybrid nanofluids using two step method and its thermo physical properties," *Colloids Surface*, vol. 8, pp. 41–48, 2011.

[25] S. S. U. Devi and S. A. Devi, "Numerical investigation of three-dimensional hybrid $Cu-Al_2O_3$/Water nanofluid flow over a stretching sheet with effecting lorentz force subject to newtonian heating," *Canadian Journal of Physics*, vol. 94, no. 5, pp. 490–496, 2016.

[26] S. A. Devi and S. S. U. Devi, "Numerical investigation of hydromagnetic hybrid $Cu - Al_2O_3$/Water nanofluid flow over a permeable stretching sheet with suction," *International Journal of Nonlinear Sciences and Numerical Simulation*, vol. 17, no. 5, pp. 249–257, 2016.

[27] M. Afrand, D. Toghraie, and B. Ruhani, "Effects of temperature and nanoparticles concentration on rheological behavior of $Fe_3O_4 - Ag/EG$ hybrid nanofluid: an experimental study," *Experimental Thermal and Fluid Science*, vol. 77, pp. 38–44, 2016.

[28] S. Hussain, S. E. Ahmed, and T. Akbar, "Entropy generation analysis in MHD mixed convection of hybrid nanofluid in an open cavity with a horizontal channel containing an adiabatic obstacle," *International Journal of Heat and Mass Transfer*, vol. 114, pp. 1054–1066, 2017.

[29] N. Acharya, R. Bag, and P. K. Kundu, "Influence of hall current on radiative nanofluid flow over a spinning disk: a hybrid approach," *Physica E: Low-dimensional Systems and Nanostructures*, vol. 111, pp. 103–112, 2019.

[30] M. M. Maskeen, A. Zeeshan, O. U. Mehmood, and M. Hassan, "Heat transfer enhancement in hydromagnetic Alumina-Copper/Water hybrid nanofluid flow over a stretching cylinder," *Journal of Thermal Analysis and Calorimetry*, vol. 138, no. 2, pp. 1127–1136, 2019.

[31] A. Aziz, W. Jamshed, T. Aziz, H. Bahaidarah, and K. Ur Rehman, "Entropy analysis of Powell-Eyring hybrid nanofluid including effect of linear thermal radiation and viscous dissipation," *Journal of Thermal Analysis and Calorimetry*, vol. 143, no. 2, pp. 1331–1343, 2021.

[32] S. Ghadikolaei, M. Yassari, H. Sadeghi, K. Hosseinzadeh, and D. Ganji, "Investigation on thermophysical properties of $TiO_2 - Cu/H_2O$ hybrid nanofluid transport dependent on shape factor in mhd stagnation point flow," *Powder Technology*, vol. 322, pp. 428–438, 2017.

[33] W. Jamshed and A. Aziz, "Cattaneo–Christov based study of $TiO_2 - CuO/EG$ Casson hybrid nanofluid flow over a stretching surface with entropy generation," *Applied Nanoscience*, vol. 8, no. 4, pp. 685–698, 2018.

[34] U. Nazir, N. H. Abu-Hamdeh, M. Nawaz, S. O. Alharbi, and W. Khan, "Numerical study of thermal and mass enhancement in the flow of carreau-yasuda fluid with hybrid nanoparticles," *Case Studies in Thermal Engineering*, vol. 27, p. 101256, 2021.

[35] R. W. Fox, A. McDonald, and P. Pitchard, "Introduction to fluid mechanics, 2004," 2006.

[36] R. Bansal, *A Textbook of Fluid Mechanics*. Firewall Media, 2005.

[37] J. N. Reddy and D. K. Gartling, *The Finite Element Method in Heat Transfer and Fluid Dynamics*. CRC press, 2010.

[38] P. A. Davidson and A. Thess, *Magnetohydrodynamics*, vol. 418. Springer Science & Business Media, 2002.

[39] M. Gad-el Hak, *Advances in Fluid Mechanics Measurements*, vol. 45. Springer Science & Business Media, 2013.

[40] R. W. Lewis, P. Nithiarasu, and K. N. Seetharamu, *Fundamentals of the Finite Element Method For Heat and Fluid Flow.* John Wiley & Sons, 2004.

[41] J. Kunes, *Dimensionless Physical Quantities in Science and Engineering.* Elsevier, 2012.

[42] R. K. Tiwari and M. K. Das, "Heat transfer augmentation in a two-sided lid-driven differentially heated square cavity utilizing nanofluids," *International Journal of heat and Mass transfer*, vol. 50, no. 9-10, pp. 2002–2018, 2007.

[43] R. E. Powell and H. Eyring, "Mechanisms for the relaxation theory of viscosity," *nature*, vol. 154, no. 3909, pp. 427–428, 1944.

[44] T. Hayat, M. Qasim, and S. Mesloub, "MHD flow and heat transfer over permeable stretching sheet with slip conditions," *International Journal for Numerical Methods in Fluids*, vol. 66, no. 8, pp. 963–975, 2011.